CONDUCTIVE CONCRETE FOR BRIDGE DECK DEICING AND ANTI-ICING

A Final Report

Submitted to

Nebraska Department of Roads

For

Project No. SPR-PL-1(037) P512

by

Christopher Y. Tuan, Ph.D., P.E.
Associate Professor of Civil Engineering
University of Nebraska-Lincoln

July 2004

CHAPTER 1

INTRODUCTION

1.1 Problem Statement

Concrete bridge decks are prone to ice accumulation. The deck freezes before the approaches do, making wintry travel on highways hazardous. Traditionally, removing ice from pavement can be accomplished by a combination of several methods, such as plowing, natural melting, traffic movement and chemical treatment. Because the bond between ice and pavement is strong, removal by plowing alone may not be effective. Chemical treatment helps break the bond by melting into the ice and spreading under the ice layer. Most highway winter maintenance depends on using chemicals and fine granular particles as a primary means for deicing and anti-icing[46]. The use of road salts and chemicals for deicing is an effective method for ice removal but causes damage to concrete and corrosion of reinforcing steel in concrete bridge decks. This problem is a major concern to transportation and public works officials due to rapid degradation of existing concrete pavements and bridge decks. The search for improved deicing methods has been a research focus for quite some time. The use of electric heating cables and heated fluid in pipes has been attempted, however, those techniques were too expensive to operate and difficult to maintain.

1.2 Background Information

Conductive concrete is a cementitious composite containing a certain amount of electrically conductive components to attain stable and high electrical conductivity. Due to its electrical resistance and impedance, a thin conductive concrete overlay can generate enough heat to prevent ice formation on a bridge deck when connected to a power source.

Conductive concrete is a relatively new material technology, which has been used for anti-static flooring, electromagnetic shielding, and cathodic protection of steel reinforcement in concrete structures. However, its applications have been limited because the earlier conductive concrete mixes did not meet strength requirements and/or were too expensive to produce.

A conductive concrete mix patented by Xie et al.[82] at the Canadian National Research Council contained carbon and metallic particles and fibers. However, that mix has not been utilized in roadway deicing applications. The patent claims a wide practicable range of volumetric ratios of conductive materials, including coke breeze, steel shavings and steel fibers. However, some of the ratios claimed (e.g., "up to 8 percent of steel fibers by volume") are impossible to achieve in a concrete mix. Furthermore, the volume ratios of conductive materials and the corresponding electric resistivity in their mix design are not explicitly specified for different applications.

1.3 Research Objectives

The objectives of this research were:

(1) Design a conductive concrete mix specifically for bridge deck overlay for deicing and anti-icing application;

(2) Evaluate the conductive concrete mix developed to ensure that its mechanical and physical properties meet the ASTM and AASHTO specifications for bridge deck overlay construction;

(3) Conduct deicing and anti-icing experiments using a small-scale conductive concrete overlay in a natural environment to determine factors affecting its heating performance; and

(4) Implement a conductive concrete overlay as a heating system for bridge deck deicing in a demonstration project.

The tasks of this study included (1) conduct literature review of existing deicing methods and previous projects including heating systems for bridge deck deicing; (2) assess the impact of cold climatic factors on the conductive concrete mix design; (3) design a conductive concrete mix suitable for bridge deck overlay construction; (4) conduct laboratory experiments to evaluate the durability and the properties of the conductive concrete mix; (5) conduct experiments in a natural environment to develop guidelines for operating a heating system consisting of a conductive concrete overlay; and (6) implement the conductive concrete deicing technology in a demonstration project.

1.4 Organization of the Report

This report documents the development and testing of a conductive concrete mix especially designed for highway bridge deck overlay deicing and anti-icing. The details of a demonstration project at Roca, Nebraska, to implement the conductive concrete deicing technology are presented.

Chapter 2 provides a summary of literature review of concrete behavior in cold weather and protections against frost action, existing deicing methods, previous projects utilizing various heating systems, the experience with fiber reinforced concrete and the conduction of electricity through conductive concrete. Chapter 3 documents the development of a conductive concrete mix at the University of Nebraska especially for bridge deck deicing and anti-icing. Chapter 4 describes the evaluations of the mechanical and physical properties of the conductive concrete. Chapter 5 covers the deicing experiments utilizing a 4 ft by 12 ft test slab with a conductive concrete overlay during winter storms. Chapter 6 discusses in

detail about the implementation of a conductive concrete overlay for bridge deck deicing at the Roca Spur Bridge. The heating performance and operational costs are presented. Chapter 7 provides conclusions and recommendations.

CHAPTER 2

LITERATURE REVIEW

General information about concrete in cold weather is summarized herein. Existing deicing and anti-icing methods have been surveyed and compared.

2.1 Protections against Frost Action

2.1.1 Concrete in Cold Weather

ACI 306R[6] considers the weather to be cold when two conditions exist: (1) when the average of the maximum and minimum air temperatures recorded on 3 consecutive days is less than 5°C (40°F); and (2) when the air temperature during at least 12 hours in any 24-hour period is 10°C (50°F) or lower. Under such conditions, normal weight concrete should not be placed unless its temperature is at least 13°C (55°F) for thin sections (300 mm (12 in.)) or at least 5°C (40°F) when the minimum dimension of the concrete element is at least 1.8m (72 in.). Cold weather can damage concrete during the early stages in two ways. First, the low temperature in the concrete slows down both the setting and the early hardening process. Second, water may freeze in the concrete during the setting and early hardening periods after which the concrete can never reach the anticipated strength.

There are two ways to overcome the harmful effects of cold weather[56,59,64]:

1. to produce concrete with an accelerating admixture. The most common accelerators used is calcium chloride. The benefit of using calcium chloride (1% by weight of cement) is to increase the early strength of concrete and to reduce the required protection time against freezing.

2. to keep the temperature of concrete above the damaging level until it reaches adequate strength. To obtain the required temperature for freshly mixed concrete in cold weather, it is often necessary to heat mixing water, aggregates, or both, depending on the severity of the weather. Heating the mixing water is the most practical and efficient procedure. Water is not only easy to heat, but each pound of water heated to a given temperature has roughly five times as many heat units as there are per pound of aggregate or cement at the same temperature. Mixing water should be heated so that the fluctuations in temperature from batch to batch are avoided. Very hot water should not be allowed to touch the cement because it may cause quick or flash set. When heating aggregates is used as an alternative method, the aggregates should be heated uniformly to eliminate all frozen lumps, ice, and snow and to avoid overheating or excessive drying.

2.1.2 Deterioration of Concrete

Damage to concrete pavements, bridge decks and railings due to freeze-thaw cycles (frost action) in cold climates is one of the major problems for state and local governments. This problem results in a major expense for repair and replacement of existing concrete pavements and bridge decks. Frost damage in concrete can take several forms. The most common is cracking and spalling. In the following section, these types of damage will be briefly discussed.

2.1.2.1 Deterioration line (D-line cracking)

This type of cracks[1,24,56,59,74] usually run approximately parallel to joints or edges of concrete surfaces. As deterioration progresses, these parallel cracks occur farther away from the joints.

Figure 2.1 D-line cracking spreading from sidewalk joint

This type of cracking has been designated as D-line cracking, as shown in Fig. 2.1.

2.1.2.2 Pattern Cracking

Pattern cracking[24] occurs in concrete surfaces due to either reduced volume at the surface or an increased volume in the interior of the concrete. Freeze-thaw cycles may cause pattern cracking in the concrete surface by expansion of freezing water either in voids of the cement paste or in the aggregate pores, as shown in Fig. 2.1.

2.1.2.3 Spalling

Spalling[21] is the local disintegration of a portion of the concrete surface, usually that which covers over the top reinforcing bars, as shown in Fig. 2.2.

Figure 2.2 Spalling of concrete surface, exposing a reinforcing bar

2.1.2.4 Scaling

Scaling[1,18,24,56,59] of concrete surfaces is a type of deterioration which exposes the coarse aggregate due to removal of the mortar, as shown in Fig. 2.3.

The main cause for concrete scaling is due to repeated freeze-thawing cycles.

Figure 2.3 Scaling of concrete slab surface

2.1.3 Freezing and Thawing Mechanism

The mechanisms of freezing effects have been a subject of research[24,56,59,62,65,66,68,69,78] for many years. Many theories have been proposed to explain the deterioration and damage of concrete exposed to freezing and thawing. The two popular hypothetical mechanisms for frost actions in concrete are the generation of hydraulic pressure caused by water freezing in large cavities and the osmotic pressure resulting from partial freezing of solutions in capillaries.

2.1.4 Factors Affecting Frost Resistance of Concrete

The ability of concrete to resist damage due to frost action depends on the characteristics of both cement paste and aggregates. Frost resistance[24,56,59,62,65,66,69] depends

on the interaction of several factors such as the location of escape boundaries, the pore structure of the system, the degree of saturation, the rate of cooling, and the tensile strength of the material. One of the basic approaches in preventing concrete deterioration due to freezing and thawing is to produce durable concrete. Methods for producing durable concrete include production of high quality portland cement paste by limiting the water cement ratio, using high quality aggregates, and air-entraining admixture to produce air voids which will relieve hydraulic pressure and reduce the growth of capillary ice.

2.1.4.1 Shrinkage and Moisture Movement of Concrete

Shrinkage[5,48,54,58,59,62,69] is the shortening of concrete during hardening and drying due to water movement. Different stages of water movement, which cause different types of shrinkage, will be discussed in this section.

Plastic shrinkage (early volume change)

Plastic shrinkage is caused by the rapid evaporation of water from the concrete surface such that it exceeds the rate at which bleeding water rises to the surface. Plastic shrinkage causes cracking in the superficial layer of fresh concrete. Plastic shrinkage can be affected by different parameters such as water absorption and evaporation sedimentation and segregation, cement hydration, thermal changes, and variables in the surrounding environment, including temperature, humidity, and wind speed.

Autogenous shrinkage

This type of shrinkage happens due to the withdrawal of water from the capillary pores by the hydration of the hitherto unhydrated cement. Typical values of autogenous shrinkage are about 40×10^{-6} at the age of one month and 100×10^{-6} after 5 years. Autogenous shrinkage increases at higher temperatures, and with a higher cement content.

Autogenous shrinkage is relatively small except at extremely low water/cement ratios. For practical purposes, autogenous shrinkage need not be distinguished from shrinkage caused by concrete drying out.

Drying shrinkage

Withdrawal of water from concrete stored in unsaturated air causes drying shrinkage strains. Part of the drying shrinkage can be reversible if the concrete is exposed to wet conditions. The main factors affecting drying shrinkage are water cement/ratio, aggregate contents, concrete admixtures, time and humidity, and geometry of the concrete element. ACI 209R-92[5] gives the following general expression for predicating shrinkage over time for moist-cured concrete:

$$s_t = \frac{t}{35 + t} s_{ult} \qquad (2\text{-}1)$$

where s_t is the shrinkage after t days since the end of 7-day moist curing, s_{ult} is the ultimate shrinkage, and t is time in days since the end of moist curing. This general expression can be modified by a number of coefficients to allow for various factors such as initial moist curing, relative humidity, volume to surface ratio, fine aggregate percentage and cement content.

Carbonation shrinkage

Dissolution of $Ca(OH)_2$ crystals and deposition of $CaCO_3$ in spaces free from stress cause carbonation shrinkage. Carbonation increases the shrinkage at moderate humidity greater than 25 percent and less than 100 percent. The sequence of drying and carbonation affects the total magnitude of shrinkage. Simultaneous drying and carbonation produces lower total shrinkage than when drying shrinkage is followed by carbonation because a large part of the carbonation occurs at relative humidity above 50 percent. When concrete is subjected to alternating wetting and drying in air containing CO_2, shrinkage due to

carbonation during the drying cycle increases and the magnitude of irreversible shrinkage increases.

2.1.4.2 Alkali-Aggregate Reaction

Chemical reactions involving alkali ions from portland cement (or from other sources), hydroxyl ions and certain siliceous constituents that may be present in aggregate can cause an expansion and cracking, leading to loss of strength, elasticity and durability of concrete. This phenomenon is referred to as an alkali-silica reaction[56,59,62,69]. The reaction starts with an attack on the siliceous minerals in the aggregate by the alkaline hydroxides in pore water derived from the alkalis (Na_2O and K_2O) in the cement. As a result, an alkali-silicate gel is formed, either in planes of weakness or pores in the aggregate or on the surface of the aggregate particles. In the latter case, a characteristic altered surface zone is formed. This may destroy the bond between the aggregate and the surrounding hydrated cement paste. The alkali-silica reaction occurs only in the presence of water. For the reaction to proceed, a minimum relative humidity of about 85 % at 20°C (68°F) in the interior of concrete is required. At higher temperatures, the reaction can take place at a somewhat lower humidity. The alkali-silica reactions are accelerated as the temperature is increased, but beyond a certain point higher temperatures decrease this expansion. But the increase in temperature does not increase the total expansion induced by the reaction. The alkali-silica expansion was found to be increased at three temperatures: 10°C (50°F) > 60°C (140°F) >38°C (100°F). The effect of temperature may be due to the fact that an increase in temperature lowers the solubility of $Ca(OH)_2$ and increases that of silica.

The expected increase in the pavement temperature due to heating is limited to 3°C to 5°C (37.4°F - 39.2°F). These temperatures are less than the temperatures which cause an increase in alkali-silica reaction.

2.2 Using Deicing Chemicals

The most common deicing chemical used by highway agencies is sodium chloride (NaCl). Recent statistics indicate that about 10 million tons of sodium chloride are used each winter in the United States[46]. Sodium chloride, often referred to as road salt, is usually used alone or mixed with fine granular particles. The application rates of road salt are varied due to different weather conditions, service levels and demand of highway users. The application rates range between 13 to 68 g/m^2 (170 to 890 lbs/12 ft lane-mile). The temperature for deicing applications using road salt ranges from -10°C to 1°C (14°F to 34°F). A recent interview with Nebraska Department of Roads officials has revealed that the deicing operation in Omaha uses road salt mixed with sand. The application rate ranges between 15 to 23 g/m^2 (200 to 300 lbs per 12 ft lane-mile) and about 1.82×10^6 kg (2000 tons) of salt and 4.54×10^6 kg (5000 tons) of sand are usually used in a winter season.

Calcium chloride ($CaCl_2$) has a lower freezing point than sodium chloride, and adheres better to the road at lower temperatures. Some highway agencies reported using calcium chloride alone at temperatures as low as -25°C (-14°F)[46,52]. Because of this advantage, calcium chloride is sometimes used in combination with sodium chloride to provide low temperature deicing. It is also common to pre-wet salt to improve the melting and workability of the salt treatment, and thereby reduce salt usage. Calcium chloride is more expensive than road salt and has some detrimental effects. One of these effects is that the residual calcium chloride remains wet on the road surface, causing slick pavement. It also causes melted snow

to refreeze into ice when temperature decreases[46,56,59]. Because of these effects and the high cost, calcium chloride is seldom used alone in the United States.

Using chloride deicing salt causes many problems, including damage to concrete pavement and bridge decks (e.g. surface scaling and corrosion of reinforcement)[1,10,56,57,59,86], corrosive damage to automobile bodies and pollution due to concentrations of sodium and chloride in roadside soils and water runoff. Furthermore, salt produces osmotic pressure causing water to move toward the top layer of the slab where freezing takes place [10,56,59]. This action is more severe than ordinary freezing and thawing. Many studies[46,77] have been initiated in the United States and European countries to investigate more efficient ways for storing and dispensing salt for deicing. An objective was to reduce salt usage for deicing to help reduce the detrimental effects. The use of pre-wet salt and brine is one option to control the dispensing rate and get better spreading instead of using dry salt, which tends to be blown off the road by traffic.

2.3 Alternative to the Use of Chloride

The search for new deicing chemicals has been a popular area for research and experimentation for many years. One promising alternative is Calcium Magnesium Acetate (CMA). Comparing CMA to NaCl[41,46,52,54,77,86], CMA is slower acting and less effective at low temperatures and in freezing rain, dry snow and light traffic. CMA also requires a larger truck capacity and a larger enclosed storage space than salt. Research findings indicate that CMA is not likely to have adverse effects on human health or to the environment[40,67,76]. CMA is more expensive than salt. The following deicing chemicals have been used by many highway agencies:

- Urea[46,86] is a soluble nitrogenous compound, either organic or synthetically produced. It is commonly used by airports as an ice control chemical due to its low corrosivity. Urea is an acceptable deicing chemical for temperature above 15°F (-9°C). However, urea is less effective and more expensive than salt.
- Magnesium chloride[46,86] is sometimes used as a substitute for calcium chloride because it is less expensive and works at similarly low temperature. Magnesium chloride can be used in its solid form with application rate ranges between 8 to 11 g/m^2 (100 to 150 lbs/12 ft lane-mile). Magnesium chloride is effective in melting dry snow but less effective in melting ice.
- Formamide[46,86], or a mixture of formamide and water, are liquid deicers which can be used effectively in automatic ice prevention systems. Formamide is less corrosive than sodium or calcium chloride but is much more expensive. When applied to a pavement, it is relatively nonslippery. Because formamide has a high freezing point 2.55°C (36.6°F), formamide is usually mixed with water before application. Formamide will not freeze at -18°C (0°F) with a concentration range of about 33 to 88%. A lower or higher concentration of formamide at -18°C (0°F) will cause crystallization of ice or the formation of slush.
- Tetrapotassium pyrophosphate (TKPP)[46,86] is effective for temperatures above 25°F (-4°C). TKPP has no side effects on concrete and cannot penetrate concrete to affect reinforcing steel. However, TKPP is corrosive to exposed steel (i.e., automobile chassis and brakes), and costs approximately 15 times that of salt.

Other chemical mixtures, such as CMA mixed with potassium acetate, CMA mixed with salt, formamide mixed with Urea and water, and TKPP mixed with formamide, have also been used for deicing. Some commonly used deicing chemicals are compared in Table 2.1.

Table 2.1 Comparison of deicing chemicals

Deicing Chemical	Temperature Range	Application Rate	Approximate Cost
Sodium chloride[46,77,86] (NaCl)	-10°C to 1°C (14°F to 34°F)	13 to 68 g/m^2 (170 to 890 lb/12ft lane-mile)	\$29/m^3(\$26/ton)
Calcium chloride[46] ($CaCl_2$)	-25°C(-13°F)	Not used alone in the U.S.A.	\$294/m^3(\$267/ton)
Salt mixed with Calcium chloride[46,77] ($CaCl_2$)	-17°C to 0°C (0°F to 32°F)	21-50 l/m^3 salt (5 to 12 gal/ton)	\$108/m^3(\$98/ton)
Calcium Magnesium Acetate[46,77,86] (CMA)	-5°C to 0°C (23°F to 32°F)	15 to 39 g/m^2 (200 to 500 lb/12ft lane-mile)	\$738/m^3(\$670/ton)
Urea[46,86]	-9°C (16°F)	26 to 136 g/m^2 (340 to 1780 lb/12ft lane-mile)	\$145-\$290/m^3 (\$130-\$260/ton)
Magnesium chloride[86]	-15°C (5°F)	8 to 11 g/m^2 (100 to 150 lb/12ft lane-mile)	Not Available
Formamide[86]	-18°C (0°F)	Not Available	\$290-\$435/m^3 (\$290-\$390/ton)
Tetrapotassium[46,86] pyrophosphate (TKPP)	-4°C (25°F)	49 g/m^2 (640 lb/12ft lane-mile)	\$435/m^3(\$390/ton)

2.4 Insulation against Freezing

One method to reduce salt usage is to provide insulation against frost and ice formation[19,17,35,61]. This concept was used to insulate the underside of a bridge deck and the subgrade of highway pavements and airfield runways.

The main objectives of using insulation materials such as urethane foam, plastic foam, and Styrofoam, are to reduce heat loss from the surface and prevent ice and frost formation, and to decrease the number of freeze-thaw cycles and salt usage.

Since 1962, polystyrene foam (Styrofoam) has been used in Michigan[61], Iowa[61], Minnesota[61], and Alaska[27] as insulation beneath the roads and airfields to prevent subgrade freezing. Canada[49], Sweden[73] and Britain[44] experimented using polystyrene foam for insulation under highway pavements. The polystyrene effectively prevented frost action in the subgrade. Fig. 2.4 shows Styrofoam insulating layer used on graded subgrade for flexible pavement in Michigan (1962).

Figure 2.4 Styrofoam insulating layer used on graded subgrade for flexible pavement in Michigan (1962)

In Missouri[12] (1961-1962) and Nebraska[26] (1964-1965), urethane foam was used to insulate the underside of bridge decks and upper half of the girders. A 19 mm (3/4 in.) urethane foam was used in Missouri, while a 19 mm (3/4 in.) and a 32 mm (1-1/4 in.)

urethane foams were used to compare their performance in Nebraska. The observations and results from both states indicated that there was a large scatter in the data from day to day. The urethane foam was generally not effective in achieving the two main objectives of the application. There was no reduction in the number of freeze- thaw cycles, and the salt usage was about the same as with the uninsulated deck. However, the urethane foam insulation resulted in reducing the severity of frost and ice formation. In the Nebraska[26] study, there was a bond problem for the 32mm (1-1/4 in.) insulation, and in some areas there was a complete loss of the material due to debonding from the concrete.

2.5 Heating Systems

Pavement heating systems have been applied to control snow and ice formation on bridges and ramps as an alternative to the conventional methods of plowing and using deicing chemicals. Heating systems[47,86] for use in pavements have typically been embedded resistive electrical heaters or pipes containing a heated fluid. The circulating fluid systems generally use fossil fuel energy sources. The use of low-grade, renewable thermal energy sources, such as geothermal water and warm ground water below the frost line, have also been tested.

2.5.1 Heating Using Ground Source Heat Pipes

The use of gravity-operated heat pipes to transport thermal energy to a road surface was investigated and developed[47] during the 1970s. This system depends on condensation of an evaporated liquid and the latent heat of vaporization released. Since this system does not require any mechanical or electrical parts, the gravity-operated heat is considered a favorable heat exchanger. Ammonia has been used as the working fluid in these heat pipes because it is not susceptible to freezing. The main parameters affecting the cost of ground heat pipes are

the surface area and the length of the pipes. A heating system with 60 evaporator pipes using the manifold ground heat exchanger was used to heat a bridge deck in Laramie, Wyoming[47] in 1981. The bottom surface of the heated deck was also insulated. The results showed that the heated surface was about 2°C to 14°C (35°F to 57°F) warmer than the unheated portion of the bridge during heating. This heating was sufficient to prevent freezing of the bridge deck surface and resulted in melting snow. The main disadvantage was the complication of the construction and the assembly of the heat pipes. It was reported that approximately 40% of the total cost of this ground heat system was related to drilling and grouting evaporator pipes.

2.5.2 Heating Using Infrared Heat Lamps

Infrared heat lamps were used to heat the underside of the deck of the Mississippi Avenue Bridge[86] in southeast Denver, Colorado to prevent icing. The system, consuming about 75 W/m^2 of surface (7 W/ft^2), was found to be inadequate due to excessive lag time and insufficient power. The effect of insulation, also a part of the study, was found to depend on the wind direction. Insulation helped to prevent icing when the wind direction was parallel to the bridge and increased icing when wind direction was perpendicular to the bridge direction.

2.5.3. Heating Using Electric Heating Cables

In 1961, electric heating cables[38] for snow removal and ice control were installed on the approach to a highway drawbridge in Newark, New Jersey. Fig. 2.5 shows electric cables in the bridge approach roadway, Newark, New Jersey 1961. The cables were installed in two lanes of 256 m (840 ft) long bridge approach roadway. The installation involved four steps: 1) laying a layer of coarse aggregate, 2) laying the heating cables, 3) spreading a 13 mm (1/2

in.) coat of sand-mix asphalt by hand, and 4) laying a 38 mm (1-1/2 in.) final course by paving machine. The installation cost was about \$54/m^2 (\$5.0/ft^2). This cost did not include any transformers or service facilities. The required power was 378 and 430 W/m^2 (35 and 40 W/ft^2) for the bridge and the land fill areas, respectively. This power was sufficient to produce heat to melt 25 mm (1 in.) of snow per hour. This installation was later abandoned because the electric cables were pulled out of the asphaltic concrete overlay due to traffic movement.

Another electrically heated construction was installed in 1964 on two ramps and a bridge deck at the U. S. 46 and 17 interchange[86] in Teterboro, New Jersey. This system has been operating satisfactorily. The power consumption is about 323 and 430 W/m^2 (30 to 40 W/ft^2) and the annual operating cost is approximately \$5/m^2 (\$0.45/ft^2).

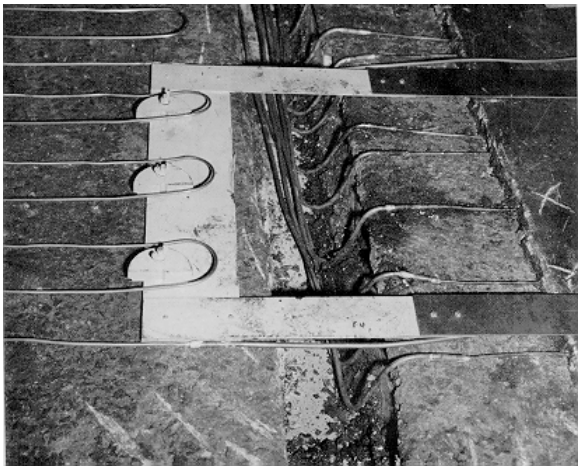

Figure 2.5 Electric cables in the bridge approach roadway, Newark, New Jersey 1961

Electrical heating units were installed in 1970 in a concrete bridge deck in Omaha[86], Nebraska. The system contained sensing elements to activate the heating units. However, this automatic system was sometimes unreliable and manual activation was necessary. Similar systems[86] have been installed in Ohio, Oregon, Pennsylvania, South Dakota, Texas

and West Virginia. Unsatisfactory performance was reported about these systems either because of problems with the heating elements or with the high power consumption.

2.5.4 Heating Using Heated Fluids

A hot water heating system was installed in 1950 in approximately 122 m (400 ft) long reinforced concrete pavement and the deck of a canal bridge in Oregon[86]. Heat was obtained from a natural hot water well. The system consisted of a grid in the pavement of 13 mm (1/2 in.) copper pipes spaced at 457 mm (18 in.) on centers, through which an anti-freeze solution was circulated after leaving a heat exchanger located in the hot water well. The continuous circulation of the anti-freeze through the system kept the deck free of snow and ice.

A heating system consisting of 9.5 mm (3/8 in.) rubber hoses spaced at 152 mm (6 in.) on centers, 25 mm (1 in.) copper manifolds, 127 mm (5 in.) PVC supply and return lines, and a gas boiler were installed in 1993 in a pedestrian overpass, in Lincoln, Nebraska[25,32]. Fig. 2.6 shows the layout of the deck heating system.

Figure 2.6 Deck heating system on approaches of a pedestrian overpass in Lincoln, Nebraska, 1993

The heating system was installed in the deck of a 367-m long by 3.7-m wide viaduct. The fluid used was propylene glycol with water at a flow rate of 454 L/min. to deliver 473 W/m^2 of heat flux to the deck. The heating system was designed to be regulated by moisture and temperature sensors cast in the deck, which turn the system on when the deck temperature is less than 4°C (40°F) and shut off the boiler when the deck reaches a temperature of 13°C (55°F). However, the automatic system did not work and manual activation was required. This heating system is not in service due to a leak in the PVC supply and return lines. The operation cost per storm was about $250 to melt 76 mm (3 in.) of snow. The installation cost of the heating system[25] was $161/$m^2$.

A heating system, consisting of 25 mm (1 in.) diameter steel pipes and carrying Freon heated up to 149°C (300°F) by a propane-fired boiler, was installed in the Buffalo River Bridge[60], Amherst, Virginia, in November 1996, as shown in Fig. 2.7. Heat is obtained from the latent heat released during condensations of the evaporated Freon. A computer and sensors on the deck control this system. The operating temperature is set at 1.7°C (35°F) or below, and the system shuts off when the deck temperature reaches 4.4°C (40°F). However, the freon cooled and condensed before it reached the upper third of the bridge. Several different fluids were being tested to identify a replacement for Freon. The heating system cost was about $181,000 and the estimated operating costs were about $1000 annually.

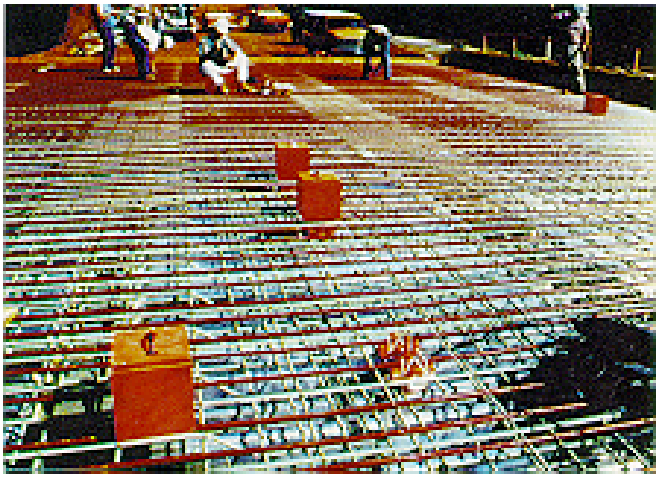

Figure 2.7 Deck heating system in the Buffalo River Bridge, Amherst, Virginia, 1996

2.5.5 Electrically Conductive Concrete

Conductive concrete may be defined as a cement-based composite that contains a certain amount of electrically conductive components to attain stable and relatively high electrical conductivity. Some of the applications for using conductive concrete are: (1) electromagnetic shielding often required in the design and construction of facilities and equipment to protect electrical systems or electronic components; (2) radiation shielding in nuclear industry; (3) anti-static flooring in the electronic instrumentation industry and hospitals; and (4) cathodic protection of steel reinforcement in concrete structures.

Xie et al.[80,82,83], summarized several researchers efforts in investigating the compositions of conductive concrete. The conductive concrete cited in the literature can be classified into two types: 1) conductive fiber-reinforced concrete, and 2) concrete containing conductive aggregates. The first type has higher mechanical strength but lower conductivity with a resistivity value of about 100 Ω.cm. The reason for the lower conductivity is due to the small fiber-to-fiber contact areas. The second type has a higher conductivity with a

resistivity value of 10 to 30 Ω.cm, but relatively low compressive strength (less than 25 MPa). Lower mechanical strength is due to the high water content required during mixing to offset the water absorption by conductive aggregates, such as carbon black and coke. Xie et al.[80,82,83] patented a new conductive concrete mix developed at the Institute for Research in Construction, National Research Council of Canada. With the newly developed mix, both high conductivity and mechanical strength were achieved simultaneously. However, this mix has not been utilized in roadway deicing applications.

The various heating systems described in Sec. 2.5 are compared in Table 2.2.

Table 2.2 Comparison of different heating systems

Heating System	Approximate cost*	Annual operating cost*	Power consumption
Infrared heat lamp[86]	\$96/m^2 (\$8.9/ft^2)	Not available	75 W/m^2 (7 W/ft^2)
Electric heating cable[38,86]	\$54/m^2 (\$5/ft^2)	\$4.8/m^2 (\$0.45/ft^2)	323 to 430 W/m^2 (30 to 40 W/ft^2)
Hot water[25,32]	\$161/m^2 (\$15/ft^2)	\$250/storm [76mm (3 in.) snow]	473 W/m^2 (44 W/ft^2)
Heated gas[60]	\$378/m^2 (\$35/ft^2)	\$2.1/m^2 (\$0.20/ft^2)	Not available

Note :

1. Cost figures were quoted directly from the literature, and conversion to present worth was not attempted.
2. Costs and energy consumption are estimates based on the limited data obtained in this study.

2.6 Previous Experience with Fiber-Reinforced Concrete

Fiber-reinforced concrete has been used for roadway pavements in the United States since 1971[42,55,63]. The benefits from adding steel fibers to concrete mix[14,56,69,70] are not limited to increasing the ultimate flexural strength, shear and torsional strength, fatigue strength and impact resistance. Other benefits include increasing the ductility, energy absorption capacity, ultimate strain capacity and post-crack load carrying capacity[8,69,70].

The steel fiber content used in different concrete overlays[42] has ranged from 36 to 157 kg/m^3 (60 to 265 lb/yd^3), with aspect ratios ranging from 40 to 200. Steel fibers have varied in length from 13 to 64 mm (0.5 to 2.5 in.). Using 2 percent of steel fibers by volume is considered an upper limit[8,13,16] beyond which poor surface finishability will result.

The recommended[13,16,22] minimum thickness for fiber-reinforced concrete overlay is between 76 to 102mm (3 to 4 in.) to avoid cracks due to curling or warping. The degree of bond between an existing pavement surface and an overlay can be categorized as bonded, partially bonded, or unbonded. If a good bond is obtainable at the interface, a 51-mm (2-in.) thick overlay may be applied on an existing pavement.

Steel fiber-reinforced concrete shows a slightly greater resistance to chloride penetration than regular concrete, observed during the testing[70] of 50-mm (2-in.) thick specimens using 8 percent sodium chloride solution. The scaling resistance of steel-fiber reinforced concrete, tested[70] with a 4 percent calcium chloride solution, was shown to improve with lower water/cement ratio. Specimens with less permeability also showed higher resistance to scaling caused by deicing chemicals.

Grondziel[36] reported that rusting of steel fibers was found only at or near the surface and not inside the cross section. Several studies[36] also indicated that the forces due to the

volumetric expansion caused by steel corrosions are insufficient to split the cement paste surrounding the steel fibers.

Fine transverse cracks were reported[22] to have appeared on overlays after construction due to thermal stresses and concrete shrinkage. Reflective cracks were also observed[13,16,22,63] over existing cracks in the old pavements. To avoid longitudinal and transverse cracks, the maximum spacing[13,16,22,36,42,55] between joints should be less or equal to 12m (40 ft), previous joints in the old pavement should be matched, and pressure relief joints should be provided at a spacing between 300 to 450m (1000 to 1500 ft) .

2.7 Conduction of Electricity through Concrete

Conventional concrete is not electrically conductive. The electric resistivity of normal weight concrete ranges between 6.54 – 11 kΩ•m.[11,79] A hydrating concrete consists of pore solution and solids, including aggregates, hydrates and unhydrated cement. The electric resistivity of the pore solution in cement paste is about 0.25-0.35 Ω•m[79]. Most common aggregates (e.g., lime stone) used in concrete, with electric resistivity ranging between 3×10^2 and 1.5×10^3 Ω•m[79], are non-conductive.

Conduction of electricity through concrete may take place in two ways: electronic and electrolytic. Electronic conduction occurs through the motion of free electrons in the conductive media, while electrolytic conduction takes place by the motion of ions in the pore solution. Whittington et al.[79] investigated conduction of electricity through conventional concrete using cement paste and concrete specimens. Electric resistivity was found to increase with time for both specimens because conduction in these specimens depended on the ions' motion in the pore solution. In addition, the electric resistivity of the concrete specimens was higher than that of the cement paste specimens, due to the restricted ions'

movement from non-conductive aggregates used in the concrete specimens. In 1978, Farrar[29] used "Marconite," a carbon by-product from oil refining, to replace sand in a conductive concrete mix. The electric resistivity of the conductive concrete using Marconite ranges between 0.5 to 15 Ω•cm. The use of Marconite was limited to small-scale applications such as electromagnetic shielding and anti-static flooring because it was expensive. Conduction of electricity in this case was through the movement of electrons with the particles in continuous contact within the concrete. This phenomenon is called "electrical percolation" in concrete[29,83]. Xie et al.[83] used steel and carbon fibers as the conductive media and investigated the effect of fiber size on the percolation threshold, which was found to increase with decreasing fiber length. More short fibers than long fibers were required to create a conductive media within the concrete matrix. Conduction through hardened concrete depends on movement of electrons which requires a good contact between conductive particles. Using longer fibers could reduce the minimum contact required.

Approaches to improving the electrical conductivity of a concrete mix include: (1) use of conductive aggregates such as iron ore, raw slag, etc.; and (2) increasing the conductivity of the cement paste by adding conductive materials such as steel shavings, coke breeze, steel or carbon fibers, etc.

2.7.1 Electrical Conduction Models for Concrete

Different models were proposed to predict conduction of electricity through concrete. Maxwell[50] (1904) derived the first relation between electric and phase composition of composites conductivity. He based his model on three assumptions: (1) the composite has a matrix with conductivity σ_1, (2) spherical particles has conductivity σ_2 dispersed in the matrix

in a regular arrangement, and (3) the particle size was much smaller than the distance between two particles. The electrical conductivity of the composite, σ_c, was expressed as:

$$\frac{\sigma_c}{\sigma_1} = \frac{2\sigma_1 + \sigma_2 - 2\varphi(\sigma_1 - \sigma_2)}{2\sigma_1 + \sigma_2 + \varphi(\sigma_1 - \sigma_2)} \qquad (2\text{-}2)$$

where φ is the volumetric fraction of particles in the composite. The above expression was found by Xie[81] to be incorrect for mortar and concrete systems.

Whittington et al.[79] proposed an electrical conduction model for concrete. In their model, three paths of the electric current through concrete were assumed: (1) through the aggregate and paste in series, (2) through the aggregate particles in contact with each other, and (3) through the paste. The fractional cross-sections of the three paths in (1), (2), and (3) were represented in the model by x, y, and z respectively. The aggregate ratio in path (1) is represented by w. The resistance of each circuit and the total resistance of the model can be determined by assigning values to the parameters w, x, y, and z.

Xie et al.[81] derived a conductivity model for hydrating cement systems. They assumed uniform distribution of each component in a hydrating cement composite. The size of each component is small compared with the specimen size. A general expression for the electrical conductivity of a multiphase composite was proposed by Xie et al.[81]:

$$\sigma_c = \sum_{i=1}^{N} \Psi_i \sigma_i \qquad (2\text{-}3)$$

where σ_i is the electric conductivity of its component and ψ_i is its area fraction in the cross section. The conductivity of the solids can be neglected compared with that of pore solution for a hydrating cement composite system. The conductivity in Eq.(2-2) can be expressed as:

$$\sigma_c = \psi_p \sigma_1 = (1 - \psi_s)\sigma_1 \qquad (2\text{-}4)$$

where ψ_p and ψ_s are the area fraction of pores and solids, respectively. σ_l is the conductivity of pore solution.

2.7.2 Equivalent Circuit Models for Cement Paste Systems

AC impedance spectroscopy is a useful method that can be used to describe many of the electrical properties of materials and their interfaces. Due to the complexity of cement paste microstructure and the hydration process, it is difficult to interpret an impedance spectrum. To select an equivalent circuit model requires continuous modeling with a selected equivalent circuit until the electrical response of the small element of the microstructure of the cement paste is well simulated.

McCarter et al.[51] proposed an electrical circuit model for hydrated cement paste. The model consists of three main elements in series: (1) a parallel combination of a resistor and a frequency-dependent capacitor to consider electrode effects, (2) electrode/cement paste interface represented by charge transfer resistance and double-layer capacitance, and (3) the cement bulk paste represented by a resistance parallel to capacitance circuit in series with a high-frequency resistance.

Scuderi et al.[75] proposed an equivalent circuit for hydrating cement paste with different water/cement ratios. Their model consists of five elements: (1) a resistor parallel capacitor to represent the electrode-cement paste interface, (2) an element accounting for the diffusion impedance associated with the electrode interface, (3) two elements (resistor and capacitor) to represent the bulk impedance of the cement paste, and (4) a resistor in series with other elements to represent the high-frequency intercept with the real axis in an impedance spectrum.

Gu et al.[37] proposed an electrical network of hydrating cement paste. Their model consists of three elements in series: (1) resistance of solid, (2) resistance of liquid, and (3) resistance of the interface phases and the capacitance on the interface in multiple unit cell (solid-liquid interface).

The available equivalent electrical circuit cited in the literature indicates that the impedance behavior of hydrating cement paste depends on the existence of solid-liquid interface. In the case of hardened concrete, the presence of water is limited; therefore, conventional concrete is considered a good insulator. To improve the electrical conductivity of the conventional concrete, external conductive material must be added to the concrete matrix. This conductive material will be responsible for reducing the overall impedance of the hardened concrete and hence, increase the electric conductivity of the concrete.

CHAPTER 3

CONDUCTIVE CONCRETE MIX DESIGN

3.1 Background

Conductive concrete is a relatively new material technology developed to achieve high electrical conductivity and high mechanical strength. Conductive concrete has been used for anti-static flooring, electromagnetic shielding, and cathodic protection of steel reinforcement in concrete structures. Conventional concrete mix consists of cement, fine and coarse aggregates, and water. Supplementary cementitious materials such as fly ash and silica fume, and chemical admixtures for accelerating set time, air entrainment, retarding set time, and water reduction are often used in a concrete mix. In a conductive concrete mix design, electrically conductive materials are used to replace a certain portion of the fine and coarse aggregates.

In this chapter a conductive concrete mix developed at the University of Nebraska is discussed in detail. The optimization of the mix design is also presented.

3.2 Conductive Concrete Mix Design

3.2.1 Mix Design by Xie et al. (1995)

The conductive concrete mix developed by Xie et al.[82] at the Institute for Research in Construction of the Canadian National Research Council claims a wide practicable range of volumetric ratios of conductive materials, as shown in Table 3-1. However, some of the ratios claimed (e.g., “up to 8 percent of steel fibers by volume”) are impossible to achieve in a mix. Further, the volume ratios of conductive materials and the corresponding electric resistivity of their mix design are not explicitly specified for different applications.

Table 3-1 Conductive concrete mix design (Xie et al.)[82]

Composition	Percentage
Conductive fibers	0% - 8% by vol.
Conductive particles	0% - 80% by vol.
Water/cement ratio	0.35-0.75 by weight
Sand/cement ratio	0-2.0 by weight
Stone/cement ratio	0-2.0 by weight
Dispersant/cement ratio	0.1%-5% by weight

3.2.2 Mix Design by Yehia and Tuan (1998)

In 1998, Yehia and Tuan[84] at the University of Nebraska-Lincoln developed a conductive concrete mix specifically for bridge deck deicing. In this application, a conductive concrete overlay is cast on the top of a bridge deck for deicing and anti-icing. In this mix, steel shavings and fibers were added to the concrete as conductive materials. Over 100 trial batches of conductive concrete were prepared and their properties evaluated. Optimization of the conductive concrete mix design for bridge deck overlay is discussed in detail in Section 3.5.

3.3 Material Properties

3.3.1 Steel Shavings

Steel shavings, as shown in Fig. 3-1, are an industrial waste from steel fabricators in the form of small particles of random shapes. Cast iron steel shavings were used in the trial

conductive concrete mixes. Before steel shavings are mixed into concrete, any grease or oil on the surface must be removed. Surface contamination may significantly reduce the electrical conductivity and the mechanical strength of the conductive concrete.

Figure 3-1 Steel Shavings

Results from sieve analyses of the steel shavings are shown in Fig. 3-2. Four samples taken from the steel shavings were tested and similar distributions were obtained. The particle size ranged between 0.15 and 4.75 mm (0.007 to 0.19 in.).

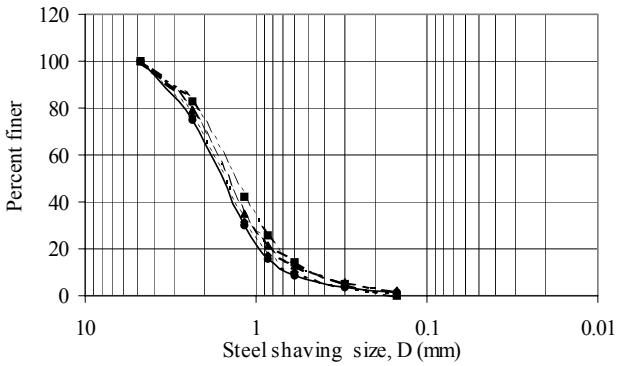

Figure 3-2 Results from sieve analysis

3.3.2 Steel Fiber

Low carbon steel fibers, as shown in Fig. 3-3, with four different aspect ratios between 18 to 53, were used in the mix. The characteristics[31] of the steel fibers are given in Table 3-2. The fiber has a rectangular cross section with corrugated surface, which ensures the bond with concrete.

Table 3.2 Steel fiber characteristics

Tensile strength	414-828 MPa @ 21°C (60,000-120,000 psi @ 70°F)
Modulus of elasticity	200,000 MPa @ 21°C (29,000,000 psi @ 70°F)
Density	7865 kg/m^3 (491 lb/cu ft)
Melting point	1507°C (2745°F)
ASTM	A820 Type II

Figure 3-3 Low carbon steel fibers

3.3.3 Other Materials

The materials used in the trial conductive concrete mixes are summarized in Table 3-3.

Table 3-3 Materials used in the conductive concrete mixes

Material	Description
Cement	Type I or Type III
w/c	0.3 - 0.4
Fly Ash	Class C
Silica Fume	Rheomac SF 100
Fine aggregates (sand and gravel)	Nebraska 47B
Limestone	½ in. (maximum aggregate size)
Superplasticizer	Rheobuild 1000

3.4 Mixing Procedure

One essential difference between mixing conventional concrete and conductive concrete is the addition of steel fibers and steel shavings. Steel fibers and steel shavings may be added during the mixing of cement and aggregates under either wet or dry conditions.

Uniform disbursement of the steel shavings and fibers must be maintained during the mixing. The guidelines specified by ACI Committee 544[7] for mixing steel fibers in concrete should be followed.

3.5 Optimization

A primary objective of this research was to determine the optimum volumetric ratios of the steel fibers and steel shavings in the mix design to achieve the required strength and electrical conductivity for bridge deck overlay deicing. Conductive concrete test specimens from three main categories were evaluated during the optimization process:

Category 1: containing steel fibers only;

Category 2: containing steel shavings only; and

Category 3: containing both steel shavings and steel fibers.

Compressive strength, electric resistivity, workability and finishability were used as primary evaluation criteria for each trial batch.

3.5.1 Category 1 and Category 2

The electric resistivity test results showed that using steel fibers or steel shavings alone could not provide an electric resistivity lower than the 10 Ω•m necessary for deicing application. The test results are summarized in Table 3.4. It is necessary to add both steel fibers and steel shavings to the mix in order to achieve the required electrical conductivity.

Table 3.4 Summary of test results – Optimization category 1 and 2

Composition	**Compressive Strength MPa (psi)**	**Electric Resistivity (Ω•m)**
Conventional concrete	65 (9425)	5.4×10^5
Concrete with 2% steel fibers (category 1)	54 (7918)	5.4×10^5
Concrete with 5 % steel shavings (category 2)	29 (4264)	6.6×10^3
Concrete with 15 % steel shavings (category 2)	25 (3638)	2.4×10^3
Concrete with 20 % steel shavings (category 2)	24 (3581)	2.2×10^3

Notes :
(1) All ratios are by volume.
(2) 2% by volume of steel fibers is the upper limit, beyond which poor surface finishability will result.

3.5.2 Category 3

The optimization of Category 3 specimens consisted of two stages. In the first stage, the impact of using different steel fiber and steel shavings ratios on the mechanical strength and electrical conductivity was assessed. Additional experiments were conducted in the second stage to identify the optimum volumetric ratios of steel fibers and shavings to use in the mix design.

3.5.2.1 First-Stage Evaluation

Over 50 trial mixes were prepared using seven different volumetric ratios of steel shavings (3, 5, 10, 15, 20, 30, and 40 percent) and two volumetric ratios of steel fibers (1.5 and 2 percent). Electric resistivity and compressive strength were determined for each batch. The test results are summarized in Table 3.5.

Table 3.5. First-stage test results - Category 3

Steel shavings by volume	Steel fibers by volume	Compressive strength MPa (psi)	Electric resistivity* (Ω.cm)
3%	1.5%	43.9 (6800)	410x 10^3
5%	1.5%	44.8 (6500)	20x 10^3
10%	1.5 and 2%	44.1 (6400)	600 to 800
15%	1.5 and 2%	42.1 (6100)	100 to 200
20%	1.5 and 2%	35.9 (5200)	75 to 100
30%	1.5%	18.3 (2650)	60
40%	1.5 and 2%	13.4 (1950)	30 to 50

* All tests were conducted at room temperature 23°C (74°F).

3.5.2.1.1 Mechanical and Physical Properties

The workability and surface finishability of the trial mix were similar to those of conventional concrete. Fig. 3-4 shows a typical conductive concrete mix, and Fig. 3-5 shows the finishing process for a specimen. For conductive concrete mixes with 10 to 20 percent steel shavings and 1.5 to 2 percent steel fibers by volume, the compressive strength ranges between 35-40 MPa (5000-6000 psi) and the electric resistivity ranges between 5 to 10 Ω•m. The electric resistivity of the mixes with 3 to 5 percent steel shavings was too high to be conductive. Mixes with 30 to 40 percent steel shaving were highly conductive, but the compressive strength was reduced significantly and did not meet the compressive strength, 21 MPa (3000 psi), the minimum required for bridge deck overlay.

Figure 3-4 Typical conductive concrete mix

Figure 3-5 Surface finishability of conductive concrete

3.5.2.1.2 Small Slab Heating Experiments

A number of slabs, 305mm x 305mm x 51mm (1 ft × 1 ft × 2 in.), were used to determine the energy consumption and the associated temperature distributions in slab heating experiments. As shown in Fig. 3-6, steel plates were cast in the slab for electrodes. Fig. 3-7 shows a specimen under testing. Initially slab heating tests were conducted at 23°C (74°F) or

room temperature. Two thermocouples were installed in each slab to measure the mid-depth and surface temperature, and both were located at the center of the slab. The experimental results from six slabs showed that the temperature at the mid-depth of the slabs increased at a rate of approximately 0.56°C/min. (1°F/min.) with 35 volts. The current going through the conductive concrete varied from about 0.2 A to 5 A. Figs. 3-8(a)-(c) show the changes in the core and surface temperature of the 305mm x 305mm x 51mm (1 ft × 1 ft × 2 in.) slabs with time for different ratios of conductive material. Some of the slabs were placed in a refrigerator before testing, and the results showed a consistent heating rate with different initial temperatures. Conductive materials (i.e., steel fibers and shavings) from different sources were used for the slabs, and the heating characteristics were consistent. The power input was variable because there was no constant power control on the power supply. Average power of 516 W/m^2 (48W/ft^2) was consumed by the conductive concrete to raise the slab temperature from -1.1^{o}C (30^{o}F) to 15.6^{o}C (60^{o}F) in 30 minutes. This power level is consistent with the successful deicing applications using electrical heating cited in the literature[38,86].

The following guidelines may be drawn from the first-stage test results:

1. Use steel shavings of 20 percent per volume of conductive concrete as an upper bound; poor workability and surface finishability will result if higher volumetric ratios are used. In addition, using higher ratios of steel shavings requires an increase in w/c ratio to improve workability which consequently reduces the compressive strength of the mix.
2. Use steel fibers of 1.5 percent per volume of conductive concrete as an upper bound; higher ratios will make mixing difficult and produce poor surface finish.

Figure 3-6 Steel plates are used for electrodes

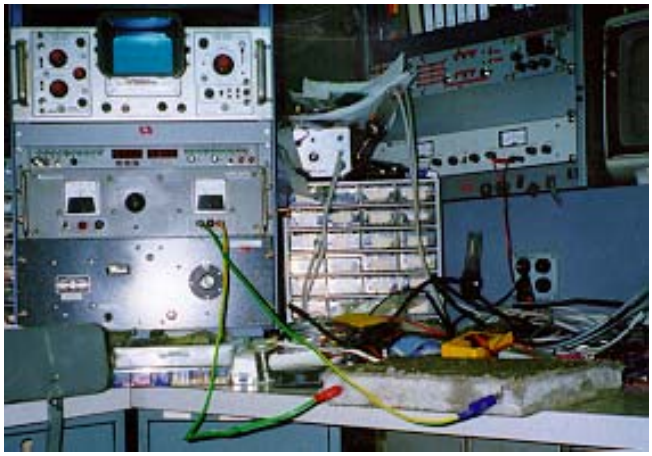

Figure 3-7 Small conductive concrete slab heating test

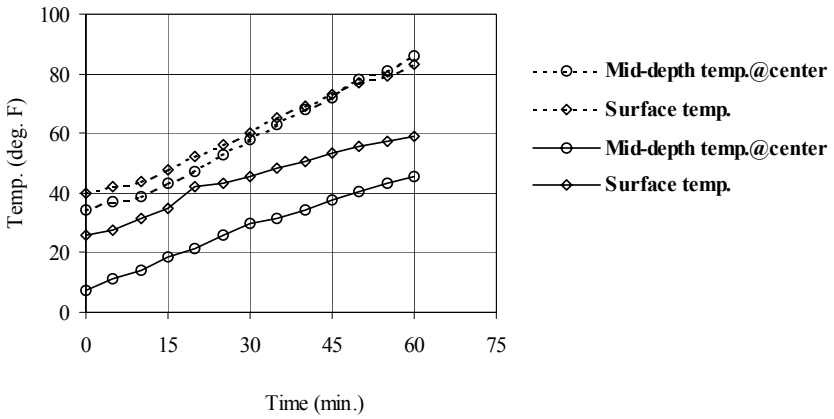

(a) Temperature time history

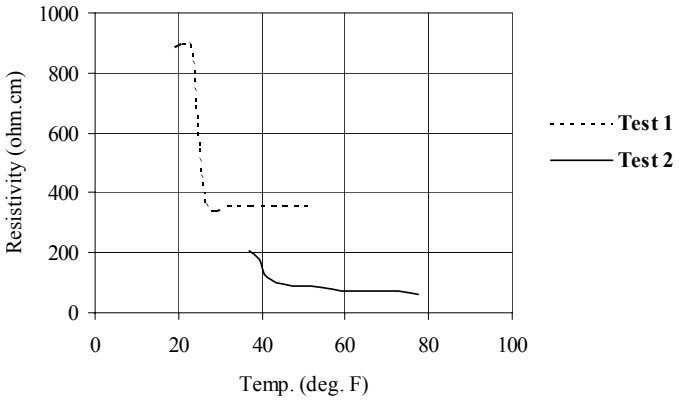

(b) Change of slab resistance with slab temperature

Figure 3-8 (a) Slab heating test - 20% conductive material

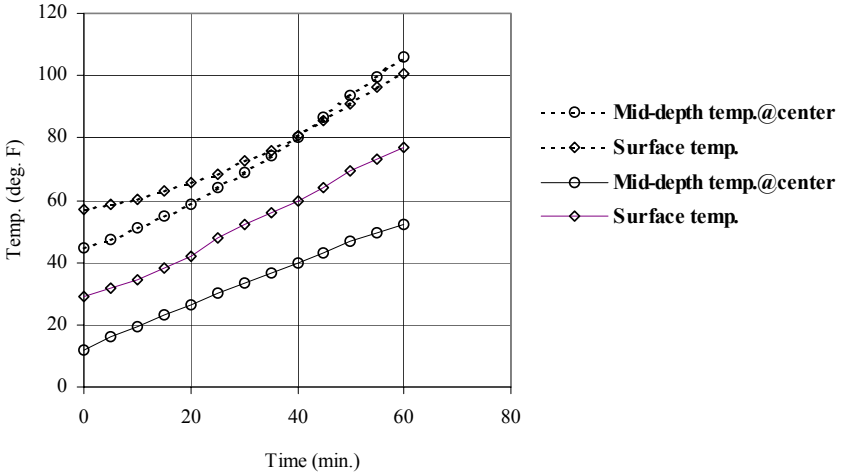

(a) Temperature time history

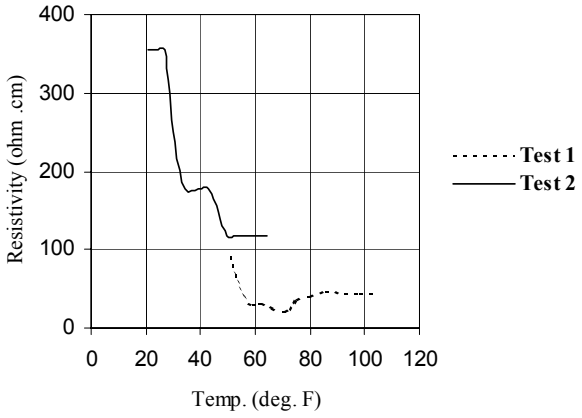

(b) Change of slab resistance with slab temperature

Figure 3-8(b) Slab heating test - 15 % conductive material

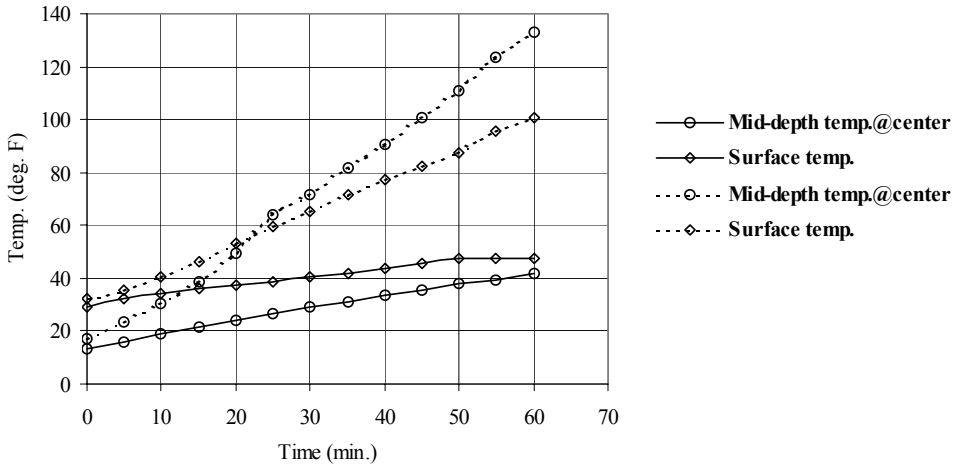

(a) Temperature time history

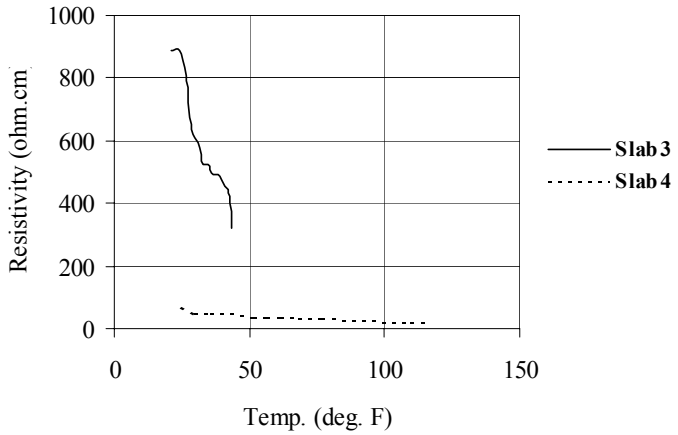

(b) Change of slab resistance with slab temperature

Figure 3-8(c) Slab heating test - 15 % conductive material

3.5.2.2 Second-Stage Evaluation

The conductive concrete mix design was further investigated based on the first-stage results. Steel shavings of 10, 15 and 20 percent was used with 1.5 percent of steel fibers per volume of conductive concrete, respectively. Over 25 batches of conductive concrete were prepared. Fig. 3-9 shows some of the conductive concrete test specimens prepared for the second evaluation stage.

Figure 3-9 Conductive concrete test specimens
Category 3 (stage two evaluation)

From each batch, three 152mm x 305mm (6 in. x 12 in.) cylinders were tested for compressive strength, and two beams of 533mm x 152mm x 152mm (6 in. x 6 in. x 21 in.) were tested to determine the flexural strength. Two slabs of 305mm x 305mm x 51mm (1 ft × 1 ft × 2 in.) were used to determine the required power to heat the slabs and the associated temperature distributions.

3.5.2.2.1 Mechanical Properties

The compressive strength and the modulus of rupture were determined for each batch, and the average strength after 28 days are given in Table 3-6.

Table 3-6. Compressive strength and modulus of rupture- Category 3

Steel shavings* by volume	Compressive strength MPa (psi)	Modulus of rupture MPa (psi)
10%	43 (6272)	5.8 (851)
15%	46.5 (6741)	6.7 (976)
20%	35 (5044)	6.4 (923)

*All mixes contained 1.5 percent steel fibers by volume.

To compensate for the increase of surface area with higher ratios of steel shavings, the w/c ratio was increased to maintain workability. As a result, the compressive strength decreases with the increase of steel shavings. However, the compressive strength is in the range of 35 to 42 MPa (5000 to 6000 psi), adequate for overlay construction.

Two beams were tested for flexural strength of the conductive concrete with center-point loading. The modulus of rupture of the conductive concrete is about 1.5 to 2 times that of the conventional concrete ($7.5\sqrt{f_c'}$). This increase was probably due to the use of steel fibers.

3.5.2.2.2 Effect Of Hydration Time on Electrical Conductivity

The electrical conductivity of a concrete mix changes with hydration time due to variation of the moisture content. The moisture inside a mix improves electrical conductivity. To determine the change of electrical conductivity of a conductive concrete mix with hydration time, electric resistivity was calculated from the voltage and current data recorded

during the slab heating tests. The electric resistivity, ρ, can be calculated from the electrical resistance, ***R***, of the slab:

$$R = \rho \frac{L}{A} \quad \text{----------(3-1)}$$

where ***R*** is determined from the applied voltage and the associated current, ***L*** is the electrode spacing, and ***A*** is the cross-sectional area of the slab parallel to the electrodes. Electrical conductivity is the reciprocal of electric resistivity, which is a material constant. Table 3-7 shows the hydration effect on the electric resistivity of conductive concrete mixes with 10, 15, and 20 percent of steel shavings and 1.5 percent of steel fibers.

Table 3-7. Effect of hydration time on electric resistivity

	10% steel shaving	**15% steel shaving**	**20% steel shaving**
Test date	**Average resistivity (Ω.cm)**	**Average resistivity (Ω.cm)**	**Average resistivity (Ω.cm)**
10–day	148.50	39.08	6.66
20–day	177.15	40.16	6.89
30-day	211.58	48.19	7.64
30-day + 2 days in freezer	341.25	62.10	10.91

Notes :
(1) 1.5 % steel fiber was used in all mixes.
(2) All tests were conducted at room temperature 23°C (74°F).

The electric resistivity steadily increases during hydration. However, the electric resistivity of a mix would stabilize and eventually approach a constant value as the hydration process diminishes. The long-term electric resistivity values of the mixes are given in Table 3-8.

Table 3-8. Long-term evaluation of the electric resistivity

Steel shavings by volume	Electric resistivity (Ω.cm)	
	After 6 months	After 1 year
10%	6200	7300
15%	740	860
20%	350	410

Notes :
(1) 1.5 % steel fiber was used in all mixes.
(2) All tests were conducted inside a freezer at temperature 0°C (32°F).

3.5.2.2.3 Slab Heating Tests

Two slabs of 305mm x 305mm x 51mm (1 ft × 1 ft × 2 in.) from each trial mix were tested using 35 volts of DC power, and the corresponding current was recorded. Fig. 3-10 shows a slab under testing using DC power. Fig. 3-11(a) shows the slab heating rate for different steel shavings ratios, and Fig. 3-11(b) shows the change in electric resistivity with slab temperature. The average power consumption and heating rates for the conductive concrete mixes with 15 to 20 percent steel shavings and 1.5 percent steel fibers were consistent with those obtained from the first-stage tests.

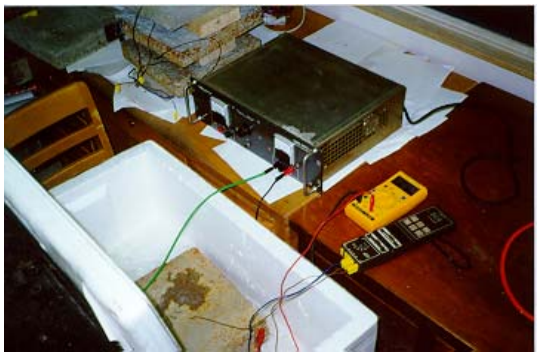

Figure 3-10 Slab under testing using DC-power

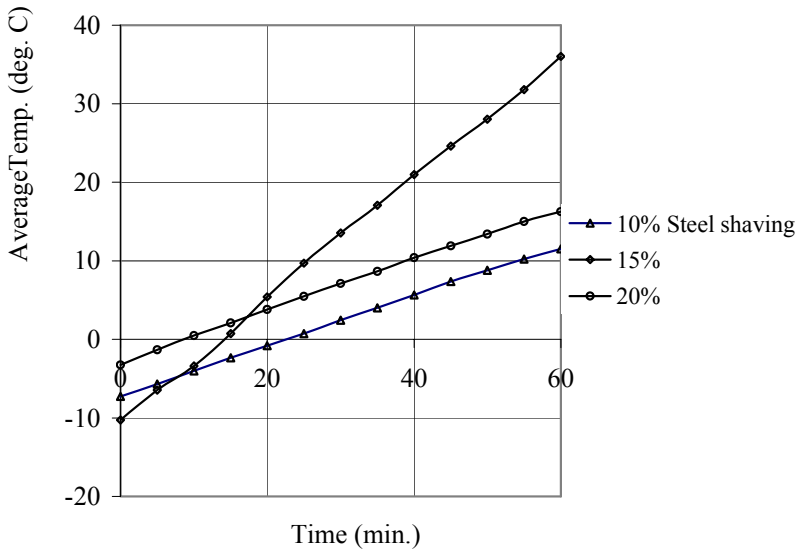

(a) Temperature time history

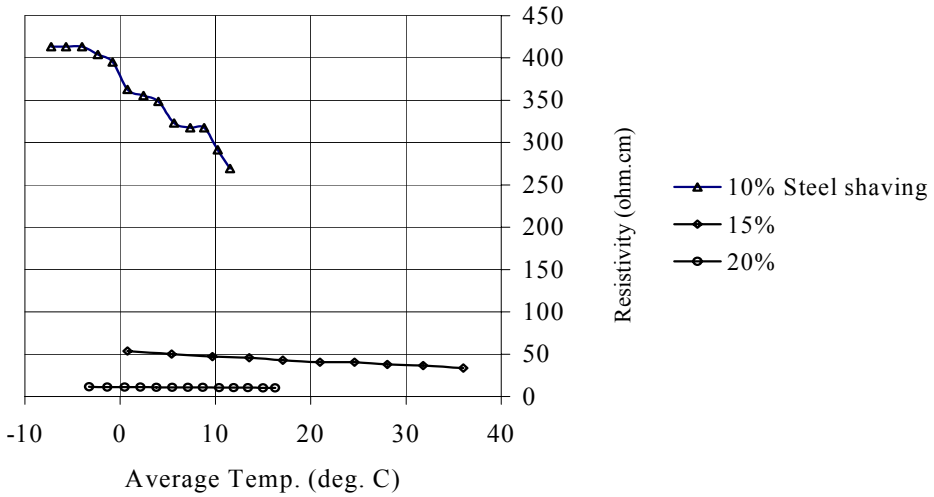

(b) Change of electric resistivity with slab temperature

Figure 3-11 Slab heating tests

3.5.2.2.4 Conduction of Electricity through Conductive Concrete

Several tests were conducted using AC and DC power to study the conduction of electricity through the conductive concrete mix developed at the University of Nebraska. A model[30,39] commonly used to describe the behavior of a semi-conductor or a diode, shown in Fig. 3-12, is also applicable to conductive concrete. The movement of electrons is presumed to flow through a resistor in parallel with a variable resistor and a capacitor. Conduction of electricity through conductive concrete, as depicted in Fig. 3-13, may be divided into three zones: (1) linear, (2) operational, and (3) saturation. In the linear zone, the relation between the applied voltage and the current going through the mix is linear. The electric charges accumulate in the capacitor, and the heating rate is minimal. In the operational zone, a nonlinear relation exists between the applied voltage and the associated current. There is more current flow through the conductive concrete and the heating rate increases. In the saturation zone, the applied voltage is high enough to break down the capacitor. The current going through the conductive concrete rapidly increases like a short circuit. For efficient heating operation using conductive concrete, the break down point of the capacitor must be determined first, and the applied voltage may be reduced to the operational zone. The heating rate of the conductive concrete can then be controlled by maintaining the voltage and current within the operational range. With a validated model to describe the electric heating characteristics of the conductive concrete mix, the optimum electrode spacing can be determined for a specified bridge deck overlay thickness.

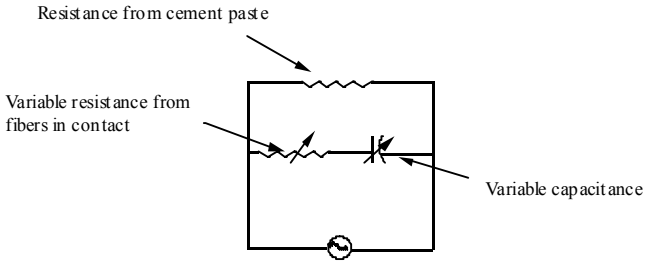

Figure. 3-12 A model for conduction of electricity through conductive concrete

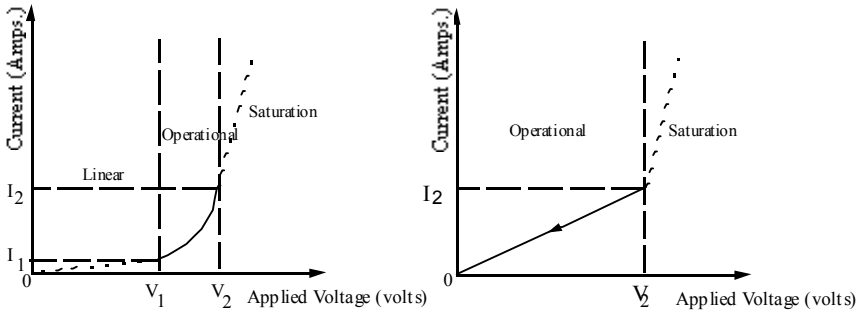

(a) Starting from zero to saturation

(b) Starting from saturation - Voltage can be reduced to control heating rate

*V_1 and I_1 values are temperature dependent

Slab	Electrode spacing (in)	Steel* Shaving %	V_2	I_2
30cm x 30cm x 5cm (1ft x 1ft x 2 in.)	12	15	110	>10
		20	98	>10
91cm x 61cm x 9cm (2ft x 3ft x 3.5 in.)	24	20	196	>10

* 1.5% steel fibers were used in all mixes

Figure 3-13 Conduction of electricity through conductive concrete - model parameters

3.5.2.2.5 Slab Heating Rate Comparison - AC vs. DC Power

The optimization in the second stage included comparison of slab deicing performance between use of direct current (DC) and alternate current (AC) power. Three specimens with 10, 15, and 20 percent of steel shaving with 1.5 percent of steel fibers, respectively, were tested with the same initial temperature using 76 volts of DC and AC power. These tests were conducted while the slabs were placed inside a freezer at a temperature of 0°C (32°F).

The "breakdown" voltage of each slab was applied first, and the tests were continued by reducing voltage to the operational range. Fig. 3-14 shows the heating characteristics of the 15 and 20-percent slabs in terms of energy consumption.

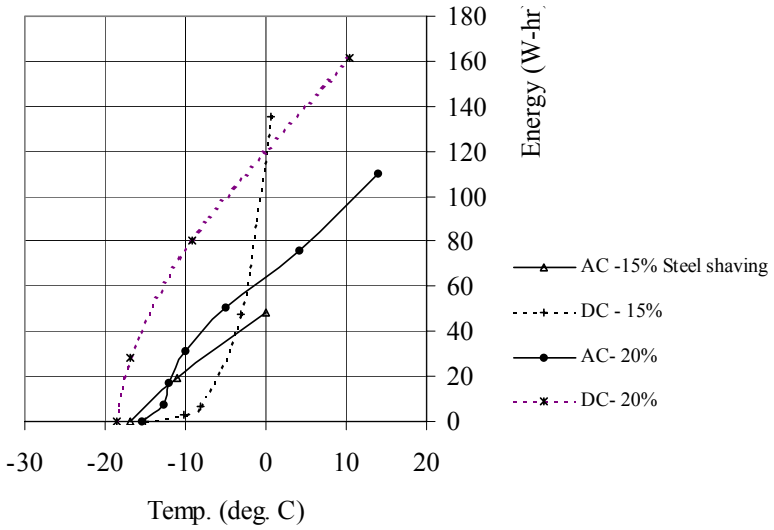

Figure 3-14 Power consumption – AC vs. DC

The following was observed during the slab heating tests:

(1) Once the DC has established a path through a slab, the current will go through the same path and it is likely to create "hot spots" in the slab;

(2) Due to the sinusoidal variation of the AC voltage, the current going through the slab takes a different path every cycle, which minimizes the possibility of creating hot spots. In other words, heating using AC power will be more uniform than using DC power; and

(3) Using AC power, as shown in Fig. 3-14, is more energy-efficient than using DC power for the same temperature rise in the slab.

3.5.2.2.6 Size Effect

The heating performance using AC power of two slabs, 91cm x 61cm x 9cm (3 ft x 2 ft x 3.5 in.) and 30cm x 30cm x 5cm (1 ft x 1 ft x 2 in.), was compared for size effect. Figs. 3-15(a) and (b) show part of the specimens used in the study. These slabs were cast with 20 percent of steel shaving and 1.5 percent of steel fibers. The "breakdown" voltage required for an electrode spacing of 61cm (2 ft) is twice that for 30cm (1 ft). The slab heating rate depends upon the amount of current going through, which is inversely proportional to the cross-sectional area of the slab parallel to the electrodes. Once the break-down point is reached, the applied voltage can be varied to control the current, which, in turn, controls the heating rate.

Figure 3-15(a) 1 ft x 1ft x 2 in. slabs

Figure 3-15(b) 3 ft x 2ft x 3.5 in. slabs

3.5.2.2.7 Evaluation of the Electric Resistivity

The electric resistivity of each batch was back calculated from the slab heating tests using Eq.(3-1), where the electrical resistance of the slab was determined from the applied voltage and the associated current recorded during the tests. The resistivity value thus obtained was consistent from all the batches. The electric resistivity was higher at a lower temperature under a constant voltage. This phenomenon was also reported by Whittington et al.[79] The electric resistivity for different volumetric ratios of conductive materials are given in Tables 3-5, 3-7, and 3-8.

3.5.3 Problems and Solutions

Two problems were encountered during the optimization process. First, a secured bond between the electrodes and conductive concrete is necessary to provide good conductivity. As a result, inconsistent results were obtained from slabs prepared from the

same mix in the heating tests. Some of these slabs were cut to expose the steel plates. A smooth interface was found between the concrete surface and the steel plate, indicating that the bond between the two surfaces was poor, as shown in Fig. 3-16.

Conductive adhesives were used by Whittington et al.[79] and Xie et al.[80] to ensure good conductivity between the electrodes and the specimens. However, using conductive adhesive is not cost-effective for field application. Several approaches to improving the bond between the electrodes and conductive concrete were studied. The best solution is to have perforated steel plates or have gaps between steel plates greater or equal to the maximum aggregate size to allow concrete to flow through to ensure a good bond. Perforated steel plates were used for electrodes in the slab heating tests, and excellent electrical conductivity was obtained. Figs. 3-17(a)-(c) show several electrode designs with good electrical conductivity.

Figure 3-16 Smooth surface between the steel plate and concrete surface

The second problem was to provide a thin thermal insulation layer between the conductive concrete overlay and the concrete bridge deck to minimize heat loss. Epoxy coating and mortar were used, but the insulation was not as good as expected. Sawdust mortar[59] consisting of equal parts of portland cement, sand, and sawdust by volume, has been identified to be a good thermal insulator. Fig. 3-18 shows a specimen with sawdust layer cast before the conductive concrete layer. Furthermore, it is very cost-effective to utilize the sawdust, which is an industrial waste.

Figure 3-17(a) Steel plate with opening

Figure 3-17(b) 1 in. steel plate welded on WWF with 0.5 in. spacing

Figure 3-17(c) 3/4 in. corrugated steel plate welded on steel posts with 1.25 in. spacing

Figure 3-18 Sawdust layer was used as insulation layer

The following conclusions were drawn from the optimization process:

1. The required electrical conductivity and mechanical strength of a bridge deck overlay for deicing can be achieved by using 15-20 percent of steel shaving and 1.5 percent of steel fibers per volume of conductive concrete.
2. The workability and surface finishability of the conductive concrete mix developed at the University of Nebraska are excellent and comparable to those of regular concrete.
3. The heating rate of the slabs using AC and DC power was similar. However, AC power is preferred since the heating is more uniform than using DC power.

4. Using a thermal insulation layer underneath a conductive concrete overlay will reduce the energy consumption in deicing and anti-icing operations.
5. Once the electric resistivity of a mix is determined, the optimum electrode spacing can be determined for a bridge deck overlay for minimum power consumption.
6. Perforated steel plates should be used for electrodes to provide good electric conductivity across the interface with conductive concrete.

CHAPTER 4

EVALUATION OF MECHANICAL AND PHYSICAL PROPERTIES OF THE CONDUCTIVE CONCRETE MIX

4.1 Background

In the first stage of the experimental program, the volumetric ratios of the trial batches of conductive concrete were optimized. The objectives of the second stage of the experimental program were to evaluate:

1. The mechanical and physical properties of the optimized mix, and
2. The deicing performance of a conductive concrete overlay in natural environment.

The mix design containing 20% steel shavings and 1.5% steel fibers per volume from the optimization process has been tested extensively to evaluate its mechanical and physical properties. Material testing was conducted in accordance with the ASTM[9] and AASHTO[2] specifications. The compressive strength, flexural strength, rapid freeze-thaw resistance, permeability, shrinkage and thermal conductivity of the mix have been determined. Conductive concrete overlay from the same mix was also cast on the top of two concrete slabs to be tested in a natural environment for deicing and power consumption evaluation.

In this chapter, descriptions of materials testing, test specifications, test specimens, the number of specimens tested in each category, and the test date since casting are presented. The test results also are summarized.

4.2 Specimen Fabrication

The specimens were prepared following the ASTM[9] and AASHTO[2] specifications. The specimens were cast using the same mix used for the overlay. After casting, the specimen were cured in curing tank until the testing dates, recommended by the specifications, as shown in Fig. 4-1. Descriptions of materials testing, test specifications, test specimens, the number of specimens tested in each category, and the test date since casting are presented in Table 4-1.

Figure 4-1 Specimens in curing tank

Table 4-1 Summary of material testing

Test	Test Specifications	Specimen Size	**No. of specimens per test**	**Test date since casting**
Compressive strength	ASTM C 39-86 AASHTO T 22-92	Cylinder 152mm x 305mm (6" x 12")	3	7, 14, 28, 56 and 90 days
Stress-Strain relation	ASTM C 469-94	Cylinder 152mmx305mm (6" x 12")	3	28, 56, and 90 days
Modulus of elasticity	ASTM C 469-94	Cylinder 152mm x 305mm (6" x 12")	3	28, 56, 90, and 180 days
Flexural Strength	ASTM C 293-79 ASHTO T 177-81	Beam 762mmx152mmx140mm (30" x 6" x 5.5")	3	7, 14, 28, 56 and 90 days
Rapid freeze and thaw resistance	ASTM C 666-92 /AASHTO T 161-93 Procedure "A" – Freezing and thawing in water	Prism 406mm x 89mm x 76mm (16" x 3.5" x 3")	17	Starts after 14 days
Shrinkage	Refer to Sec. 4.3.5	Prism 102mm x 102mm x 610mm (4" x 4" x 24")	12	10, 28, 56, 90, and 180 days
Permeability	Refer to Sec. 4.4.1	102 mm x 25 mm (4 in. diameter and 1 in. thick)	3 conductive concrete specimens	Starts after 6 months
Thermal conductivity	Refer to Sec. 4.4.2	Cylinder 102mm x 203mm (4" x 8")	6	Starts after 6 months

4.3 Mechanical Properties

Testing of mechanical properties of the mix included: compressive strength, flexural strength, freeze and thaw resistance and shrinkage.

4.3.1 Compressive Strength

The tests were conducted using a 400-kip Forney compression machine as shown in Fig. 4-2.

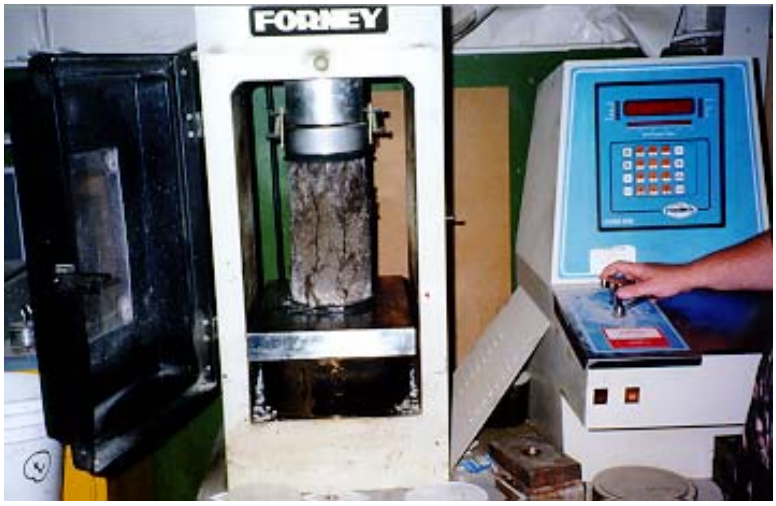

Figure 4-2 400-kip compression testing machine

The change of the compressive strength for 90 days since casting is shown in Fig. 4-3. After 28 days, the compressive strength reached a value of 31 MPa (4500 psi). The specimens showed ductile behavior due to the steel fiber. The same behavior was reported by Fanella et. al[28] for fiber reinforced concrete in compression. Typical failure mode is shown in Fig. 4-4.

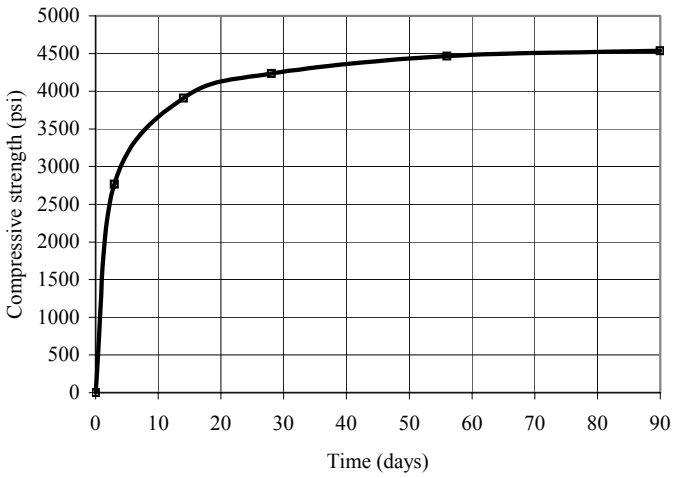

Figure 4-3 Compressive strength with time

Figure 4-4 Typical failure mode of concrete in compression

4.3.2 Stress-Strain relation and modulus of elasticity

4.3.2.1 Stress-Strain Relation

A 400-kip Forney compression machine was used in the test, and a compressometer was used to monitor the deformation of each specimen, as shown in Fig. 4-5.

Figure 4-5 Test setup for stress-strain relationship

ASTM C 469-94 recommendations for preparing the test specimen and loading rates were followed. The compressive strength was determined before testing to determine the rate of loading. The loading rate was controlled by the deformation of the specimen. The load was applied and the corresponding strain value was recorded until the load reached 60-70% of the ultimate load. Fig. 4-6 shows stress-strain curves obtained from the compression tests conducted on the 28^{th} day after casting.

4.3.2.2 Modulus of Elasticity

Three methods may be used to calculate the modulus of elasticity of concrete: (1) tangent modulus, (2) secant modulus, and (3) chord modulus. Tangent modulus can be

obtained by the slope of a line drawn tangent to the stress-strain curve at any point on the curve. Secant modulus represents slope of a line drawn between the origin and a point in the curve corresponding to 40% of the ultimate stress at failure load. Chord modulus is given by the slope of a line drawn between a point in the curve corresponding to 50 micro-strains and a point in the curve corresponding to 40% of the ultimate stress at failure load. The modulus of elasticity of the conductive concrete was calculated using all three methods, as shown in Fig. 4-7. The moduli of elasticity of the conductive concrete are compared against the predicated value by using the ACI equation for the same compressive strength in Table 4-2. The reduced modulus was probably due to portions of the fine and coarse aggregates were replaced by steel fibers and shavings, which added ductility to the concrete mix. This same behavior was reported by Fanella et. al.[28] for fiber reinforced concrete in compression.

Table 4-2 Modulus of elasticity of conductive concrete

Modulus of elasticity	**Conductive concrete**	**ACI Equation**
Tangent modulus	7.14×10^5	$E = w_c^{1.5}\, x\, 33\sqrt{f_c^{`}} = 3.8x\, 10^6$ psi
Secant modulus	5.27×10^5	
Chord modulus	4.95×10^5	

w_c unit weight for conductive concrete = 144 lb/ft^3

$f_c^{`}$ compressive strength = 4500 psi

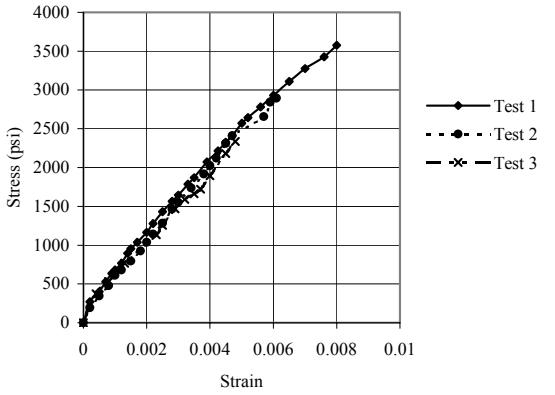

Figure 4-6 Stress strain relations of conductive concrete

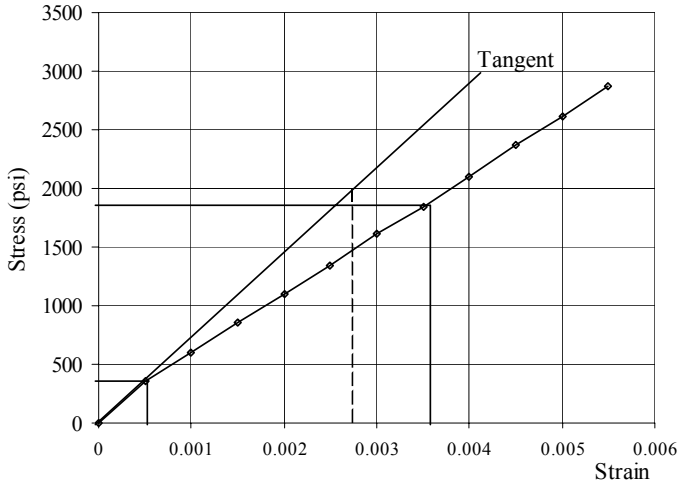

Figure 4-7 Modulus of elasticity of conductive concrete

4.3.3 Flexural Strength

A Tinius Olsen Universal testing machine with a maximum load capacity of 120 kips (534 kN) was used to test the specimens in two different setups. The first setup was a single point load and the second a two point-loads with 9-in. spacing. Fig. 4-8 shows test setup with single point load.

Figure 4-8 Flexural strength – test setup

The modulus of rupture of the conductive concrete was about 1.5 times that of conventional concrete having the same compressive strength, as shown in Fig. 4-9. This increase in the

modulus of rupture was probably due to the use of steel fibers, this finding is consistent with other experimental results cited in the literature[8,14,56,70,69].

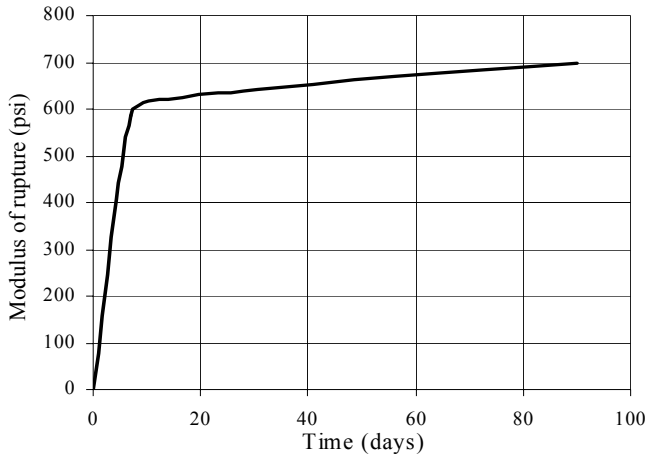

Figure 4-9 Flexural strength with time
[using simple beam with center-point loading]
(ASTM C293-79 – AASHTO T 177-81)

4.3.4 Rapid Freeze and Thaw Resistance

The Procedure A of ASTM C 666-92[9] or the AASHTO T 161-93[2] Specification was followed for rapid freeze-thaw resistance testing. Procedure A requires that specimens must freeze and thaw in water. Specimens were cured for 14 days after that test started. Fig. 4-10 shows freeze and thaw testing equipment. Freezing and thawing cycles were maintained in temperature range from 4.4 to –17.8°C (40 to 0°F). This temperature range was reached in a period of 2-3 hours. The transverse frequency (dynamic frequency), mass, average length and cross-section dimensions of the concrete specimen were taken at temperature range –1.1°C to +2.2°C (30°F to 36°F). After the initial readings, the measurements were taken at intervals

less than 36 cycles. Specimens were placed in a styrofoam box and covered with ice while taking measurements to maintain temperature of the specimens in the range of –1.1°C to +2.2°C (30°F to 36°F), as shown in Fig. 4-11. Table 4-3 summarizes the test results. The tests were stopped after 312 rapid freeze-and-thaw cycles, and none of the specimens failed. The reduction of dynamic modulus of elasticity was in the range of 6-15 percent. This excellent performance illustrates that the steel fibers helped in resisting the internal stresses induced by the contraction and expansion due to freeze and thaw action. Fig. 4-12 shows the specimens before and after testing.

Table 4.3 Resistance of concrete to rapid freezing and thawing

ASTM C 666-92 -AASHTO (T161-93)

No. of specimens	17
No. of cycles	312
No. of failed specimens	NONE
% Change in dynamic modulus of elasticity	6-15%

Figure 4-10 Freeze and thaw testing equipment

Figure 4-11 Freeze and thaw specimens during taking measurements

Figure 4-12 Freeze and thaw specimens – before and after 312 cycles

4.3.5 Shrinkage

The main objective of this test was to determine the drying shrinkage of the conductive concrete specimens. Drying shrinkage is the withdrawal of water from concrete stored in unsaturated air. Demac points, spaced at about 20cm (8 in.), were attached along the length on two opposing faces of each specimen, as shown in Fig. 4-13. Precise distances between Demac points were measured using a dial gage, as shown in Fig. 4-14. Specimens were cured for 10 days and stored at room temperature afterwards. Initial readings were taken after mounting the Demac points, and after that readings were taken every 7 to 10 days for a minimum duration of 6 months to monitor the shrinkage. Shrinkage strains were calculated from the Demac readings. Typical average shrinkage strain is compared against the ACI 209[5] predictive equation in Fig. 4-15. Shrinkage strains from the conductive concrete specimens were less than those predicted by the ACI 209[5] equation by about 25 to 30 percent. This reduction was probably due to the steel fibers, which restricted the shrinkage.

Figure 4-13 Specimens for shrinkage test

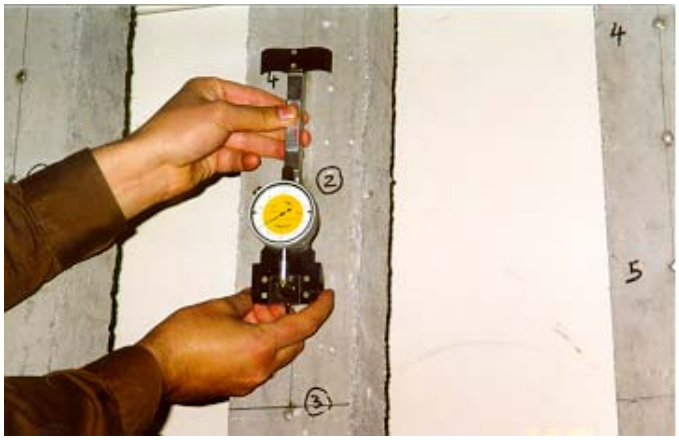

Figure 4-14 Shrinkage strain measurements

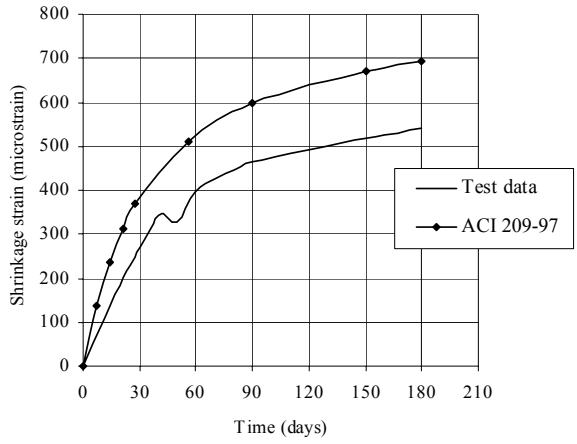

Figure 4-15 Shrinkage strain vs ACI 209-97 predicted strain

4.4 Physical Properties

The physical properties of the conductive concrete tested were permeability and thermal conductivity.

4.4.1 Permeability

The procedure described herein is not a standard permeability test. However, the teat has been used for permeability evaluation of polymer concrete and concrete rehabilitated with polymer flood coating[23,71]. Six specimens, 25.4 mm x 101.6 mm (4-in. diameter and 1 in. thick), were used for each test, as shown in Fig. 4-16. Three specimens were from the conductive concrete mix and three specimens were from conventional concrete mix. The conventional concrete specimens were used for comparison.

Figure 4-16 One-inch thick specimens for permeability test

A temperature-controlled box, dessicators, and a computer for temperature control were used in the test, as shown in Fig. 4-17. A steady-state water flow through the concrete specimen under gravity was measured, and the weight loss per unit time of each specimen was recorded. As shown in Fig. 14-18, high vacuum grease was used to seal around a small plate containing water on top of the specimen to provide 100 percent humidity. Initial weight readings were taken and specimens were individually placed inside a moisture-free dessicator (using desiccant) in a temperature-controlled box, as shown in Fig. 14-19. The temperature inside the box was in the range of 24-26°C (75-79°F). The weight readings of the specimens were

taken at 24-hour intervals for 10 days. Two groups of specimens were prepared for the test one group was prepared in unsaturated air and the other group in saturated surface dry (SSD) condition.

The weight of each specimen was plotted versus time and curve-fitted to determine a linear trend. The rate of permeability through the 2.54-cm (1-in.) thick specimens was determined by the slope of the line. Figs. 4-20(a) and (b) show the permeability test results, and the permeability rates of the conductive concrete are compared against those of conventional concrete in Table 4-4. The permeability of the conductive concrete was comparable to that of a high-strength concrete.

Table 4-4. Summary of the permeability tests

Specimen type	**Permeability Rate (cm^3/sec)**	
	Conductive concrete	**Conventional concrete**
Stored in unsaturated air	0.0034	0.0033
Saturated surface dry	0.0068	0.0079

Figure 4-17 Temperature-controlled box for permeability test

Figure 4-18 Permeability test specimen preparation

Figure 4-19 Specimens inside moisture-free desiccators

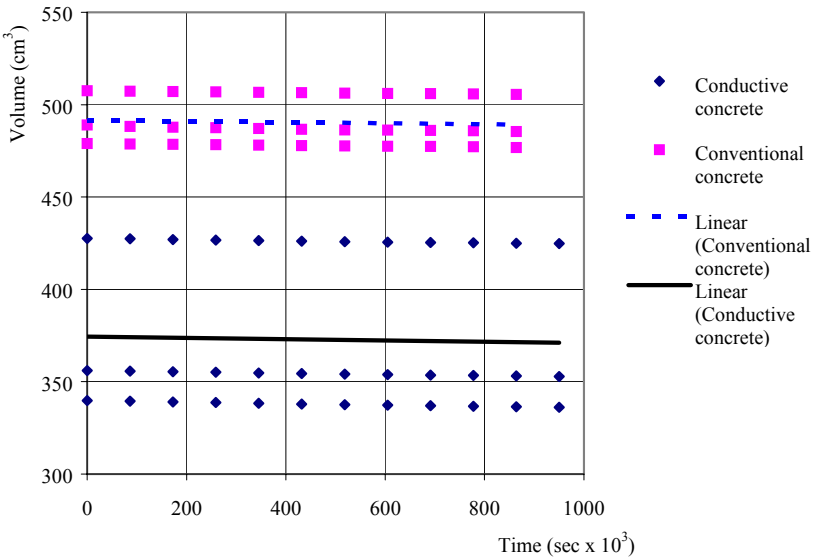

Figure 4-20(a) Specimen stored in unsaturated air

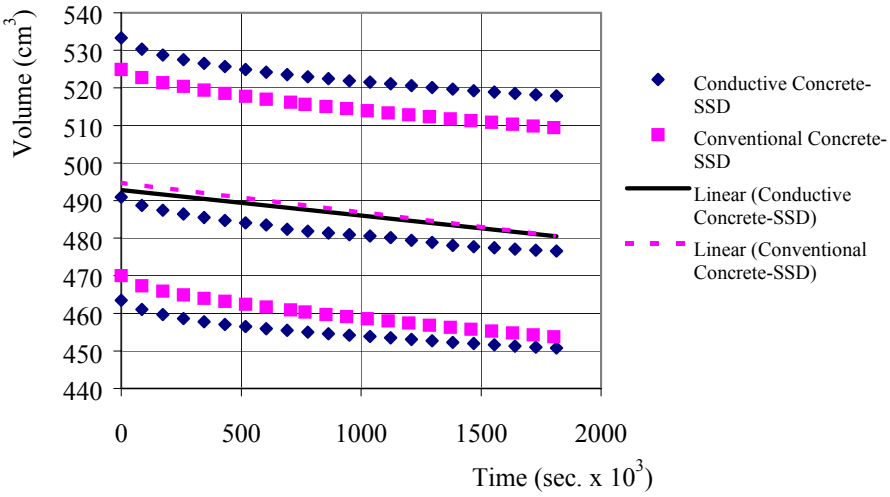

Figure 4-20(b) Saturated surface dry specimens

4.4.2 Thermal Conductivity

4.4.2.1 Theoretical Approach

Conductive concrete may be considered as a "composite" whose constituents are steel fibers, steel shavings, and regular concrete. Based on the volume fraction of the steel fibers and shavings contained in the composite, expressions of "apparent" thermal properties of conductive concrete may be derived from those of the constituent materials[20].

Expressions may be derived for the "apparent" thermal conductivity of a conductive concrete mix based on the volume fraction of steel fibers and shavings added, and on the thermal conductivity of steel and concrete (κ_s = 47 W/m-^{o}K and κ_c = 0.87 W/m-^{o}K, respectively, evaluated at 0^{o}C). The optimized conductive concrete mix has 20 percent of steel fibers and shavings by volume. Assuming the two materials conduct heat "in parallel," an upper bound of the apparent thermal conductivity can be calculated as

$$\kappa^* = \kappa_s \times 0.2 + \kappa_c \times 0.80 = 10.1 \text{ W/m-}^o\text{K} \qquad (4\text{-}1)$$

4.4.2.1 Experimental Approach

A test procedure was developed for determining the thermal conductivity of the conductive concrete mix for a temperature range between –5 to 20^{o}C (23 to 68^{o}F). Six cylinders of 102mm x 203mm (4 in. x 8 in.) were prepared. A thermal insulation layer, using the sawdust mortar, was cast around each cylinder, as shown in Fig. 4-21(a). Two thermocouples 5cm (2-in.) apart, as shown in Fig. 4-21(b), were placed along the direction of the heat flow inside each cylinder. For each test, the specimen and the heat source were placed inside a Styrofoam box to minimize heat loss. The thermal conductivity tests were

conducted with the Styrofoam box in a freezer at a temperature of 0°C (32°F). Heat flux at the bottom of the specimen was controlled to reach a thermal equilibrium and the temperature in the specimen was monitored. A test was stopped when a constant temperature differential was observed between the two points inside the cylinders. Fig. 4-22 shows typical temperature distributions during a test. The thermal conductivity of the conductive concrete, κ_{cc}, was calculated as follows,

$$\frac{q}{A} = -\kappa_{cc} \frac{\Delta T}{\Delta x} \qquad (4\text{-}2)$$

where **q** is the heat transfer rate, 660 watts from a hot plate, **A** is area of hot plate, and ΔT and Δx are respectively the temperature differential and the distance (i.e., 5cm or 2 in.) between the two thermocouples. The thermal conductivity values computed from the test data are given in Table 4-5, with an average value of 13.5 W/m-°K. A 20 percent reduction of the thermal conductivity was applied to account for the heat loss. This percentage represents the ratio between the cross section area of the cylinder and that of the insulation layer. The thermal conductivity values from the two approaches are comparable and were used for a heat transfer analysis described in Chapter 5.

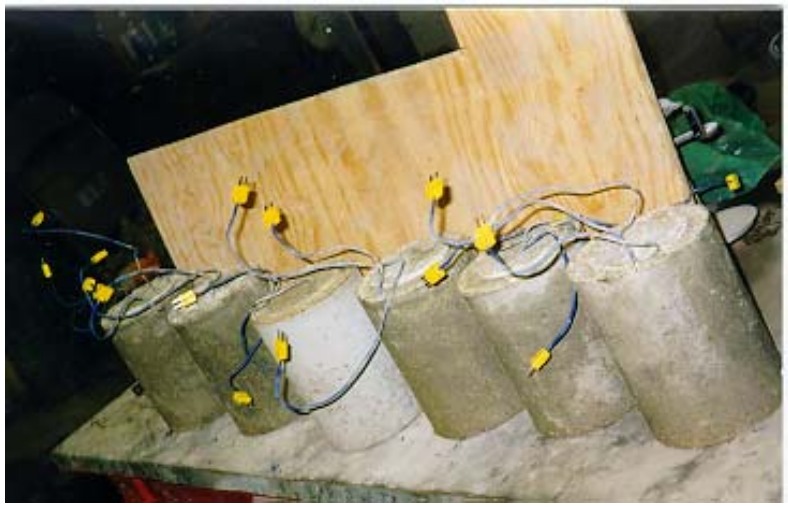

Figure 4-21(a) Cylinders with sawdust mortar insulation layer

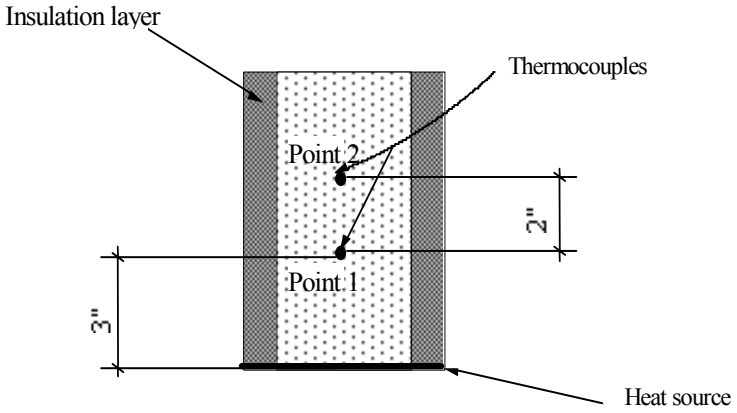

Fig. 4-21(b) Thermal conductivity test specimen

Table 4-5. Summary of the thermal conductivity tests

Specimen No.	Temp. Difference ΔT (°K)	Thermal conductivity (W/m-°K)
1	283.6	13.6
2	285.7	13.5
3	281.2	13.7
4	286.0	13.4
5	285.5	13.5
6	286.7	13.4
Average		13.5
With 20% heat loss		10.8

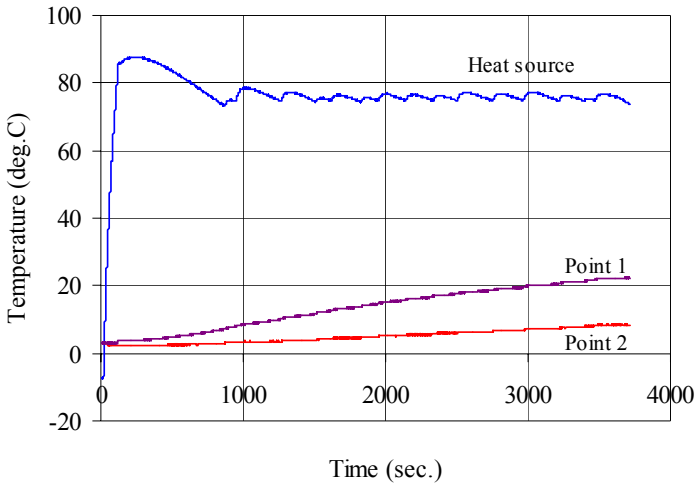

Figure 4-22 Typical temperature distribution during thermal conductivity tests

4.5 Test Results

Table 4-6 summarizes the test results of both mechanical and physical properties of the conductive concrete developed at the University of Nebraska.

Table 4-6 Mechanical and physical properties of the conductive concrete

Test	Result
Compressive strength	31 MPa (4500 psi)
Flexural strength	4.6 MPa (670 psi)
Rapid freeze and thaw resistance	None of the specimen failed after 312 cycles
Shrinkage	Less than that predicted by ACI-209 equation by 20-30%
Modulus of elasticity	3634 MPa (5.27×10^5 psi)
Permeability	Permeability rate was similar to that of high strength concrete
Thermal Conductivity	10.8 W/m-°K.

The mechanical and physical properties of the conductive concrete mix after 28 days have met the ASTM and AASHTO Specifications for bridge deck overlay construction.

CHAPTER 5

DEICING EXPERIMENTS WITH CONDUCTIVE CONCRETE OVERLAY

5.1 Introduction

The conductive concrete mix was optimized[84,85] and the mechanical and physical properties of the conductive concrete mix were evaluated[84] in accordance with the ASTM and AASHTO specifications. The compressive strength, flexural strength, rapid freeze and thaw resistance, permeability, and shrinkage of the conductive concrete mix after 28 days have met the AASHTO requirements for bridge deck overlays.

Two concrete slabs, 2m by 2m and 1.2m by 3.6m (7 ft x 7 ft and 4 ft x 12 ft), were constructed with a 9-cm (3.5 in.) thick conductive concrete overlay cast on top for conducting deicing experiments in the natural environment. The objectives of the experiments were to utilize the conductive concrete mix for an overlay application and to conduct deicing experiments for heating performance and power consumption evaluation.

The experiment setup, data acquisition and analysis, energy costs, detailed analyses of the temperature distributions in the overlays and the energy consumption during winter storms are presented in this Chapter.

5.2 Conductive Concrete Overlay Construction

5.2.1 The Concrete Slabs

Two 152-mm (6-in.) thick concrete slabs, one 2m by 2m (7 ft by 7 ft) and the other 1.2m by 3.6m (4 ft x 12 ft), were first constructed to simulate typical concrete bridge decks. An 89-mm (3.5-in.) thick overlay using the conductive concrete mix was cast on the top of

each slab. Fig.5-1(a) shows the preparation for the conventional concrete layer, and Fig.5-1(b) shows the conventional concrete layer after casting with surface roughened. Figs. 5-2(a) and (b) show the details of the two slabs.

Figure 5-1(a) Slabs ready for casting the conventional concrete layer

Figure 5-1(b) 6-in. conventional concrete layer

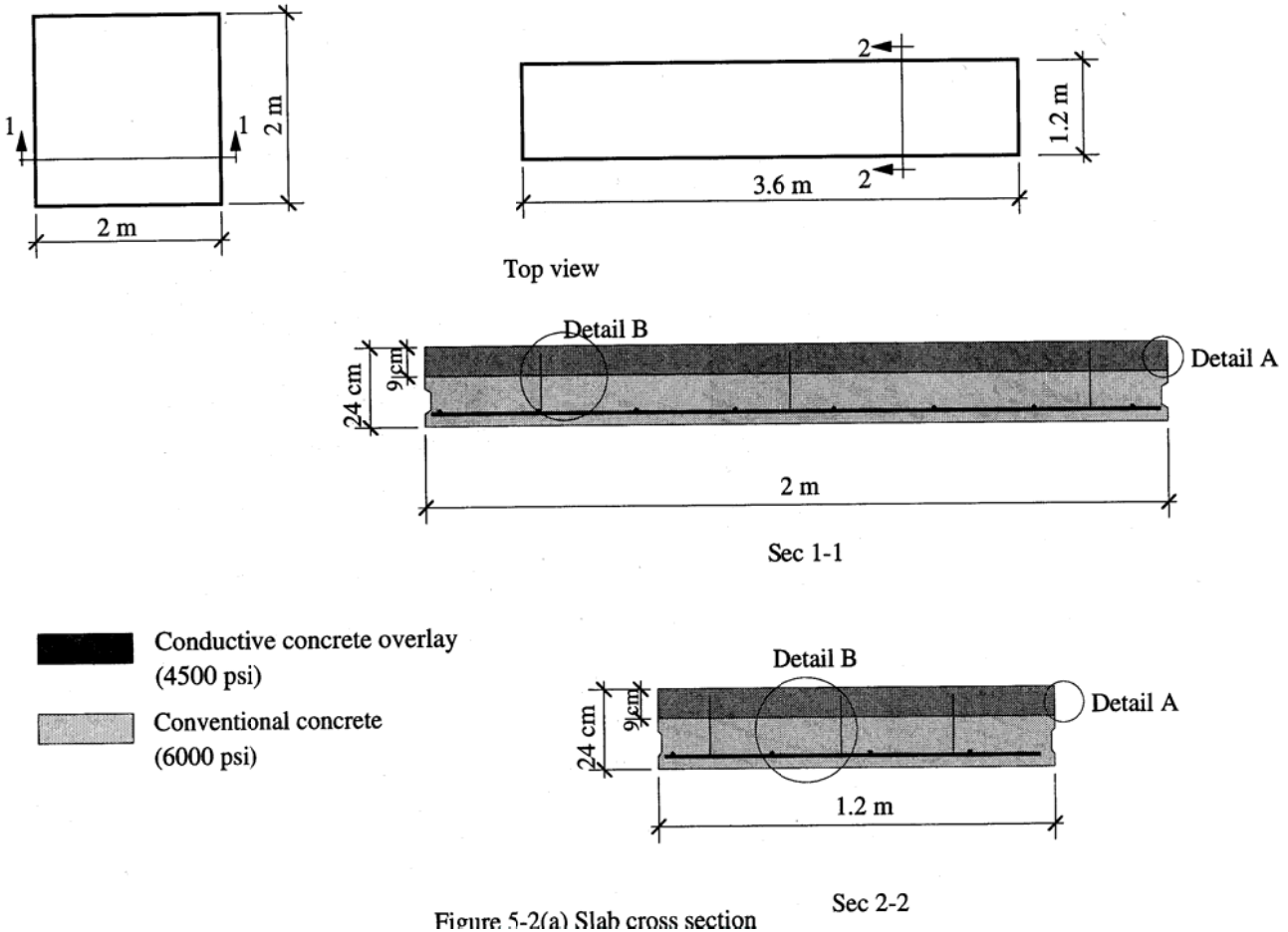

Figure 5-2(a) Slab cross section

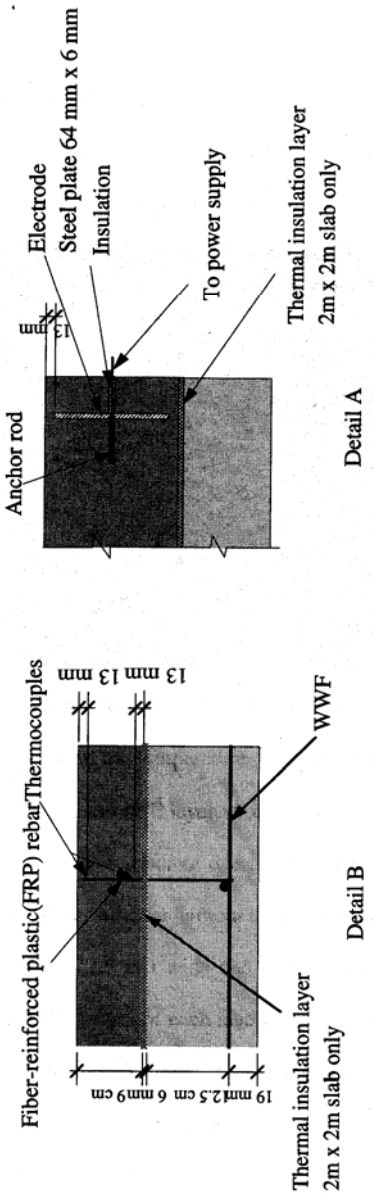

Figure 5-2(b) Thermocouples and steel plates in the overlay

As shown in Fig. 5-3, fiber-reinforced plastic (FRP) shear studs were used to resist horizontal forces between the concrete slab and the overlay. FRP shear studs were used to avoid short circuit of electricity during the deicing experiments.

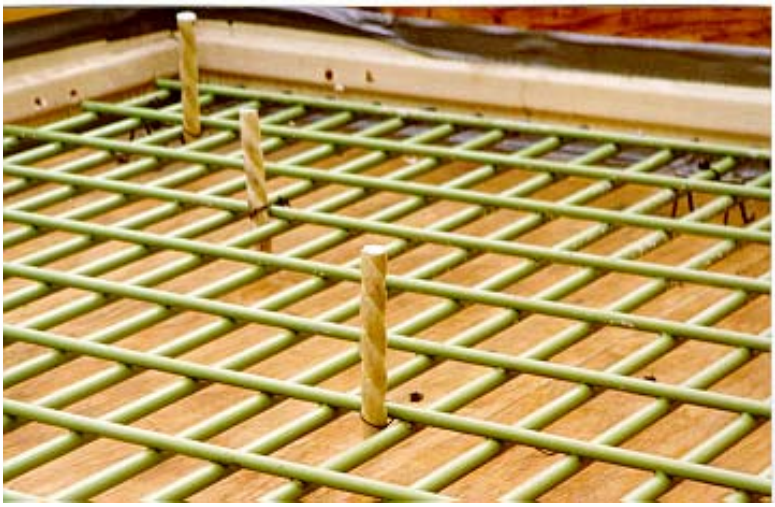

Figure 5-3 Fiber-reinforced plastic rebar used as shear studs

To investigate the effect on the temperature distribution and power consumption, a 6-mm (0.25-in.) thick sawdust mortar[59] layer was cast between the 2m by 2m (7 ft by 7 ft) concrete slab and the conductive concrete overlay for thermal insulation. The 1.2m by 3.6m (4 ft by 12 ft) slab was constructed without the thermal insulation for comparison.

Two steel plates, 64-mm (2.5 in.) wide and 6-mm (0.25 in.) thick, as shown in Fig.5-4, were installed along the length of each slab for electrodes. The steel plates had perforations greater than or equal to the 13-mm (0.5-in.) maximum aggregate size to allow concrete to flow through to provide good conductivity across the interface.

Figure 5-4 Steel plates with opening were used as electrodes

The two slabs' dimensions were selected to provide the same volume of conductive concrete overlay for comparison of power requirements.

5.2.2 The Conductive Concrete Mix

Steel fibers and steel shavings were added to regular concrete to achieve the required electric resistivity for deicing application. The mix, containing 20 percent of steel shavings and 1.5 percent steel fibers by volume, was cast as an overlay on the top of each concrete slab.

The mixing of the conductive concrete was carried out at a Lyman-Richey (Ready Mixed Concrete) plant in Omaha, Nebraska, as follows:

1. 1.1 cubic meter (1.5 cu. yd.) of wet concrete was mixed first without adding any conductive material;
2. Silica fume was added to the concrete;
3. Steel shavings were added to the concrete;
4. Another 0.8 cubic meter (1 cu. yd.) of wet concrete was added; and

5. Steel fibers were added last, and all the materials were mixed in the drum for at least 30 minutes before pouring.

A total of 1.9 cubic meter (2.5 cu. yd.) of conductive concrete was dispensed for the overlays and test specimens. Fig. 5-5 shows that the workability and finishability of the mix were similar to those of conventional concrete. Fig. 5-6 shows that the overlays had smooth surfaces after finishing.

Figure 5-5 Conductive concrete mix showed excellent workability and surface finishability

Figure 5-6 Slabs after finishing

5.2.3 Instrumentation

5.2.3.1 Thermocouples

Type TX, SERV-RITE thermocouple wires from Pneumo Corporation were embedded in the overlays for monitoring the temperature distributions. The 20-gage thermocouple wire was made of a copper/constantan material, valid for a temperature range between –60 and 100°C (-76 and 212°F). Five thermocouples were installed in the thermal insulation layer as shown in Fig. 5-7. Ten thermocouples, five at 13mm (0.5 in.) and the other five at 80 mm (3.25 in) from the top surface, were placed in the square slab, as shown in Fig. 5-8(a). Another four thermocouples were installed (No. 5 to 8) in the middle of the overlay. As shown in Fig. 5-8(b), sixteen thermocouples were laid out in the rectangular slab: two thermocouples, one at 13 mm (0.5 in.) and the other at 80 mm (3.25 in.) from the top surface, were installed at each of the locations (No. 1 to 4 and C1 to C3). Another two thermocouples (C4 and C5) were installed at 45mm (1.75 in.) from the top surface. Figs. 5-9 (a) and (b) show distribution of the thermocouples within the overlay.

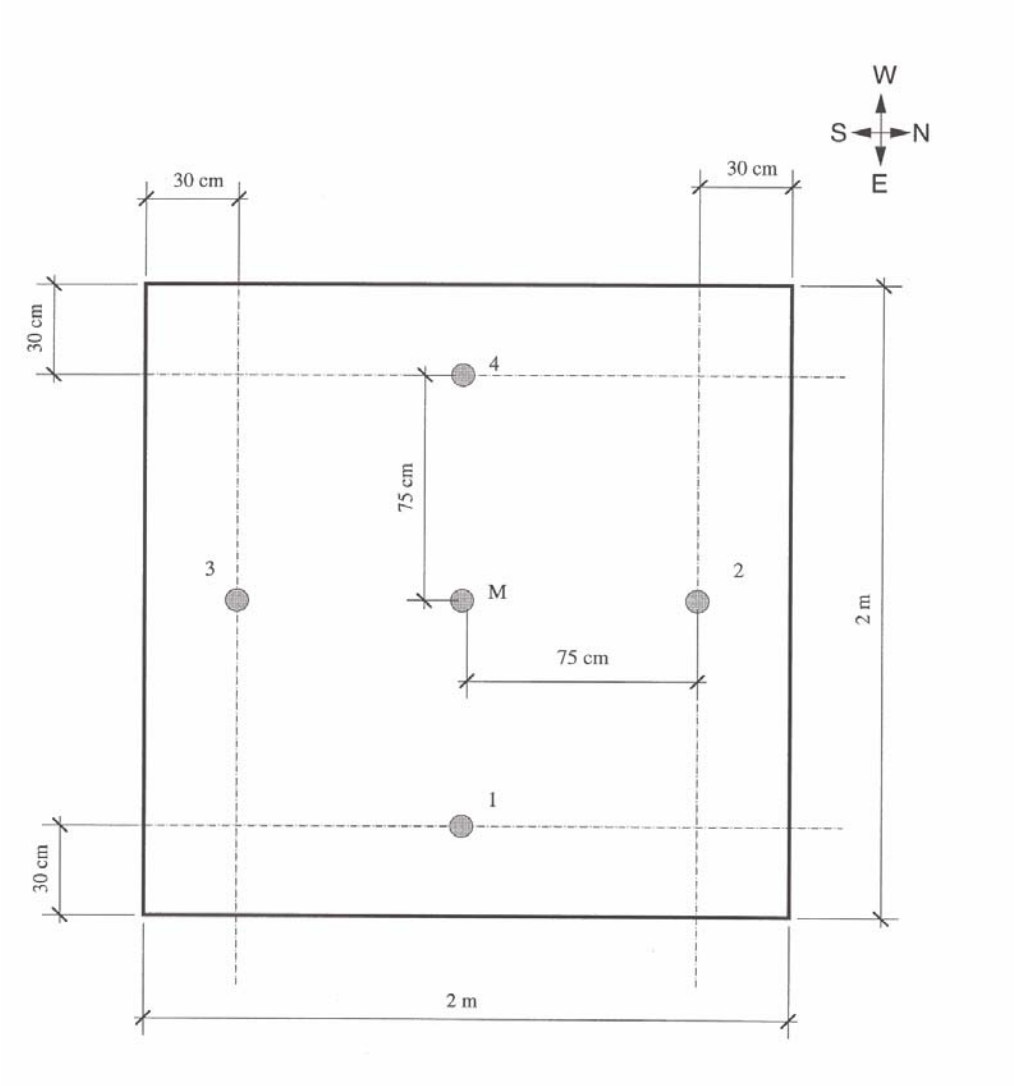

Figure 5-7 Thermocouple locations in the insulation layer

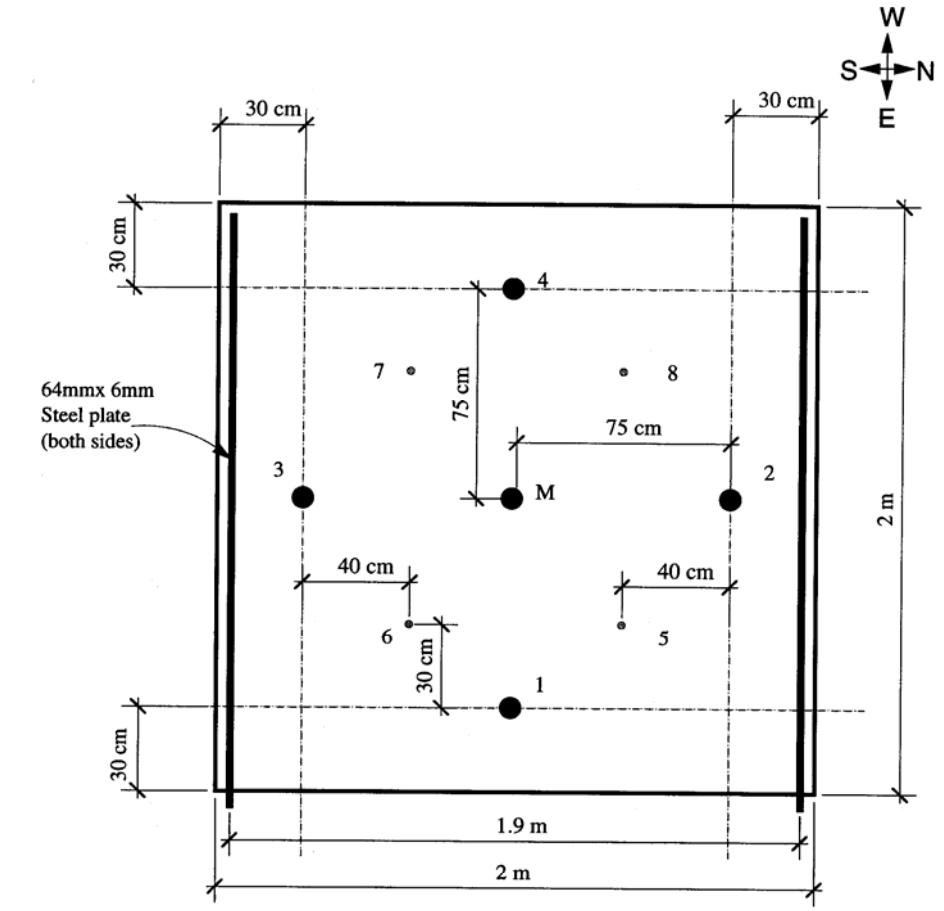

● Top & Bottom (13mm & 80mm from the top surface)

• Middle (45 mm from the top surface)

Figure 5-8(a) Thermocouple locations in the 2m by 2m overlay

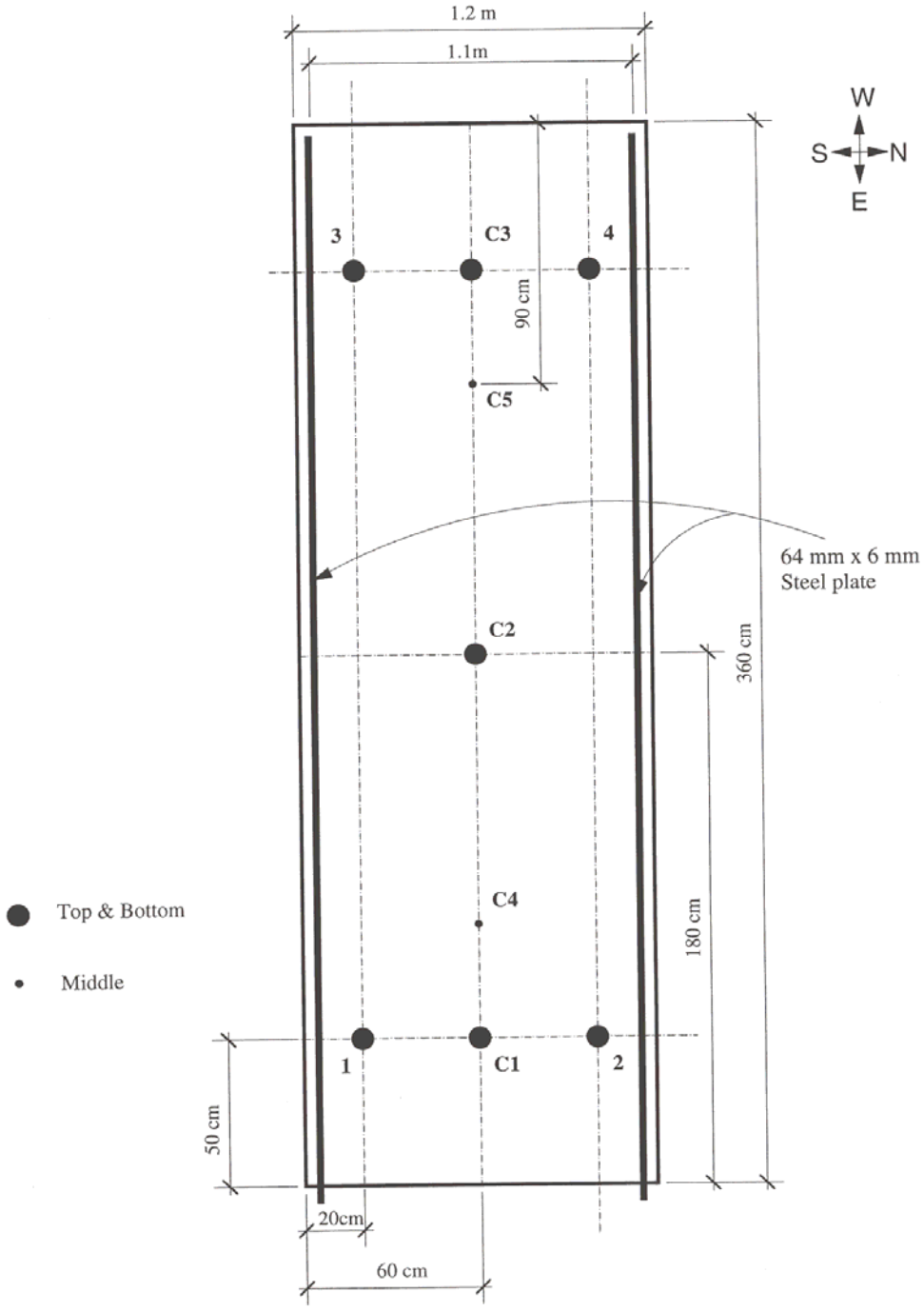

Figure 5-8(b) Thermocouple locations in the 1.2 m by 3.6 m overlay

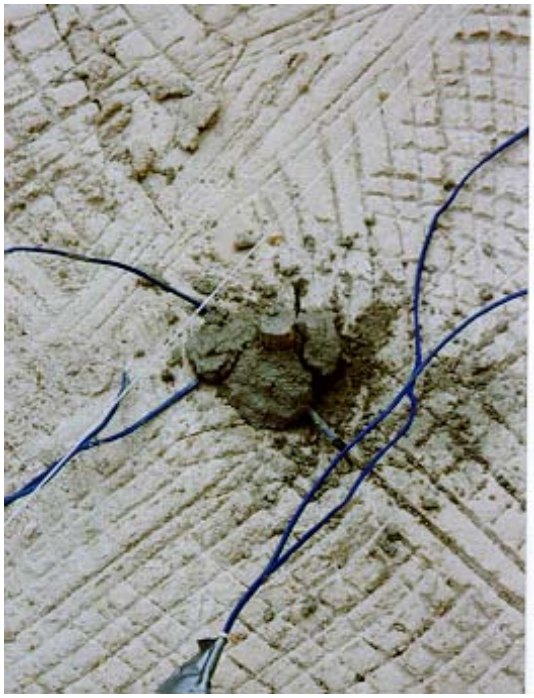

Figure 5-9(a) Thermocouples placed at two levels

Figure 5-9(b) Thermocouple layout before casting overlay

5.2.3.2 Weather Station

An Accu-Weather (model WX 200) electronic weather station was mounted at 1.8m (6 ft) above the overlay surface to record the ambient air temperature, relative humidity, and wind speed/direction during the experiments, as shown in Figs. 5-10 (a) and (b). The temperature, humidity, and wind sensors were, The weather station scanned and recorded air temperature and relative humidity data every 10 seconds and wind speed and direction every 5 seconds.

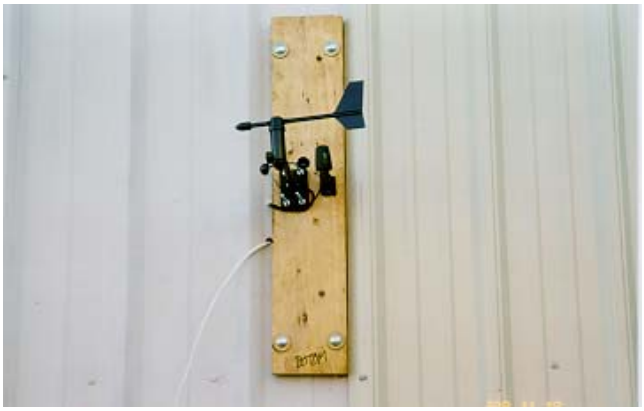

Figure 5-10(a) Temperature, humidity, and wind sensors

Figure 5-10(b) An Electronic Weather Station

5.2.3.3. AC Power Supply

A 220V, 60 Hz, AC power was used to energize the overlays. A VARIAC was used to regulate the applied voltage. A transformer was used to elevate the applied voltage to a maximum of 420 volts. An amp-meter was used to record the electrical current going through each overlay. The overlays were connected to the AC power in parallel. The total current available for both the overlays was limited to 10 Amps, which was the maximum capacity of the transformer. Fig. 5-11(a) shows the equipment used to elevate the voltage from 220 volts to 420 volts. Fig. 5-11(b) shows the two slabs connected to the power source.

5.2.3.4. Data Acquisition System

A MEGADAC 3415AC data acquisition system from OPTIM Electronics Corporation was used to record the overlay temperature readings. Sixteen thermocouple channels were scanned simultaneously at one sample per second during the deicing experiments, and the thermocouple readings were recorded manually along with the weather data once every 30 minutes during the deicing experiments.

Figure 5-11(a) The VARIAC, Transformer and Amp-meters for Power Control

Figure 5-11(b) Slabs connected to power source

5.3. Deicing and Anti-icing Experiments

Deicing experiments were conducted in five snowstorms under two scenarios: deicing and anti-icing. While the overlays were preheated before and heated during the storms in an anti-icing scenario, they were heated only during the storms in a deicing scenario. In each experiment, the applied voltage, electric current through each overlay, overlay temperature, air temperature, humidity, and wind speed/direction were recorded. Table 5-1 summarizes the climatic data acquired during the experiments.

The heating rate of the conductive concrete depends upon the amount of current going through, which can be controlled by maintaining the applied voltage in the operational range and limiting the current. The "breakdown" voltage was in the range of 450-480 volts for the 1.2m by 3.6m (4 ft by 12 ft) overlay, and 780-840 volts for the 2m by 2m (7 ft by 7 ft) overlay. For rapid heating, it was desirable to apply voltage as close to the saturation zone as possible.

Table 5.1 Climatic data in anti-icing and deicing experiments

Date	Experiment type	Snow accumulation mm. (in.)	Wind speed Km/hr (mph)	Wind direction	Air temperature °C (°F)	Relative humidity (%)
Feb. 11, 1999	Anti-icing	75 (3)	5 to 15 (3 to 9.6)	W to NW	-5 to –3 (22 to 26)	74 to 97
Feb. 17, 1999	Anti-icing	200 (8)	4 to 9 (2.7 to 5.4)	W to SW	0.6 to 2 (33 to 36)	71 to 97
Feb. 20, 1999	Deicing	50 (2)	4 to 6 (2.7 to 4)	W	3 (37)	59 to 67
Feb. 22, 1999	Anti-icing	275 (11)	19 to 40 (12 to 25)	W to SW	-3 (26)	59 to 97
March 8, 1999	Deicing	250 (10)	16 to 32 (10 to 20)	W to NW	0 (32)	97 to 87

* Data are for 1.2m x 3.6m (4ft x 12ft) slab.

However, the transformer could only provide up to 420 volts with a maximum current of 10 Amps. Consequently, the following sequence was carried out during the experiments: (1) a 420-volt voltage was applied first, and the current was recorded; and (2) once the total current going through the overlays reached the 10-Amp limit, the voltage was reduced to keep the current below 10 Amps. For an electrode spacing of 1.2m (4 ft), an applied voltage of 420 V was in the operational zone. However, for an electrode spacing of 2m (7 ft), an applied voltage of 420 V was in the linear zone and the heating rate was not adequate for deicing. As a result, only the heating performance of the 1.2m by 3.6m (4 ft by 12 ft) overlay is discussed as follows.

5.3.1 Anti-icing experiments

February 11, 1999

The slab temperature was about 15°C and the ambient temperature was about 7°C at the beginning of the experiment. The applied voltage was about 310 volts and the current going through the overlay gradually increased. The heating rate was initially less than the heat loss from the underlying slab, due to rapid decrease in the ambient temperature and high wind. After about 6 hours of preheating, the heating rate was stable under –5°C ambient temperature and kept the overlay temperature in the range of 3 to 5°C during the storm. There were 75 mm (3 in.) of snow accumulation during the storm. However, snow melted as soon as it came into contact with the overlay as depicted in Fig. 5-12.

Figure 5-12. Anti-icing Experiment – February 11, 1999

February 17, 1999

After preheating at 230-volt voltage for about an hour, the overlay temperature was kept in the range of 2 to 4°C. The applied voltage was increased to about 310 volts no sooner than the storm had started. The overlay temperature was increased to the average of 6 to 8°C after 6 hours of heating. The storm lasted about three and half hours. After the storm, the applied voltage was reduced to 270 volts to keep the overlay dry. The overlay was able to retain the heat for about 3 hours after the power was turned off.

February 22, 1999

The overlay was preheated for 2 hours at an applied voltage of 420 volts. This voltage was kept constant for 5 hours. The storm started during this period, and the current going through the overlay gradually increased. The heating rate was sufficient to maintain the overlay temperature in the range of 1 to 2°C. The average ambient temperature was about –2°C and the wind speed did not vary significantly during the storm, which provided a

relatively stable test environment. Thermal equilibrium was reached under an applied voltage of 310 volts with the current in the range of 8 to 9 Amps.

5.3.2 Deicing experiments

February 20, 1999

The deicing experiment was conducted after the storm with 50 mm (2 in.) of snow accumulation. The ambient temperature was about 2 to 3°C. A voltage of 420 volts was applied and kept constant for about 4 hours, and the current gradually increased to 10 Amps. Figs. 5-13(a) and (b) show the test slab before and during the deicing experiment, respectively.

(a) Slab before testing

(b) Slab during testing

Figure 5-13. Deicing Experiment – February 20, 1999

March 8, 1999

In this deicing experiment, the power was turned on at the same time the storm started. The ambient temperature was just above freezing during most of the experiment, therefore, the applied voltage was kept at 240 volts and the heating rate was sufficient to maintain the overlay temperature in the range of 2 to 6°C.

The temperature at the centerline of the overlay was generally about 2 to 4°C (4 to 7°F) lower than areas close to the electrodes. Consequently snow accumulated and formed a strip along the middle of the overlay during heavy precipitation. This behavior was also observed when the applied voltage was reduced to limit the current to 10 Amps.

The temperature ranges of the thermocouple readings are summarized in Table 5.2, and the average temperature data from all the thermocouples are presented in Fig. 5-14.

February 11, 1999

Location	C1T	C1B	C4M	C2T	C2B	C5M	C3T	C3B
Min. ^{O}C	2.43	3.62	4.18	3.94	5.93	6.01	2.59	2.51
Max. ^{O}C	15.74	15.43	15.51	14.89	16.13	15.67	16.05	20.00

February 17, 1999

Location	C1T	C1B	C4M	C2T	C2B	C5M	C3T	1T
Min. ^{O}C	-0.54	-0.22	-1.35	-0.38	-0.38	-0.70	-0.78	0.42
Max. ^{O}C	5.93	6.41	6.80	8.86	10.51	9.88	6.72	21.23

February 20, 1999

Location	C1T	C1B	C4M	C2T	C5M	C3T	1T
Min. ^{O}C	0.02	-0.54	-0.54	-0.54	-0.62	-0.46	-0.62
Max. ^{O}C	2.19	1.95	1.71	2.51	2.43	1.79	9.57

February 22, 1999

Location	C1T	C1B	C4M	C2T	C5M	C3T	1T
Min. ^{O}C	-1.27	-1.11	-1.27	-0.78	-1.19	-1.35	-1.99
Max. ^{O}C	2.59	2.51	2.99	16.67	6.25	4.34	8.70

March 8, 1999

Location	1T	1B	C1T	C1B	2T	2B	C4M
Min. ^{O}C	0.50	0.58	0.34	0.50	0.74	1.06	0.82
Max. ^{O}C	8.94	9.49	2.27	2.67	21.92	20.46	2.99

Location	C2T	C2B	C5M	3T	3B	4T	4B
Min. ^{O}C	-1.03	0.98	0.02	0.42	0.90	1.06	0.90
Max. ^{O}C	6.17	10.12	9.17	8.15	20.00	42.97	36.07

Note: 1. Thermocouple locations are shown in Fig. 3.
2. T = top, B = bottom, and M = middle.

Table 5.2 Temperature Range of Anti-icing and Deicing Experiments

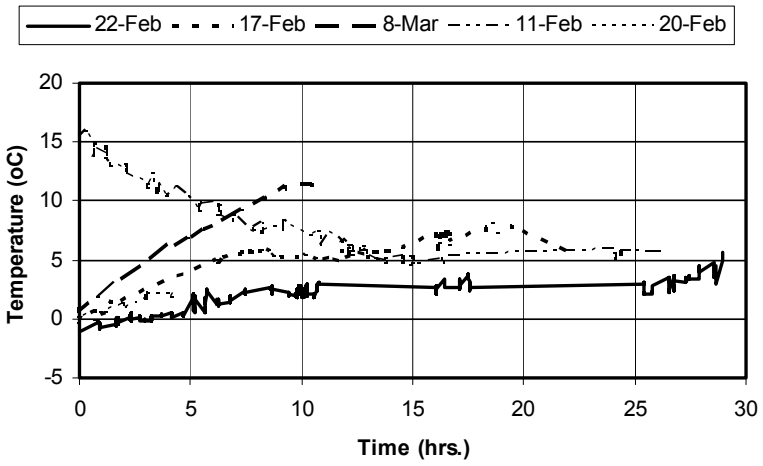

Figure 5-14 Average Anti-icing and Deicing Temperature Data.

5.3.3 Energy Consumption and Costs

During each experiment, the applied voltage and the current going through the overlay were recorded. The recorded current, however, is not the true current that should be used to calculate the energy consumption. To determine the actual current, the impedance (resistance and capacitance) of the conductive concrete overlays must be determined. The impedance of the conductive concrete depends upon the steel fiber distribution within the concrete matrix. Conductive concrete mixes with the same volumetric ratios of steel fibers and steel shaving are expected to have comparable impedance. Due to the limitations of the monitoring equipment (e.g., the oscilloscope and reference resistance), it was not possible to determine the impedance of the conductive concrete overlays or the phase of the current going through each overlay relative to the applied voltage.

The power consumption in a RC circuit (i.e., an electric circuit containing both resistors and capacitors) consists of two components: effective power, which produces the

useful work, and reactive power, which oscillates between the source and the load without producing useful work. To simplify the power consumption calculations, the applied voltage and the recorded current are used in the following equation[33]:

$$P = V_{eff}\ I_{eff}\ \cos\theta \qquad (5\text{-}1)$$

where V_{eff} is the applied voltage, I_{eff} is the total current, and θ is the phase angle between the current and the voltage. The term $\cos\theta$ is defined as the power factor (PF). In the case of a resistive circuit, $\theta = 0^{o}$ and $\cos\theta = 1$, and for a capacitive circuit, $\theta = 90^{o}$ and $\cos\theta = 0$. The PF of the conductive concrete was determined to be in the range of 0.8 to 1.0 based on tests conducted on 0.3m x 0.3m x 5 cm (1 ft x 1 ft x 2 in.) slabs. A power factor of 0.8 was used to account for the phase lag in the estimation of the energy consumption.

Table 5-3 summarizes the energy cost/m^2 of overlay surface during each storm, assuming that 1 kW-hr costs $0.08. Considering a typical highway bridge, 13m by 46m (44-ft wide, and 150-ft long), the approximate energy cost would be in the range of $430 to $600 per storm. A recent interview with Omaha Public Works[72] officials revealed that the approximate cost to operate a plow truck for snow removal is about $1000/hour during a major storm. A life-cycle cost analysis[15] including bridge deck repair costs and vehicle depreciation caused by deicing chemicals, has revealed that utilizing conductive concrete overlay on a bridge deck has the potential to become a very cost-effective deicing method.

Table 5.3 Energy Consumption and Costs

Date	Snow accumulation mm. (in.)	Preheating (hrs)	Experiment time (hrs)	Power consumption (kW-hr)	Energy Cost $/m^2 ($/ft^2)
Feb. 11, 1999	75 (3)	6	16	32.48	0.56 (0.052)
Feb. 17, 1999	200 (8)	4	18	42.64	0.73 (0.068)
Feb. 20, 1999	50 (2)	---	5	9.84	0.17 (0.016)
Feb. 22, 1999	275 (11)	2	15	33.76	0.58 (0.054)
March 8, 1999	250 (10)	---	20	46.16	0.80 (0.074)

5.4. Design Issues

5.4.1 Electrical Conduction Model Validation

As shown in Fig. 5-15, the relationship between the applied voltage and the current going through the 1.2m by 3.6m (4 ft by 12 ft) overlay was established using data from the deicing and anti-icing experiments. A voltage of 220-volt was first applied (i.e., in the lower range of the operational zone), and the current going through the overlay increased slowly with time. The current increased at a faster rate, when a voltage of 420-volt was applied (i.e., in the upper range of the operational zone). From the limited data presented herein, an exponential relationship was found to produce the best fit for each given voltage and current. The current going through the slab is expected to increase if the voltage is kept constant. The current will increase at a higher rate if the overlay temperature is in the range of 3-5°C. However, the total current allowed to go through the overlays was limited to 10 Amps in all cases. Generally, conduction of electricity in the conductive concrete overlays followed the model described in Chapter 3.

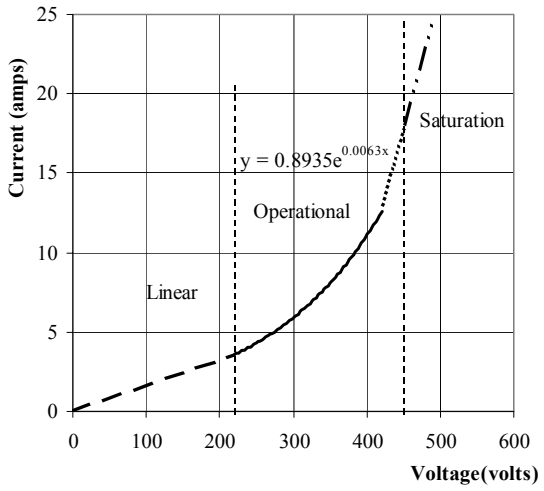

Fig. 5-15 Conduction of electricity in the 1.2m x 3.6 m x 9 cm conductive concrete overlay

5.4.2 High Voltage and Safety Concerns

Safety was a major concern due to applying high voltage to heat the overlay. Since a conductive concrete mix behaves as a resistor in parallel with a variable resistor and a capacitor, the summation of the potential drops of all the viable current paths between the two electrodes is equal to the applied voltage. Likewise, the total current going through all the viable paths is equal to the current corresponding to the applied voltage. This behavior has been confirmed by field measurements. Several measurements were taken at different locations on the overlay surface during heating experiments, and the voltage readings were in the range of 10 to 20 volts. The current readings were in the range of 20 to 30 mA. These voltage and current levels pose no hazard to the human body.

A potential safety hazard exists if steel fibers and shavings come in direct contact with electrodes and are exposed on the surface. This risk can be eliminated if the top surfaces of the electrodes are insulated to avoid direct contact with any conductive materials near the surface. It is also essential to insulate the power connection at the electrode ends.

5.4.3 Thermal Stresses Due to Overlay Heating

The maximum temperature rise in the overlay during the experiments was in the range of 15 to 20°C (27 to 36°F). The coefficient of thermal expansion of concrete[56,59,15] using limestone is in the range of 5.9 to 7.1 x 10^{-6}/°C, and that of the steel fibers and shavings is in the range of 5.5 to 11.5 x 10^{-6}/°C. If the differential thermal expansion in the conductive concrete were 7 x 10^{-6}/°C, the thermal strain caused by a 20°C temperature increase would be 7 x 10^{-6} x 20 = 140 x 10^{-6}. The modulus of elasticity of the conductive concrete[85] was about 3650 MPa (5.3 x 10^{5} psi), and the thermal stresses induced would be 140 x 10^{-6} x 3650 = 510 kN/m^2 (74

psi). This stress level is less than the allowable tensile strength of concrete[56,59] of approximately 3100 kN/m^2 (450 psi). Since the electric resistance heating of the overlay is a gradual process, the potential of concrete cracking due to "thermal shock" is minimal.

5.4.4 Interface Shear Between Bridge Deck and Overlay

As cited in the literature[13,16,22,42,56], the interface can resist shearing stresses from high traffic movements if a bond exists between an overlay and a pavement. The maximum horizontal shear stresses calculated at the interface of a 51mm (2 in.) bridge deck overlay[13] due to an 80-kN (18 kips) single-axle load plus impact (equivalent to an H20 wheel) were about 446 kN/m^2 (64 psi) and 167 kN/m^2 (24 psi), respectively. The interface (horizontal) shear strength between the overlay and the pavement, determined from direct shear tests, was about 1400 kN/m^2 (201 psi). The use of shear studs was not necessary. Roughening the existing pavement surface before casting the overlay can ensure a good bond at the interface.

5.4.5 Minimum Temperature Reinforcement in an Overlay

ACI 318-95[4] (7.12) and AASHTO[2] (8.20.1) require that at least 265 mm^2 per meter (1/8 in^2 per foot) of steel reinforcement should be provided in each direction for a concrete overlay to resist stresses due to temperature and shrinkage. Based on field experience reported by Grondziel[36] and a steel fiber manufacturer[31] that uniform disbursement of 60 kg of steel fibers per cubic meter of concrete (100 lb./cu. yd.) will provide adequate overlay strength to resist stresses from heavy traffic and thermal stresses. No minimum steel reinforcement in the overlay was necessary. There was about 120 kg of steel fibers in a cubic meter (200 lb./cu. yd.) of the conductive concrete mix, and therefore, minimum temperature reinforcement is not required.

5.4.6 Effect of Slab Geometry on Heating Rate

The "breakdown" voltage of the conductive concrete overlay was found to be directly proportional to the electrode spacing, and the amount of current going through is inversely proportional to the cross-sectional area of the overlay parallel to the electrodes. The basic equations[33] to calculate the impedance and the electric resistivity can be used to design the overlay:

$$Z = \frac{V}{I} \qquad (5\text{-}2)$$

$$Z = \frac{\rho L}{A} \qquad (5\text{-}3)$$

where Z is the impedance, V is the applied complex sinusoidal voltage, I is the complex current, ρ is the average electric resistivity of a specific cross-sectional area, L is the spacing between the electrodes, and A is the cross-sectional area of the overlay.

The electric resistivity of the material should be determined first, and electrodes spacing can be chosen for a given breakdown voltage. The heating rate is proportional to the current going through the slab. Based on the amount of current desired, the cross-sectional area (thickness and length) of the overlay can then be determined.

5.5 Electric Resistance Heating of Conductive Concrete

A coupled thermal-electric finite element analysis was conducted to study the electrical resistance heating of the conductive concrete overlay, namely, the relationship between power input, heating rate and temperature distribution of the conductive concrete overlay of the test concrete slab. The parameters of the finite element model were determined from the literature as well as from the experimental data. The thermal and electrical properties and the heating

characteristics of the conductive concrete are presented herein. The numerical results showed that the model can be used to predict the heating performance of the conductive concrete overlay.

5.5.1 Coupled-field Governing Differential Equations

The electric resistance heating, or "Joule heating," of conductive concrete may be analyzed with a set of coupled electric field and transient heat conduction equations. The three-dimensional electric field equation is given as

$$\frac{\partial}{\partial x}\left(\kappa_\phi \frac{\partial \varphi}{\partial x}\right)+\frac{\partial}{\partial y}\left(\kappa_\phi \frac{\partial \varphi}{\partial y}\right)+\frac{\partial}{\partial z}\left(\kappa_\phi \frac{\partial \varphi}{\partial z}\right) = 0 \qquad (5.4)$$

where $\varphi(x,y,z)$ is the electric potential, and κ_ϕ is the electrical conductivity (i.e., the reciprocal of electric resistivity) of the conductive concrete.

The three-dimensional transient heat conduction equation is given as

$$\rho c_p \frac{\partial T}{\partial t} = \frac{\partial}{\partial x}\left(\kappa_T \frac{\partial T}{\partial x}\right)+\frac{\partial}{\partial y}\left(\kappa_T \frac{\partial T}{\partial y}\right)+\frac{\partial}{\partial z}\left(\kappa_T \frac{\partial T}{\partial z}\right)+Q \qquad (5.5)$$

where ρ, c_p, and κ_T are the mass density, heat capacity and thermal conductivity of the conductive concrete, respectively, Q is the rate of internal heat generation per unit volume of the conductive concrete, $T(x,y,z,t)$ is the temperature field and t is time. It is assumed that κ_T remains constant in the typical temperature range of deicing experiment (-25 to 10°C).

For Joule heating of conductive concrete, Eqs.(5.4) and (5.5) are coupled in that the electrical conductivity κ_ϕ is a function of temperature T and that the internal heat generation Q is a function of the electric potential $\varphi(x,y,z)$ and can be expressed as

$$Q = \frac{\kappa_\phi(T)}{2}\left[\left(\frac{\partial \varphi}{\partial x}\right)^2+\left(\frac{\partial \varphi}{\partial y}\right)^2+\left(\frac{\partial \varphi}{\partial z}\right)^2\right] \qquad (5.6)$$

The boundary condition may be expressed as

$$\kappa_T \frac{\partial T}{\partial x} n_x + \kappa_T \frac{\partial T}{\partial y} n_y + \kappa_T \frac{\partial T}{\partial z} n_z + \beta T = \gamma \qquad (5.7)$$

where n_x, n_y and n_z are the unit normals to the boundary, β a constant and γ the heat flux associated with the convective heat losses from the exterior surfaces.

5.5.2 Transient Thermal Finite Element Analysis

A coupled-field finite element analysis was conducted for the Joule heating simulation. The finite element analysis program ***ANSYS*** was used for the thermal-electric analysis of the conductive concrete test slab. Taking advantage of the symmetry of the test slab, only half of the slab was included in the modeling. However, both electrodes must be included in the model to complete the current flow path. A 3-D thermal-electric solid element (SOLID69) was used to model the regular concrete deck, the conductive concrete overlay, the steel electrodes and, if any, a layer of ice or fresh snow on top of the conductive concrete. With the snow layer, the model consisted of 6150 nodes and 5040 thermal-electric solid elements. Fig. 5-16 shows an isometric view of the finite element model.

The hexahedral solid element has eight nodes with two degrees of freedom, temperature and voltage, at each node. The Joule heat generated by the current flow is included in the heat balance calculations. The material properties required for input include density, heat capacity, electric resistivity and thermal conductivity. The thermal-electric finite element analysis is highly nonlinear, in that the material properties may be functions of temperature and that snow and ice will undergo phase change when melting. Thus, the thermal-electric analysis requires an

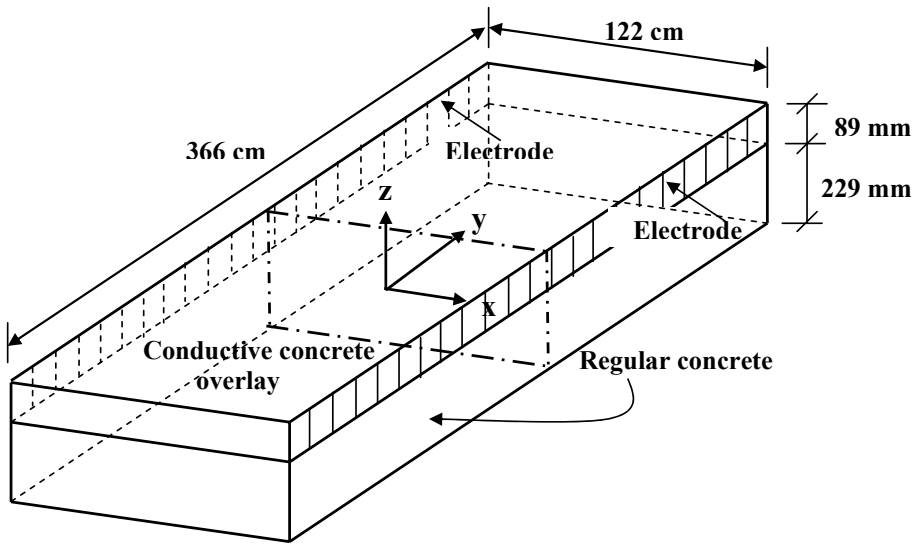

Figure 5-16 Conductive concrete overlay model

iterative solution. In simulating the deicing experiments, the applied voltage was assigned to the nodes of electrode elements and the resulting current was calculated. Other output parameters of interest includes the temperature distribution and the heat flux of the test slab surface.

Boundary Conditions

The plane of symmetry (i.e., the ***xz***-plane) was treated as an adiabatic boundary. All of the other five exterior surfaces were treated as convective with a film coefficient of 34 W/m^2-^oK, used for convection under 24 km/hr (15 mph) wind, and with the ambient temperature. Radiative heat gain and loss were ignored. Furthermore, the applied voltage was reduced during some of the deicing experiments to limit the maximum current going through the conductive concrete overlay. In those events, the temperature distribution from a previous simulation was

prescribed as the initial condition for a subsequent transient thermal analysis under a different applied voltage.

Model Parameters

Conductive concrete is a heterogeneous solid or a "composite," whose constituents are steel fibers, steel shavings, and regular concrete. Nevertheless, it may be treated as a homogeneous and isotropic material with its "apparent" properties determined based on the volume fraction of the steel fibers and shaving contained in the composite. Expressions of "apparent" physical and thermal properties of conductive concrete may be derived from those of the constituent materials[85]. The apparent physical and thermal properties for a conductive concrete mix with 1.5 percent of steel fibers and 20 percent of steel shaving by volume are presented in Table 5.4, along with the properties of other materials used in the finite element simulations. The electric resistivity of a material can be expressed as

$$Z = \frac{\psi L}{A} \qquad (5.8)$$

where $\mathbf{Z}$ is the impedance, ψ is the average electric resistivity of a cross-sectional area, L is the spacing between the electrodes, and A is the area of a cross-section of the overlay parallel to the electrodes. The electric resistivity of the conductive concrete is presented in Fig. 5-17 as a function of temperature.

Table 5.4 Electrical and Thermal Properties used in the Finite Element Simulation

Material	Density (kg/m^3)	Heat Capacity (J/kg-K)	Thermal Conductivity (W/m-K)	Electric Resistivity at 0^oC (Ω-m)
Steel	7830	420	47	1.695×10^{-7}
Concrete	2350	880	0.87	5.4×10^5
Conductive Concrete	3446	670	4.2	20
Ice	920	2050	2.2	Not applicable
Fresh snow	200	2090	0.1	Not applicable
Water	1000	4190	0.55	Not applicable

Phase Change

Ice and snow melting is a phase change process, which requires a nonlinear transient thermal analysis. When the temperature of the snow reaches 0^oC, the snow will continue to absorb heat and start changing into water. During the phase change, the temperature of the snow remains at 0^oC. The latent heat absorbed by snow, 333.5 kJ/kg is input by defining the

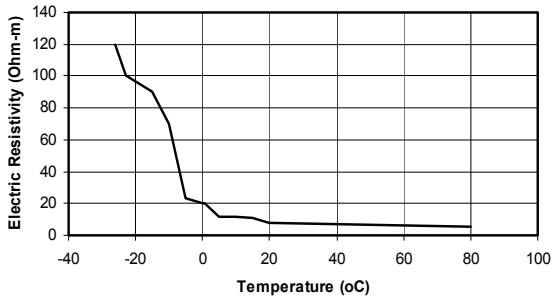

Figure 5-17 Electric Resistivity of the Conductive Concrete

enthalpy of snow as a function of temperature. Enthalpy, which has units of heat/volume, is the integral of specific heat with respect to temperature:

$$H = \int \rho_{snow}\, c_p(T)\, dT \qquad (5.9)$$

The mass density of snow is ρ_{snow} = 200 kg/m^3, and the heat capacity of snow is c_p = 2.09 kJ/kg-^{o}K. Fig. 5-18 shows the enthalpy-temperature curve used in the simulation for the snow layer in the deicing experiment. Once a snow element in the model was predicted to have melted, its material properties were replaced by those of water.

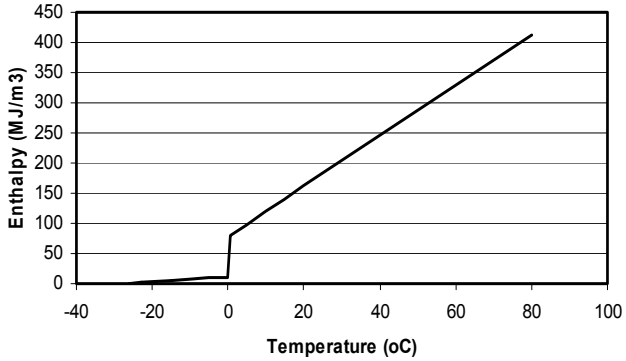

Figure 5-18 Enthalpy-Temperature Curve for Phase Change of Snow

5.5.3 Comparison of Results

Finite element simulations were conducted for both anti-icing and deicing experiments, and the results are compared against the experimental data herein.

Anti-icing simulation

In an anti-icing simulation, the finite element model did not have the snow/ice layer initially. The applied voltage was assigned to the electrode nodes and the recorded ambient temperature was used as the initial condition. The recorded time-history of the applied voltage was followed in the simulation, and the resulting current was compared against the current

recorded in the experiment. The temperatures calculated were then compared against the thermocouple readings.

At the time snowstorm started, the finite element model was modified to include the snow/ice layer and the temperature profile from the previous time step was prescribed as the initial condition for the new model. The temperature of the snow/ice layer was assumed to be the ambient temperature or at freezing, whichever is lower. From this point on, the temperature of the snow/ice layer was checked against above freezing. If the snow temperature indicated that the layer had melted, the snow layer temperature would be reset to ambient temperature or freezing, whichever is lower. This process would continue until the total snow accumulation observed in the experiment was reached. However, if the heat flux generated by the overlay is greater than the rate of snow precipitation, there will be no snow accumulation.

The anti-icing experiment conducted on February 22, 1999, was selected for finite element simulation. The overlay was preheated under 420 V for 1.72 hours before the snowstorm started. The average heat flux of the overlay surface during this period was calculated to be 320 W/m^2, which compares well with the input power density of 365 W/m^2 with about 12 percent heat loss. The maximum rate of snow precipitation, $\boldsymbol{p}$, with no accumulation can be calculated as follows:

$$\boldsymbol{p} \times \rho_{\boldsymbol{snow}} \times \text{latent heat of fusion} = 320 \ \text{W}/\text{m}^2 \qquad (5.10)$$

and $\boldsymbol{p}$ = 17.3 mm/hr (0.68 in./hr). The total snow accumulation during a period of about 7 hours was 279 mm (11 in.), and snow accumulated on the test slab. The anti-icing experiment became deicing once snow accumulated.

The time-histories of the calculated current is compared against the recorded data in Fig. 5-19. The applied voltage was reduced from 420 V to 390 V at 5.2 hours into the experiment,

and lasted for 34 minutes. The heating rate of the conductive concrete is depicted in Fig. 5-20, with an average rate of 7.8°C/hr (14°F/hr). The finite element model overestimated the temperature distribution by about 15 to 25 degrees Celsius compared to those summarized in Table 5.2. Given the complexity of the problem, however, the finite element model provides a useful tool to evaluate the electrical resistance heating behavior of conductive concrete mixes with different volumetric fractions of other added conductive materials.

Deicing simulation

The finite element model used in deicing simulation had a 51 mm (2 in.)-thick snow layer on top. The simulation procedure described previously was also followed herein. The deicing experiment conducted on February 20, 1999, was selected for simulation. The time-history of the calculated current is compared against the recorded data in Fig. 5-19. The temperature profile of the snow layer indicated that it would take about 2 hours to melt 51 mm (2 in.) of snow, as shown in Fig. 5-21.

Similar to anti-icing simulation, the finite element model overestimated temperature profile and the temperatures were generally in the 35 to 45°C range. However, the predicted values were close to the field data at certain thermocouple locations, as in the March 8, 1999 experiment. Since the conductive concrete was assumed to be isotropic and homogeneous, a fairly uniform temperature distribution was expected. The heterogeneity of conductive concrete would cause wide scatter in temperature distribution, with higher temperature

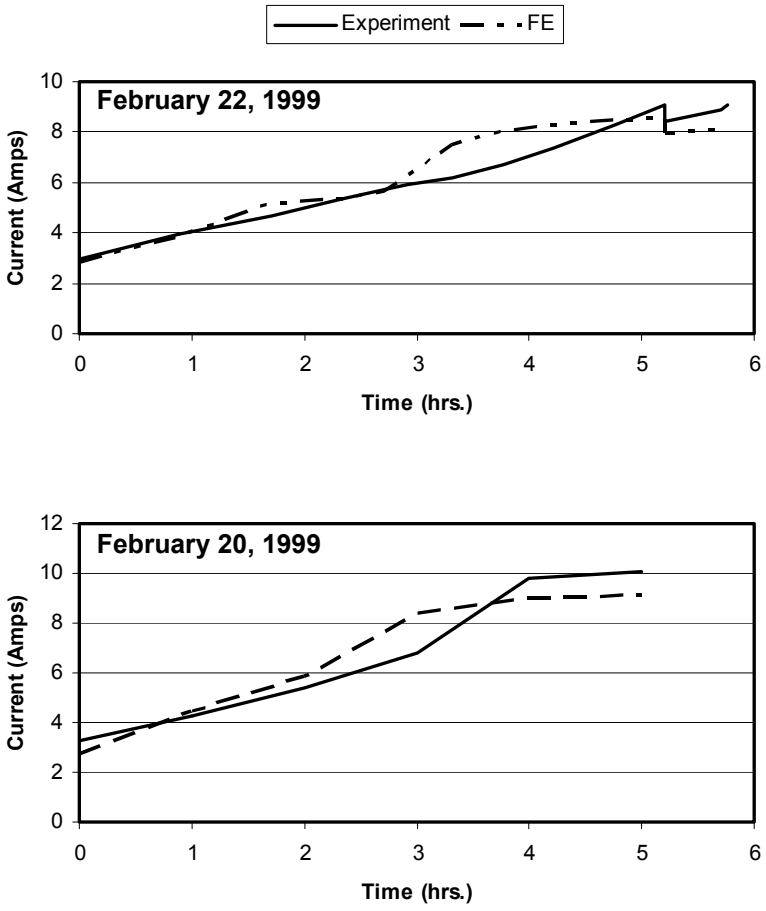

Figure 5-19 Deicing Electric Current Data (Under 420 V AC)

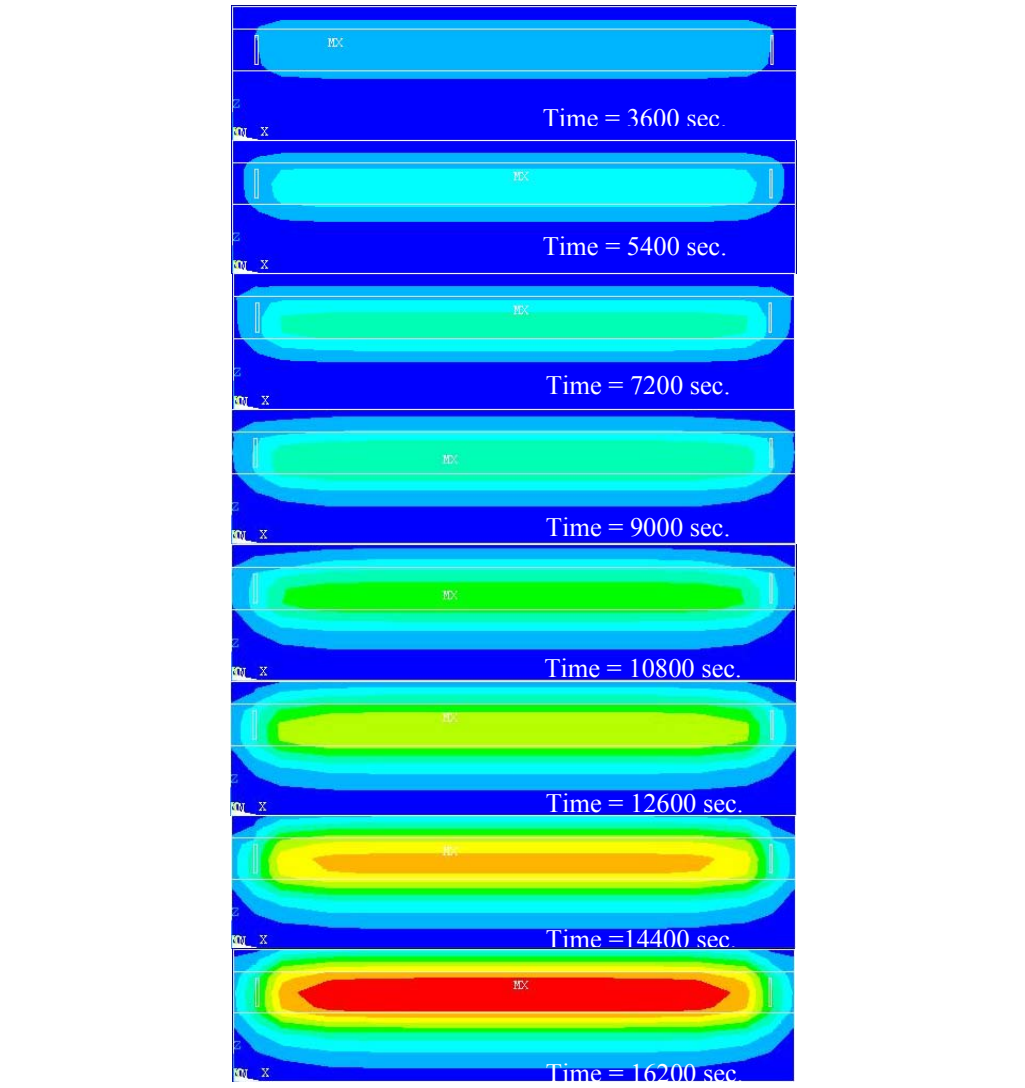

Figure 5-20 Electrical Resistance Heating of Conductive Concrete Overlay

readings close to metal fibers and particles. Another possible cause is the omission of radiant heat loss, which could be significant during night-time when the experiments were conducted.

It was observed in the deicing experiments that the temperature along the centerline of the test slab was generally lower than in the areas close to the electrodes. Consequently snow accumulated and formed a strip along the middle of the overlay as shown in Fig. 5-13(b). In reality, the temperature of the electrodes was expected to be much higher than the surrounding conductive concrete. However, the finite element model predicted higher temperature along the centerline than areas close to the electrodes. As a result, the model was unable to duplicate the snow strip along the middle of the overlay.

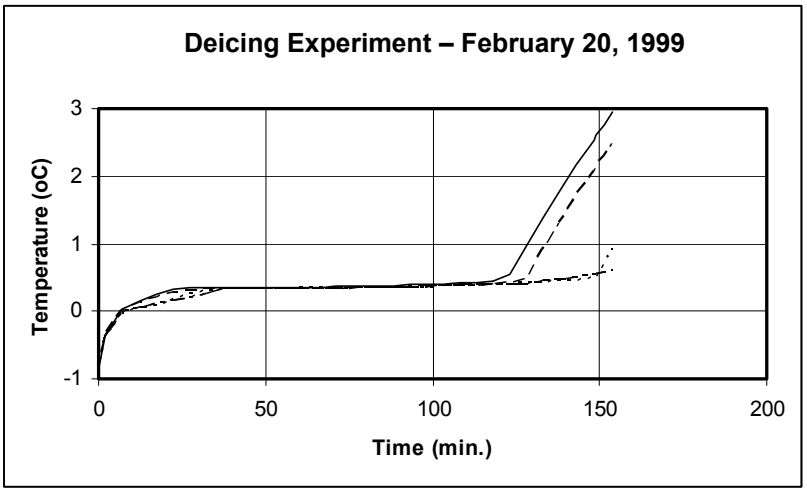

Figure 5-21 Temperature Time-histories in the Snow Layer

CHAPTER 6

AN IMPLEMENTATION OF CONDUCTIVE CONCRTE OVERLAY

6.1 Background

During Phase I of the conductive concrete research, a concrete mix containing 1.5 percent of steel fibers and 20 percent of steel shavings per volume was developed specifically for concrete bridge deck deicing. The mix had a minimum compressive strength of 31 MPa (4500 psi) and provided an average thermal power density of 590 W/m^2 (55 W/ft^2) with a heating rate of 0.14^{o}C/min (0.25^{o}F/min) in the winter environment. The average energy cost was about \$0.8/m^2 (\$0.074/ft^2) per snow storm.

Steel shavings are waste materials produced by steel fabricators in the form of small particles of random shapes. Drawbacks were noticed about using steel shavings during development of the conductive concrete: (1) there was a lack of consistency of sizes and compositions from various sources of steel shavings; (2) steel shavings acquired were usually contaminated with oil, which required cleaning; and (3) steel shavings required a specialized mixing procedure to ensure uniform dispersal in the concrete. As a follow-up effort, carbon and graphite products were used to replace steel shavings in several trial conductive concrete mix designs. Test data showed that the electrical conductivity and the heating rates could be significantly improved with the carbon products. Consequently Nebraska Department of Roads approved a demonstration project at Roca, located on Nebraska Highway 77 South about 24 km (15 miles) south of Lincoln, to implement a conductive concrete deck on a highway bridge for deicing. The Roca Spur Bridge has been instrumented with temperature and current sensors for heating performance monitoring during winter storms. Experimental data and operating costs are presented in this Chapter.

6.2 Conductive Concrete utilizing Carbon and Graphite Products

Formatted: Indent: First line: 0"

During the spring of 2001, carbon products were used to replace steel shavings in the conductive concrete mix designs. Seven commercial carbon and graphite products were used in trial batches in an experimental program. Ten trial mixes were prepared for evaluations. The criteria used for the trial mixes were workability, finishability, compressive strength, heating rate, and electric resistivity. All mixes contained steel fibers and carbon products for conductive materials. The steel fibers of variable lengths amounted to 1.5 percent and the carbon products amounted to 25 percent per volume of the conductive concrete mixes. These trial mixes are described as follows:

Formatted: Bullets and Numbering

1. 20 % Black Diamond (3/8×0)
2. 25 % Earth Link
3. 41 % Earth Link
4. 25% EC-98C (10×0)
5. 25% EC-100 (10×0)
6. 25% EC-97 (3/8×0)
7. 25% EC-100 (3/8×0)
8. 25% FP-428 (100×0)
9. 25% ALL – All graphite products were used in this mix except the Black Diamond
10. 25% Earth Link + Slag aggregate

Formatted: Indent: First line: 0"

Black Diamond (BD) is the trade name of a natural graphite crystalline in the form of pellets. Earth Link (EL) is the trade name of graphite cement, which contains approximately 70 percent of portland cement and 30 percent of graphite powder. The EC designations are used to distinguish carbon products of different particle sizes. FP-428 is a product of small carbon

particles. Crushed limestone of 13 mm (0.5 in.) maximum size was used in the trial mixes. However, 13 mm (0.5 in.) blast furnace slag was used in one trial mix to replace the limestone with an intent to improve the electrical conductivity. Coarse blast furnace slag is the co-product of molten iron production in a blast furnace. When molten, slags float on the metal. Separating the two is not exact and there is some iron residue in the slags. Six 152 × 305 mm (6 × 12 in.) cylinders and one 457 × 330 × 63.5 mm (18 in. × 13 in. × 2.5 in.) slab were prepared from each trial mix.

6.3 Test Results

6.3.1 Workability, Finishability and Compressive Strength

Workability and finishability were the two primary criteria used in the preliminary evaluation of the trial mixes. In addition, three cylinders from each trial mix were tested for compressive strength at 28 days. The test results are summarized in Table 6.1.

6.3.2 Heating Rate

Heating tests with the 457 × 330 × 63.5 mm (18 in. × 13 in. × 2.5 in.) slabs were conducted under two initial temperatures, -4°C (25°F) and 2°C (35°F). Two steel plates spaced at 305 mm (12 in.) were used for electrodes. The steel plates had perforations greater than or equal to the 13-mm (0.5-in.) maximum aggregate size to allow concrete to flow through to provide good anchorage. A Type TX thermocouple was embedded in the middle of each test slab to monitor the temperature. Alternate current (AC) power with a constant voltage of 140 volts was applied, and resulting current and slab temperature from each slab were recorded for 30 minutes. The slabs were kept inside a freezer during heating tests to maintain constant ambient temperature. The results are summarized in Table 6.2.

Table 6.1 Preliminary Test Results.

Trial Mix	Workability	Finishability	28-day Compressive Strength MPa (psi)	Remarks
1. 20% Black Diamond (3/8×0)	Good	Good	24.0 (3483)	Gas release during hydration causing volume expansion
2. 25% Earth Link	Good	Good	39.8 (5770)	
3. 41% Earth Link	Good	Good	32.7 (4735)	Required more superplasticizer
4. 25% EC- 98C (10×0)	Good	Good	47.0 (6811)	
5. 25% EC- 100 (10×0)	Good	Good	40.5 (5870)	
6. 25% EC- 97 (3/8×0)	Good	Good	41.8 (6061)	
7. 25% EC-100 (3/8×0)	Good	Good	37.4 (5416)	
8. 25% FP-428 (100×0)	Good	Good	26.3 (3817)	Required more Superplasticizer
9. 25% EC-All	Good	Good	34.5 (4997)	
10. 25% Earth Link + Slag aggregate	Good	Good	46.6 (6750)	

Table 6.2 Comparison of heating rate, operating voltage, and peak current.

Specimen	Initial Temperature	Max. Heating Rate (^{o}C/minute)	Operating Voltage (Volts)	Peak Current (Amps.)
EC-100 (3/8×0)	-4^{o}C	0.25	140	0.93
EC-100 (3/8×0)	2^{o}C	0.27	140	1.13
EC-100 (10×0)	-4^{o}C	0.26	140	0.67
EC-100 (10×0)	2^{o}C	0.38	140	0.95
EC-98C (10×0)	-4^{o}C	0.09	140	0.48
EC-98C (10×0)	2^{o}C	0.11	140	0.61
EC-97 (3/8×0)	-4^{o}C	0.38	140	0.89
EC-97 (3/8×0)	2^{o}C	0.38	140	1.00
FP-428 (100×0)	-4^{o}C	0.14	140	0.43
FP-428 (100×0)	2^{o}C	0.07	140	0.47
EC-all	-4^{o}C	**1.56**	140	**4.26**
EC-all	2^{o}C	**1.71**	140	**4.82**
41% EL	-4^{o}C	0.36	84	0.62
41% EL	2^{o}C	0.31	84	0.69
BD 20%	-4^{o}C	0.01	140	0.11
BD 20%	2^{o}C	0.09	140	0.17
Slag + 25% EL	-4^{o}C	**3.27**	140	**2.39**
Slag + 25% EL	2^{o}C	**2.28**	140	**1.97**
25% EL	-4^{o}C	0.38	140	0.80
25% EL	2^{o}C	0.37	140	1.13

Formatted ... [1]
Formatted ... [2]
Formatted ... [3]
Formatted ... [4]
Formatted ... [5]
Formatted ... [6]
Formatted ... [7]
Formatted ... [8]
Formatted ... [9]
Formatted ... [10]
Formatted ... [11]
Formatted ... [12]
Formatted ... [13]
Formatted ... [14]
Formatted ... [15]
Formatted ... [16]
Formatted ... [17]
Formatted ... [18]
Formatted ... [19]
Formatted ... [20]
Formatted: Indent: First line: 0"

6.3.3 Electric Resistivity

Based on the heating test data, approximate values of the impedance and the electric resistivity were calculated for each trial mix using the following equations:

$$Z = \frac{V}{I} \qquad (6.1)$$

and

$$Z = \frac{\rho L}{A} \qquad (6.2)$$

where Z is the impedance, V is the applied AC voltage, I is the AC current, ρ is the average electric resistivity of the specimen, L is the spacing between the electrodes or 305 mm (12 in.), and A is the cross-sectional area of the test slab parallel to the electrodes or 19355 mm^2 (30 $in.^2$). A range of the electrical resistivity with respect to the initial temperatures is given for each trial mix in Table 6.3.

Two trial mixes, EC-All and Slag+25% EL showed high electrical conductivity and heating rates. Experimental data from the heating tests of these two mixes are presented in Figs. 6-1 and 6-2, respectively. The electric resistivity of these materials is a function of temperature. As temperature increases, the materials become more electrically conductive. The higher electrical conductivity is probably due to the good gradation of carbon particles in the EC-All and the added slag in the Slag+25%EL mixes. EC-all and Slag+25%EL showed superior heating performance, as shown in Fig. 6-3.

Deleted:

Table 6.3 Electrical resistivities of carbon concrete trial mixes

Specimen	Initial Temperature	Temperature Range (°C)	Electrical Resistivity (Ω.cm)
EC-100 (3/8×0)	-4°C	-4° ~ 4.5°	564 -381
EC-100 (3/8×0)	2°C	2° ~ 10°	451 – 323
EC-100 (10×0)	-4°C	-4° ~ 4.5°	721 – 576
EC-100 (10×0)	2°C	2° ~ 15.5°	519 – 392
EC-98C (10×0)	-4°C	-4° ~ -1°	939 – 853
EC-98C (10×0)	2°C	2° ~ 4.5°	733 – 669
EC-97 (3/8×0)	-4°C	-4° ~ 10°	564 – 403
EC-97 (3/8×0)	2°C	2° ~ 15.5°	518 – 357
FP-428 (100×0)	-4°C	-4° ~ 2°	1048 – 958
FP-428 (100×0)	2°C	2° ~ 4.5°	902 – 900
EC-all	**-4°C**	**-4° ~ 38°**	**435 – 108**
EC-all	**2°C**	**2° ~ 49°**	**395 – 101**
41% EL	-4°C	-4° ~ 7°	1006 – 762
41% EL	2°C	2° ~ 13°	846 – 702
BD 20%	-4°C	-4° ~ -3°	8077 -7404
BD 20%	2°C	2° ~ 7°	7500 - 5226
slag + 25% EL	**-4°C**	**-4° ~ 40°**	**808 – 208**
slag + 25% EL	**2°C**	**2° ~ 35°**	**705 – 219**
25% EL	-4°C	-4° ~ 4.5°	1813 – 728
25% EL	2°C	2° ~ 4.5°	830 – 759

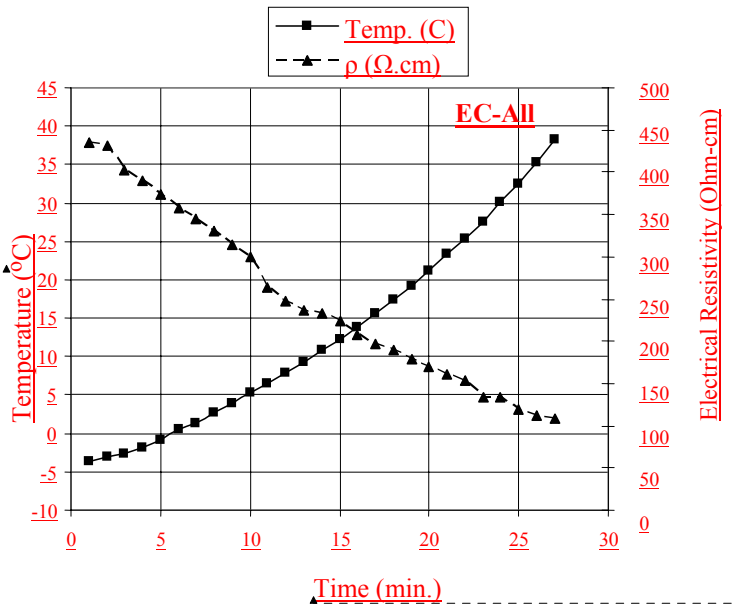

Figure 6-1 Electric Resistivity vs. Temperature – EC-All Mix

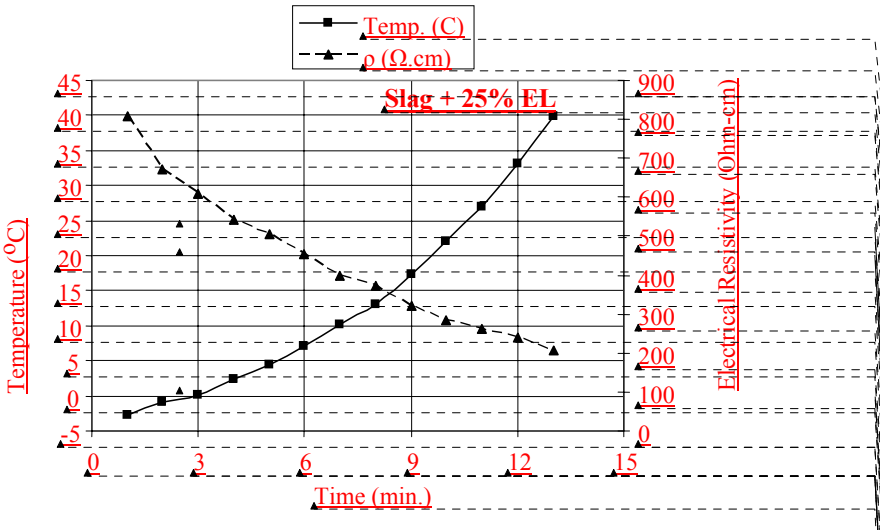

Deleted:

Formatted ... [21]

Formatted: Font: 11 pt

Formatted: Font: 12 pt

Deleted:

Formatted: Font: 11 pt

Formatted: Font: 11 pt

Formatted: Font: 11 pt

Formatted: Font: 11 pt

Formatted: Font: 12 pt

Formatted: Font: 11 pt

Formatted: Font: 11 pt

Formatted: Font: 11 pt

Formatted: Font: 11 pt

Formatted: Font: 11 pt

Formatted: Font: 11 pt

Formatted: Font: 11 pt

Formatted: Font: 11 pt

Formatted: Font: 11 pt

Formatted: Font: 11 pt

Formatted: Font: 11 pt

Formatted: Font: 11 pt

Figure 6-2 Electric Resistivity vs. Temperature – Slag+25% EL Mix

Deleted:

Heating tests have been conducted using both AC and DC power to study the conduction of electricity through the conductive concrete mix. The conductive concrete behaved like a semiconductor or a capacitor. As electrical current flows through the conductive concrete, its temperature rises and the heating rate increases. The electrical conductivity of the conductive concrete will increase as its temperature rises. The increase in electrical conductivity will cause more current to flow through under a constant voltage. Hence, the applied voltage must be controlled to maintain a gradual heating rate to avoid thermal shock to the conductive concrete.

Deleted:

Since the conductive components added only amounted to 25 percent by volume of the total materials, there are probably not enough conductive fibers and particles to form a fully interconnected electronic circuit within the concrete. Instead, these dispersed conductive materials would act as capacitors when a voltage is applied across the material. Electrical current will flow through the material if the applied voltage is high enough to cause dielectric breakdown of the material. There is a critical threshold of voltage, above which large current will go through the material like a short circuit. If the applied voltage is kept below this "break down" voltage, a "controllable" amount of current proportional to the voltage will go through the material. This behavior is similar to that of a surge protector used in computers.

6.3.4 Long-term Stability of Electric Resistivity

Deleted:

The electric resistivity of the conductive concrete is relatively low during hydration, due to the ionic conduction in the pore solution. The breakdown voltage would thus depend upon the moisture content in the material. However, there exists a stable but higher breakdown voltage after the moisture in the conductive concrete has completely dried out. For instance, no degradation in the heating performance has been observed after 5 years of deicing experiment

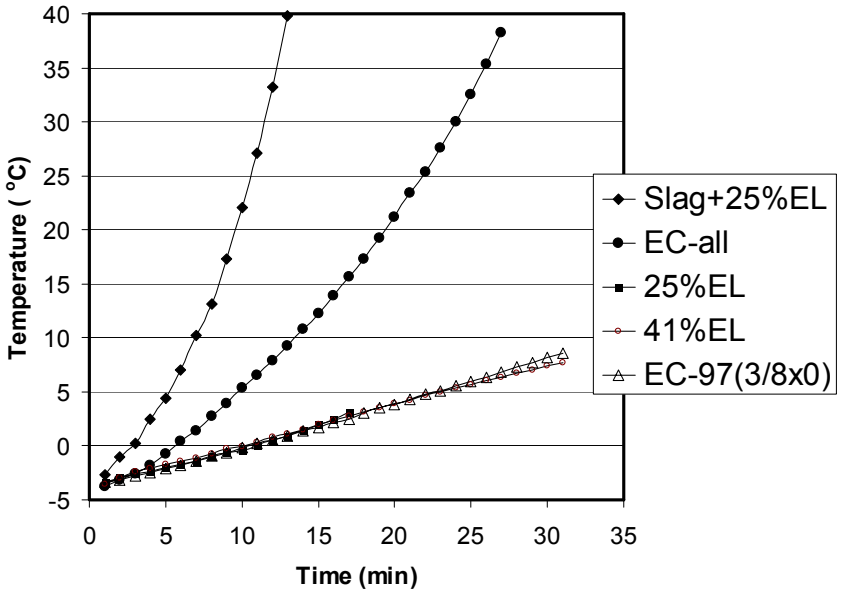

Figure 6-3 Comparison of Heating Rates of Trial Mixes

with the 1.2m by 3.6m (4 ft × 12 ft) conductive concrete test slab using steel fibers and steel shavings. To prove the same is true with the carbon concrete, a heating test was conducted on the EC-All test slab two years later. The data from the two tests are compared in Fig. 6-4. The lower electric resistivity and higher heating rate were probably due to the higher moisture content in the specimen during the earlier test.

6.4 Implementation Project – Roca Spur Bridge

Roca Spur Bridge is a 46 m (150 ft) long and 11 m (36 ft) wide, three-span highway bridge over the Salt Creek at Roca, located on Nebraska Highway 77 South about 24 km (15 miles) south of Lincoln. A railroad crossing is located immediately following the end of the bridge, making it a prime candidate for deicing application. The Roca Bridge project was let in December 2001 and construction was completed in November 2002. The bridge deck has a 36

m (117 ft) by 8.5 m (28 ft) by 102 mm (4 in.) conductive concrete inlay, which has been instrumented with thermocouples for deicing monitoring during winter storms.

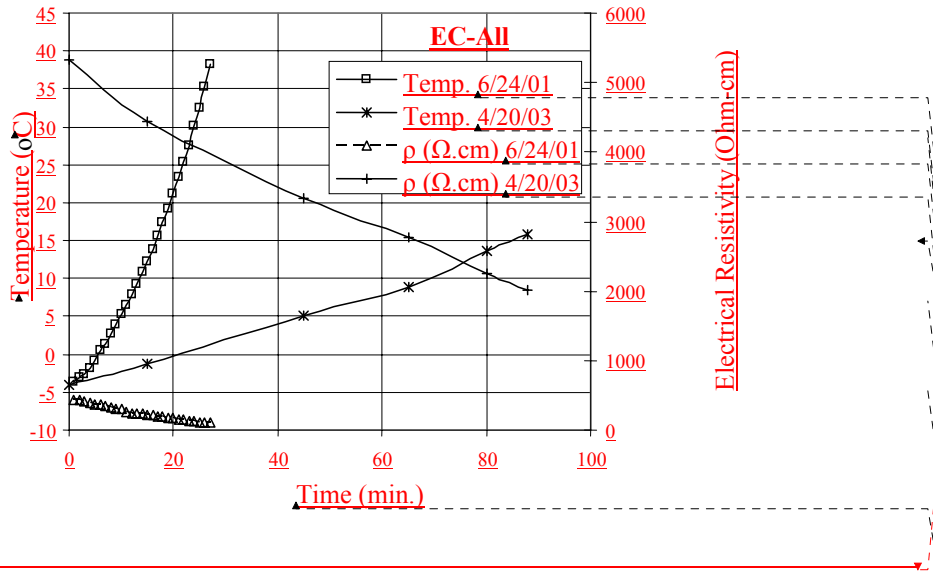

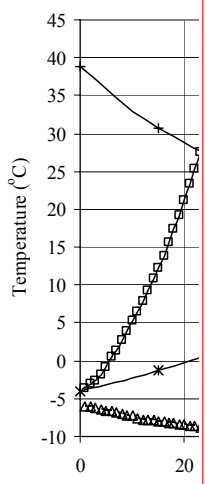

Figure 6-4 Time Effect on Electric Resistivity

6.4.1 Construction Sequence

A 102 mm (4 in.)-thick inlay of conductive concrete using the EC-All mix was cast on top of a 256 mm (10.5 in.)-thick regular reinforced concrete deck. As shown in Fig. 6-5, the inlay consisted of 52 individual 1.2m × 4.1m (4 ft × 14 ft) conductive concrete slabs. In each slab, two 89×89×6 mm (3 ½ ×3 ½ ×1/4 in.) angle irons spaced 1067 mm (3.5 ft) apart were embedded for electrodes. Thread sleeves were welded to one end of the angle irons for making

Deleted:
Formatted: Right
Formatted: Font: 11 pt
Formatted: Font: 11 pt
Formatted: Font: 11 pt
Formatted: Font: 12 pt
Formatted: Font: 11 pt
Formatted: Font: 12 pt
Formatted: Font: 12 pt
Formatted: Font: 12 pt
Deleted:

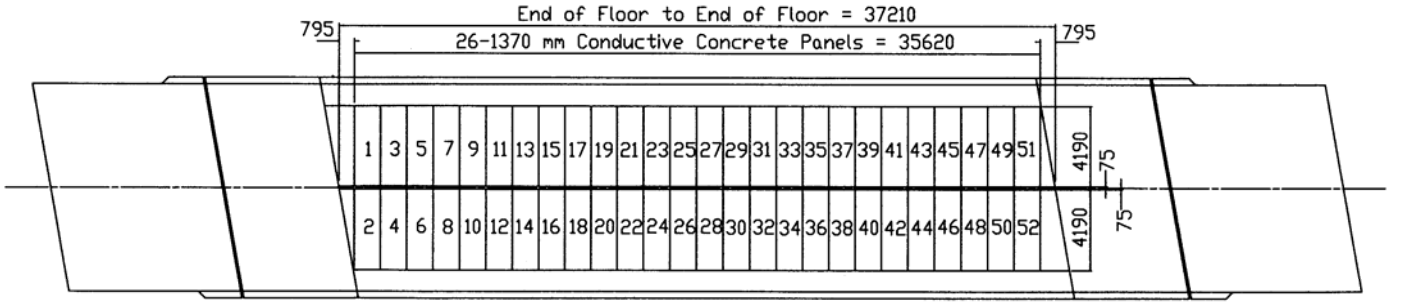

Figure 6-5 CONDUCTIVE CONCRETE PANEL LAYOUT
(Dimensions in mm)

Deleted: ¶
¶
¶
¶
¶
¶
¶
Table 3. Electrical resistivities of carbon concrete trial mixes¶
¶
¶
Specimen ... [23]

Formatted: Font: 12 pt
Formatted: Font: 12 pt
Formatted: Font: 12 pt
Formatted: Font: 12 pt
Formatted: Font: 12 pt
Formatted: Font: 12 pt
Formatted: Font: 12 pt
Formatted: Font: 12 pt
Formatted: Font: 12 pt
Formatted: Font: 12 pt
Formatted: Font: 12 pt
Formatted: Font: 12 pt
Formatted: Font: 12 pt
Formatted: Font: 12 pt
Formatted: Font: 12 pt
Formatted: Font: 12 pt
Formatted: Font: 12 pt
Formatted: Font: 12 pt
Deleted: 5
Deleted: <sp>

Deleted: Section Break (Next Page)

electrical connection. A Type TX thermocouple was installed at the center of each slab at about 13 mm (0.5 in.) below the surface to measure the slab temperature. The power chords and thermocouple wiring for each slab were secured in two PVC conduits and are accessible from junction boxes along the centerline of the bridge deck.

Deleted:

The conductive concrete inlay was cast after the regular bridge deck had been cured for 30 days. After hardening, the conductive concrete inlay was saw cut to a 102 mm (4 in.) depth along the perimeters of the individual slabs and the gaps were filled with polyurethane sealant. There was a 152 mm (6 in.) gap along the centerline of the bridge to allow power chord connections with the thread sleeves on the angle irons, as shown in Figure 6-6. The gap was then filled with a non-shrink, high-strength grout.

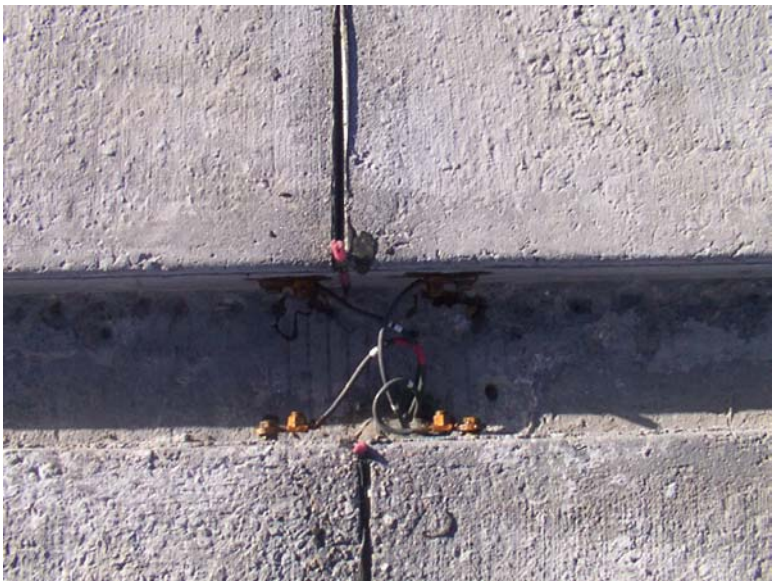

Figure 6-6 Power Chord and Angle Iron Connection

Deleted: 8

6.4.2 Integration of Power Supply, Sensors and Control Circuit

A three-phase, 600 A and 208 V AC power supply was provided by a power line nearby. A microprocessor-based controller system was installed in a control room to monitor and control the deicing operation of the 52 slabs. The system included four main elements: (1) a temperature-sensing unit; (2) a power-switching unit; (3) a current-monitoring unit; and (4) an operator-interface unit. The temperature-sensing unit took and recorded the thermocouple readings of the slabs every 15 minutes. A slab's power was turned on by the controller if the temperature of the slab was below 1.7^{o}C (35^{o}F) and turned off if the temperature was above 12.8^{o}C (55^{o}F). The power-switching unit controlled power relays to perform the desired on/off function. To ensure safety, a current-monitoring unit limited the current going through a slab to a user-specified amount. The operator-interface unit allowed a user to connect to the controller with a PC or laptop via a phone modem. The operator interface displayed all the temperature and electrical current readings of every slab in real time. A user also had the option of using a PC or laptop to download the controller-stored data into a spreadsheet.

6.4.3 Deicing Operation

The deicing controller system was completed in March 2003. Although major snow storms of 2002 were missed, the system was tested successfully under freezing temperatures. The 52 conductive concrete slabs were activated for deicing during four major snow storms of winter 2003. The climatic data of these storms were obtained from a weather station in Lincoln, Nebraska, of the National Climatic Data Center and are summarized in Table 6.4. The power was turned on 6 to 8 hours before the snow storms to preheat the slabs. The 52 slabs were divided into 26 groups with each group containing two consecutive slabs. Thus, group 1 contains slabs 1 and 2, group 2 contains slabs 3 and 4, and so on. During the December 8 storm,

Deleted:

Formatted: Indent: First line: 0"

Deleted:

Deleted:

Storm Date	Snow depth (mm)	Air temp.* (°C)	Wind speed (km/hr)	Energy (kW-hr)	Unit Cost** ($/m^2)	Powering Scheme
December 8-9, '03	165	-6.3	36	2,023	0.54	Alternating
January 25-26, '04	257	-11.1	23	2,885	0.75	Simultaneous
February 1-2, '04	145	-10.0	18	2,700	0.71	Simultaneous
February 4-6, '04	198	-7.2	19	3,797	1.00	Simultaneous

Notes:
* Average ambient temperature readings during deicing at the bridge site.
**Energy cost per unit surface area of conductive concrete inlay.

Table 6.4 Deicing Performance of Roca Spur Bridge

the odd-numbered groups were energized for 30 minutes and off for 30 minutes when the even-numbered groups were powered. This alternating form of energizing the slabs could not keep up with the low temperature, high wind and a snow rate of about 25 mm/hr (1 in./hr). As a result, the deck was partially covered with snow. The scheme was revised to energize all the slabs when the ambient temperature dropped below -1°C (30°F), and switched to alternating powering when the ambient temperature was above -1°C (30°F). The revised scheme seemed to have worked well in the later storms. Fig. 6-7 shows that the deck was free of snow cover during the February 5 storm.

Figure 6-7 Roca Bridge Deck Deicing – February 5, 2004

Formatted: Indent: First line: 0"

Formatted: Font: Bold

Deleted:

Deleted: No Slush on

The slab temperature distribution was very uniform across the deck during deicing operations, generally in the -4 to 10°C (25 to 50°F) range. As shown in Fig. 6-8, the average slab temperature was consistently about 10°C (18°F) higher than the ambient temperature. The maximum current recorded varied between 7 and 10 Amps. Fig. 6-9 shows that the electrical conductivity of the conductive concrete increased with higher average slab temperature. The peak power density delivered to the slabs varied between 360 and 560 W/m^2 (33 to 52 W/ft^2) with an average of 452 W/m^2 (42 W/ft^2). The total energy consumed by the conductive concrete slabs during the storms is summarized in Table 6.4. The energy consumed by the slabs varied from 47 to 70 kW-hr, with an average of 58 kW-hr per slab. The average energy consumption under simultaneous powering was about 3,200 kW-hr, which would cost about $260 for each major storm based on the rate of $0.08/kW-hr. The operating costs per unit area of deck surface are presented in Table 6.4. The Roca Spur Bridge project has demonstrated that using conductive concrete for deicing has the potential to become the most cost-effective roadway deicing method in the future.

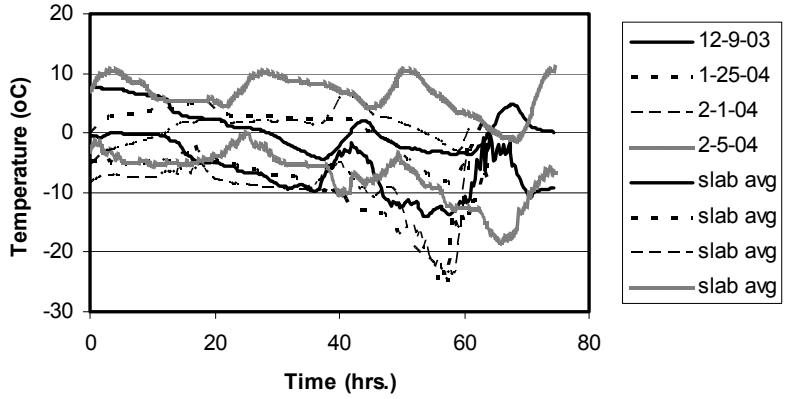

Figure 6-8 Ambient vs. Average Slab Temperature

Deleted: T…1.7…7.2…3…45…7…1 ... [24]

Formatted ... [25]

Deleted: a three-day deicing…period… ... [26]

Deleted: conductive concrete …is demonstration ... [27]

Deleted: e data…¶ ... [28]

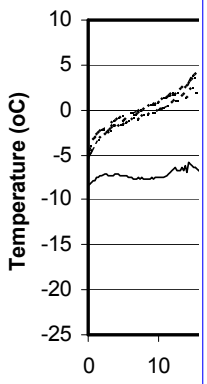

Deleted:

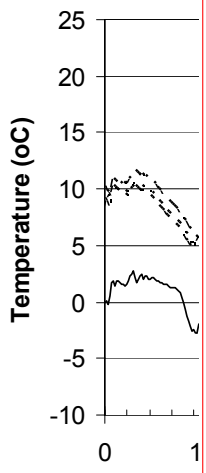

Deleted:

Deleted: 10…Temperature Data – February 1-2 ... [29]

Deleted: April 4-6

Deleted: , 2004

Deleted: 3

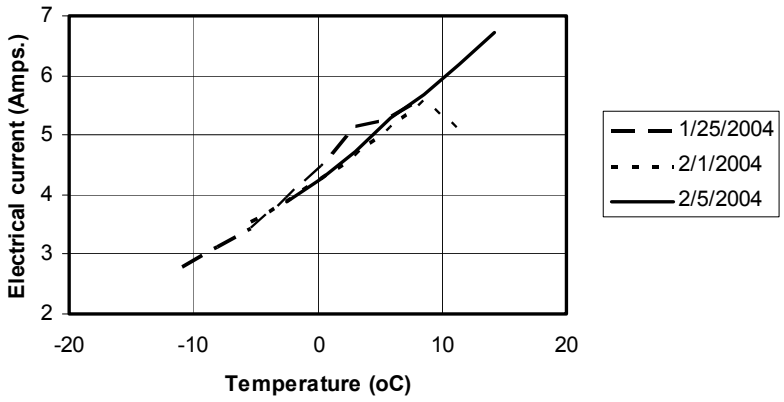

Figure 6-9 Average Current-temperature Relationship

6.4.4 Construction Costs

The construction costs of the conductive concrete inlay are itemized as follows:

- Placing, finishing, curing and saw cutting conductive concrete – $50,020
- Procuring conductive concrete materials – $80,620
- Building and installing control cabinet with sensors and power relays – $43,685
- Integrating and programming the deicing operation controller – $18,850

The total construction cost of the Roca Spur Bridge deicing system was therefore $193,175. The cost per unit surface area of the conductive concrete inlay is $635/m^2 ($59/ft^2). The heated deck of Roca Spur Bridge is the first implementation in the world using conductive concrete for deicing. The initial construction cost was high compared to the $377/m^2 ($35/ft^2) cost of a propane-fired boiler heating system recently installed in the Buffalo River Bridge in Amherst, VA in 1996[60]. Life-cycle costs, including system maintenance costs, deck repair costs and vehicle depreciation caused by deicing chemicals,

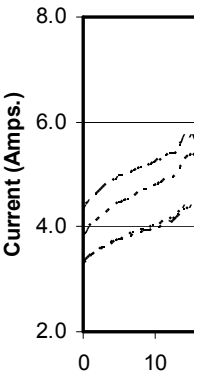

Deleted:

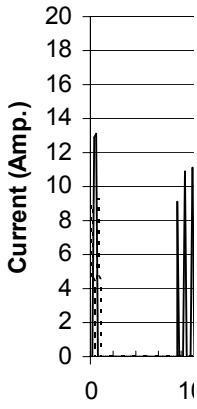

Deleted:

Deleted: 11

Deleted: Electrical Current Data – February 1-2

Deleted: April 4-6

Deleted: , 2004

Deleted: 3

Deleted: ¶
¶
Figure 10 presents the temperature traces of several slabs along with the ambient temperature.¶
The maximum current recorded varied between 9 and 18 Amps, with an average of 12.5 Amps. The peak power density delivere... [30]

Deleted:

however, should be used as the basis for cost-effectiveness comparisons of different deicing systems. In addition, the construction costs of conductive concrete overlay/inlay are expected to drop significantly when the technology becomes widely accepted.

The deicing system worked well in four major snow storms in winter 2003, and delivered an average power density of 452 W/m^2 (42 W/ft^2) to melt snow and ice. The conductive concrete deck deicing system at Roca Spur Bridge will continue to be monitored for the next several winters to evaluate its cost-effectiveness against other deicing technologies. The power controller unit of the conductive concrete overlay may be readily integrated into a RWIS to fully automate the deicing operations.

Formatted: Normal, Justified, Indent: First line: 0.5", Line spacing: Double

Deleted: ¶

CHAPTER 7

CONCLUSIONS AND RECOMMENDATIONS

Based on the findings from this study, the following conclusions were reached.

7.1 Conclusions

Mix Design

1. Use steel shaving or carbon particles of 20 percent per volume of conductive concrete as an upper bound; poor workability and surface finishability will result if higher volumetric ratios are used.
2. Using higher ratios of steel shavings or carbon particles requires an increase in w/cm ratio to improve workability, which consequently would reduce the compressive strength of the mix.
3. Use steel fibers of 2 percent per volume of conductive concrete as an upper bound; higher ratios would make mixing difficult and result in poor finish.

Optimization

4. The required electrical conductivity and mechanical strength of a bridge deck overlay for deicing can be achieved by using 15-20 percent of steel shavings or carbon particles and 1.5 percent of steel fibers per volume of conductive concrete.
5. The workability and surface finishability of the conductive concrete mix developed at the University of Nebraska are excellent and comparable to those of regular concrete.

6. The heating rates of the conductive concrete overlay using AC and DC power were similar. However, AC power is preferred since the heating is more uniform than using DC power. Using AC power would avoid "hot spots" as observed in the case of using DC power.
7. Using a thermal insulation layer underneath a conductive concrete overlay to prevent heat loss would reduce the energy consumption in deicing operations.
8. Optimum electrode spacing can be determined for a bridge deck overlay for minimum power consumption once the electric resistivity of a mix is determined.
9. Perforated steel plates should be used for electrodes to provide good conductivity across the interface with the conductive concrete.

Mix Properties

10. The mechanical and physical properties of the conductive concrete mix were evaluated in accordance with the ASTM and AASHTO specifications. The compressive strength, flexural strength, rapid freeze and thaw resistance, permeability, and shrinkage of the conductive concrete mix after 28 days have met the AASHTO requirements for bridge deck overlay construction.

Equivalent Electric Circuit Model

11. An equivalent circuit model was used to describe behavior of the conductive concrete. In this model, the conductive concrete mix is represented as a resistor, in parallel with a variable resistor and a capacitor. The resistor represents the electrical resistance of the steel shavings/carbon particles in the cement paste and the steel fibers that are directly connected. The variable resistor represents the electrical resistance of steel

fibers and steel shavings/carbon particles not directly connected. The variable capacitor represents gaps among the conductive fibers and particles within the cement paste as a dielectric material. Electrical current will flow through the material if the applied voltage is high enough to cause dielectric breakdown of the material. There is a critical threshold of voltage, above which large current will go through the material like a short circuit. If the applied voltage is kept below this "breakdown" voltage, a "controllable" amount of current proportional to the voltage will go through the material.

12. The conductive concrete behaves like a semiconductor or a capacitor. As electrical current flows through the conductive concrete, its temperature rises and the heating rate increases. The electrical conductivity of the conductive concrete will increase as its temperature rises. The increase in electrical conductivity will cause more current to flow through under a constant voltage. Hence, the applied voltage must be controlled to maintain a gradual heating rate to avoid thermal shock to the conductive concrete.

Deicing Experiments

13. Due to the potential shock hazards of using higher voltage (under the "breakdown" voltage of the conductive concrete) to heat the overlay, "step potentials" and "stray currents" have been measured during deicing operations, and the voltage and current levels were below the safe threshold for a human body.
14. The heating of the conductive concrete overlay at Roca Spur Bridge was gradual and temperature distribution across the bridge was very uniform. The average slab temperature was consistently about 10°C (18°F) higher than the ambient temperature. No sudden temperature increase or thermal shock was observed.

15. Stress due to temperature variation is in the range of 516 kN/m^2 (74 psi), which is less than the tensile strength of the concrete (3100 kN/m^2 (450 psi)).
16. The peak power density delivered to the slabs varied between 360 and 560 W/m^2 (33 to 52 W/ft^2) with an average of 452 W/m^2 (42 W/ft^2) to prevent snow accumulation and ice formation.
17. Energy costs were in the range of \$0.7 to \$1.0/m^2 (0.065/ft^2) for each major storm, based on the rate of \$0.08/kW-hr.
18. The deicing performance and the power consumption results showed that conductive concrete overlay has the potential to become the most cost-effective bridge deck deicing method.

Formatted: Font: 12 pt, Raised by 3 pt

Formatted: Font: 12 pt, Raised by 3 pt

Formatted: Font: 12 pt, Raised by 4 pt

Electric Resistance Heating Analysis

19. A coupled-field transient heat transfer analysis was conducted using a finite element model to determine the temperature distribution and power consumption in using conductive concrete overlay for bridge deck deicing. The results from the parametric study were comparable to the results from the experiments conducted during the winter of 1998.
20. The finite element model provides a useful tool to evaluate the electrical resistance heating behavior of the conductive concrete mixes with various volumetric fractions of different added conductive materials.

7.2 Recommendations for Future Research

1. A conductive concrete mix was developed at the University of Nebraska specifically for bridge deck deicing using steel fibers and steel shavings/carbon particles. These conductive materials were used to increase the electric conductivity of the concrete. Chemical admixture or other conductive materials such as iron-rich or copper-rich aggregates, to increase the electrical conductivity of concrete should be investigated.
2. The powering schemes and the control circuitry for the Roca Bridge conductive concrete overlay should be further evaluated to provide more energy-efficient deicing operations.
3. The Roca Spur Bridge deck deicing system should be monitored for at least 5 years to provide deicing and durability data for long-term performance evaluation. A life-cycle cost analysis should be performed to compare it against deicing technologies such as automated deck deicing chemicals spraying system and others.
4. Other power sources and powering schemes should be investigated for remote bridge locations. These systems would include microwave heating and photovoltaic panels.
5. The power controller unit of the conductive concrete overlay at Roca Spur Bridge may be readily integrated into a RWIS to fully automate the deicing operations. A bridge deck may be icy as long as the temperature and humidity are favorable for ice formation, not necessarily only during winter storms.

REFERENCES

1. Adkins, D. F., and Christiansen, V. T., "Freeze-Thaw Deterioration of Concrete Pavements," Journal of Material in Civil Engineering, Vol. 1, No. 2, May 1989, pp. 97-104.
2. American Association of State Highway and Transportation officials (AASHTO), "Standard Specifications for Transportation Materials and Methods of Sampling and Testing," Seventeenth Edition, 1995.
3. American Association of State Highway and Transportation officials (AASHTO), "Standard Specifications for Highway Bridges," Sixteenth Edition, 1996.
4. American Concrete Institute (ACI 318-95), "Building Code Requirements for Structural Concrete," American Concrete Institute, Detroit, MI, 1995.
5. American Concrete Institute, ACI Committee 209R, "Creep and Shrinkage in Concrete," 1992.
6. American Concrete Institute, ACI Committee 306, "Cold Weather Concreting," 1992.
7. American Concrete Institute, ACI Committee 544, "Guide for Specifying, Proportioning, Mixing, Placing, and Finishing Steel Fiber Reinforced Concrete," ACI Materials Journal, January-February, 1993, pp. 94-101.
8. American Concrete Institute, ACI Committee 544, "State-of-the Art Report on Fiber Reinforced Concrete," ACI 544. 1R-82, 1982.
9. American Society for Testing and Materials (ASTM), "Concrete and Aggregates, Section 4, V. 04.02, 1990.

10. American Society for Testing and Materials, “Significance of Tests and Properties of Concrete and Concrete-Making Materials,” 1966.
11. Anon, “ Electrical Properties of Concrete,” Concrete and Construction Engineering, London, 1963, pp. 195.
12. Axon, E. O., and Couch, R. W., “Effect of Insulating the Underside of a Bridge Deck,” Highway Research Record, No. 14, Publication 111, 1963, pp. 1-13.
13. Bagate, M., McCullough, B.F., and Fowler, D., “Construction and performance of an Experimental Thin-Bonded Concrete Overlay Pavement in Houston,” Concrete Pavement Construction, TRB 1040, Washington, D.C., 1985, pp. 25-33.
14. Banthia, N., and Mindess, S., “Fiber Reinforced Cementitious Composites: Current Practice and Future Prospects,” ACI SP-144-21, 1990.
15. Berwanger, C., and Sarkar, A. F., “Thermal Expansion of Concrete and Reinforced Concrete,” ACI Journal, November 1976, pp. 618-621.
16. Betterton, R.M, Knutson, M.J., and Marks, V.J., “Fibrous Portland Cement Concrete Overlay Research in Greene County, Iowa,” Concrete Pavement Construction, TRB 1040, Washington, D.C., 1985, pp. 1-7.
17. Britton, H. B., “The Value of Insulated Forms for Winter Bridge Construction,” Highway Research Record, No. 14, Publication 111, 1963, pp. 79-93.
18. Browne, F. R., and Cady P. D., “Deicer Mechanisms In Concrete,” American Concrete Institute, Publications SP-47-6, pp. 101-119, 1975.
19. Bukovatz J. E., and Crumpton, C. F., “Kansas’ Experience with Interlayer Membranes on Salt-Contaminated Bridge Deck,” Transportation Research Record 962, 1984, pp. 66-68.

20. Callister, W.D., Materials Science and Engineering, Chapter 16: "Composites," Wiley and Sons Publication, New York, 1985, pp.388-410.
21. Carrier, R. E., and Cady P. D., "Factors Affecting the Durability of Concrete Bridge Decks," American Concrete Institute, Publications SP-47-7, 1975, pp. 121-168.
22. Chanvillard, G., Aïtcin, P. C., and Lupien, C., "Field Evaluation of Steel Fiber Reinforced Concrete Overlay with Various Bonding Mechanisms," International Symposium on Recent Developments in Concrete Fiber Composites, TRB 1226, Washington, D.C., 1985, pp. 48-56.
23. Cheney, S., "Polymer Overlay and Injection for Concrete Bridge Deck Repair," a M.S. Thesis, under the supervision of Dr. Christopher Y. Tuan, University of Nebraska-Lincoln, March 1998.
24. Cordon, W. A., "Freezing and Thawing of Concrete Mechanisms and Control," American Concrete Institute, ACI Monograph No. 3, 1966.
25. Cress, M. D., "Heated Bridge Deck Construction and Operation in Lincoln, Nebraska," IABSE Symposium, San Francisco, 1995, pp. 449-454.
26. Downey, G. L., Delorm, R. T., Dederman, A. H., Hossack, J. W., and Strobel, G. C., "A Report on Effect of Bridge Deck Insulation on Icing Conditions," Department of Roads, State of Nebraska and U.S. Bureau of Public Roads, 1966.
27. Esch, C. D., "Insulation Performance Beneath Roads and Airfields in Alaska," Transportation Research Record 1146, 1987, pp. 23-27.
28. Fanella, D. A., and Naaman, A. E., "Stress-Strain Properties of Fiber Reinforced Mortar in Compression," ACI Journal, July-August 1985, pp. 475-483.
29. Farrar, J. J., "Electrically Conductive Concrete," GEC Journal of Science and Technology,

Vol. 45, No. 1 1978, pp. 45-48.

30. Ferdon, D., and Chen, B., "Proposed Electrical Properties of the Conductive Concrete Mix," Special Report, University of Nebraska, Computer Engineering Department, May 1999.
31. Fibercon Concrete, "A Technical Manual for the Design of Factory and Warehouse Floor Slabs using Steel Reinforcing Fibers," Fibercon International, Inc., Pennsylvania, U.S.A., 1996.
32. Ficenec, J. A., Kneip, S. D., Tadros, M. K., and Fischer L. G., "Prestressed Spliced I Girders: Tenth Street Viaduct Project, Lincoln, Nebraska," PCI Journal, September-October 1993, pp. 38-48.
33. Floyd, T. L., "Principles of Electric Circuits," 3rd Edition, Merrill Publishing Company, 1989.
34. Fontana, J. J., and Webster R. P., "Electrically Conductive Polymer-Concrete Overlays," Transportation Research Record 1041, 1985, pp. 1-10.
35. Frascoia, R. I., "Field Performance of Experimental Bridge Deck Membrane Systems in Vermont," Transportation Research Record 962, 1984, pp. 57-66.
36. Grondziel, M., "Restoration of Concrete Floors with Steel-Fiber Concrete for Aircraft at Frankfurt Airport – West Germany," Fiber Reinforced Cements and Concretes-Recent Developments, Elsevier Applied Science, 1989, pp. 610-619.
37. Gu, P., Xie, P., Fu, Y., and Beaudoin, J. J., "Microstructural Characterization Cementitious Materials: Conductivity and Impedance Methods," Materials Science of Concrete IV, The American Ceramic Society, Westerville, OH, 1995, pp. 201-262.
38. Henderson, D. J., "Experimental Roadway Heating Project on a Bridge Approach,"

Highway Research Record, No. 14, Publication 111, 1963, pp. 14-23.

39. Hey, J. C., and Kram, W.P., Transient Voltage Suppression Manual, 2nd Edition, General Electric Company, New York, 1978.
40. Hiatt, G. F. S., George, N. A., Cushman, J. R., Griffis, L. C., and Rausina, G. A., "Calcium Magnesium Acetate: Comparative Toxicity Tests and an Industrial Hygiene Site Investigation," Transportation Research Record 1157, 1988, pp. 20-26.
41. Hsu, M. T., "Production and Testing of Calcium Magnesium Acetate in Maine," Transportation Research Record 962, 1984, pp. 77-82.
42. Hutchinson, R. L., "NCHRP Synthesis of Highway Practice 99: Resurfacing with Portland Cement Concrete," TRP, National Research Council, Washington, D.C., 1982.
43. Incropera, F. P., and Dewitt, D. P., Fundamentals of Heat and Mass Transfer, Third Edition, John Wiley & Sons, New York, 1990.
44. Jones, R. H., "Developments in the British Approach to Prevention of Frost Heave in Pavements," Transportation Research Record 1146, 1987, pp. 33-40.
45. Karlekar, B. V., and Desmond, R. M., Heat Transfer, Second Edition, West Publication Co., Minnesota, U.S.A., 1982.
46. Kuemmel, D. E., "Managing Roadway Snow and Ice Control Operations," Transportation Research Record, NCHRP, Synthesis 207, 1994.
47. Lee, R. C., Sackos, J. T., Nydahl, J. E., and Pell, K. M., "Bridge Heating Using Ground-Source Heat Pipes," Transportation Research Record 962, 1984, pp. 51-57.
48. MacGregor, J. G., "Reinforced Concrete Mechanics and Design," 2nd Edition, Prentice Hall, Englewood Cliffs, New Jersey, 1992.

49. MacMaster, J. B., and Wrong, G. A., "The Role of Extruded Expanded Polystyrene in Ontario's Provincial Transportation System," Transportation Research Record 1146, 1987, pp. 10-22.

50. Maxwell, J. C., Electricity and Magnetism, Oxford University Press, 1904.

51. McCarter, W. J., and Brousseau, R., "The AC Response of Hardened Cement," Cement Concrete Research, 20, 1990, pp. 891-900.

52. Mcelroy, A. D., Blackburn, R. R., Hagymassy, J., and Kirchner, H. W., "Comparative Study of Chemical Deicers," Transportation Research Record 1157, 1988, pp. 1-11.

53. Mcelroy, A. D., Blackburn, R. R., Hagymassy, J., and Kirchner, H. W., "Study on Wetting Salt and Sand Stockpiles with Liquid Calcium Chloride," Transportation Research Record 1157, 1988, pp. 38-43.

54. Mcelroy, A. D., Blackburn, R. R., Hagymassy, J., Kirchner, H. W., and Stevens, D. L., "Comparative Evaluation of Calcium Magnesium Acetate and Rock Salt," Transportation Research Record 1157, 1988, pp. 11-19.

55. McGhee, K.H., "NCHRP Synthesis of Highway Practice 204: Portland Cement Concrete Resurfacing," TRP, National Research Council, Washington, D.C., 1994.

56. Mehta, K. P., Concrete - Structure, Properties, and Materials, Prentice-Hall, Inc., Englewood Cliffs, New Jersey, 1986.

57. Nadezhdin, A., Mason, D. A., Lawless, D. F., and Fedosoff, J. P., "The Effect of Deicing Chemicals on Reinforced Concrete," Transportation Research Record 1157, 1988, pp. 31-37.

58. Nanni, A., Ludwig, D. A., and McGillis, M. T., "Plastic Shrinkage Cracking of Restrained Fiber-Reinforced Concrete," Transportation Research Record, No. 1382, pp. 69-72, 1993.

59. Neville, A. M., Properties of Concrete, Fourth Edition, John Wiley & Sons, Inc., New York, 1996.

60. News Item, "Heated Pipes Keep Deck Ice Free," Civil Engineering, ASCE, Vol. 68, No. 1, January 1998, pp. 19-20.

61. Oosterbaan, M. D., and Leonards, G. A., "Use of Insulating Layer to Attenuate Frost Action in Highway Pavements," Highway Research Record, No. 101, Publication 1318, 1965, pp. 11-27.

62. Orchard, D. F., Concrete Technology - Properties of Material, V. 1, Fourth Edition, Applied Science Publishers LTD, London, 1979.

63. Packard, R.G., and Ray, G.K., "Performance of Fiber-Reinforced Concrete Pavement," Fiber Reinforced Concrete- International Symposium, ACI SP-81, 1984, pp. 325-349.

64. Popovics, S., Fundamentals of Portland Cement Concrete: A Quantitative Approach, Vol. 1: Fresh Concrete, John Wiley & Sons, 1982.

65. Popovics, S., Concrete-Making Materials, Hemisphere Publishing Corporation, 1979.

66. Powers, T. C., "Freezing Effects in Concrete," American Concrete Institute, Publications SP-47-1, 1975, pp. 1-11.

67. Rabideau, A. J., Weber, A. S., and Matsumoto, M. R., "Impact of Calcium Magnesium Acetate Road Deicer on POTW Operation," Journal of Water Resources Planning and Management, Vol. 113, No. 2, March, 1987, pp. 311-315.

68. Rainiero, J. M., "Investigation of the Ice-Retardant Characteristics of Verglimit-Modified Asphalt," Transportation Research Record 1157, 1988, pp. 44-53.

69. Ramachandran, V. S., Feldman, R. F., and Beaudoin, Concrete Science- Treatise on Current Research, Heyden & Son Inc., Philadelphia, PA, USA, 1981.

70. Ramakrishnan, V., “Superplasticized Fiber-Reinforced Concrete for the Rehabilitation of Bridges and Pavements,” International Symposium on Mechanical Properties of Special Concrete, TRB 1003, Washington, D.C., 1984, pp. 4-11.

71. Report on "Polymer Injection / Ultra sonic Pulse-Echo PORT/UPE" System for Concrete Bridge Deck Repair," by University of Nebraska-Lincoln, Omaha Campus, Center for Infrastructure Research- Omaha Campus, U.S. Army Corps of Engineers, (CPAR) Project, 1997.

72. Report on “Cost Analysis for Snow Removal During the winter of 1998,” Omaha Public Works, March 1999.

73. Sandegren E., “The Use of Cellular Plastic in Swedish Railways to Insulate the Track Against Frost,” Transportation Research Record 1146, 1987, pp. 28-32.

74. Schwartx, D. R., “D-Cracking of Concrete Pavements,” Transportation Research Record 134, 1987.

75. Scuderi, C. A., Mason, T. O., and Jennings, H. M., “Impedance Spectra of Hydrated Cement Pastes,” Journal of Material Science, 26, 1991, pp. 349.

76. Slick, D. S., “Effects of Calcium Magnesium Acetate on Pavements and Motor Vehicles,” Transportation Research Record 1157, 1988, pp. 27-30.

77. Transportation Research Board, “Snow Removal and Ice Control Technology,” Transportation Research Record, No. 1387, 1993.

78. Wang, K., Monteiro, P. J., Rubinsky, B., and Arav, A., “Microscopic Study of Ice Propagation in Concrete,” ACI Materials Journal, July-August 1996, pp. 370-377.

79. Whittington, H., McCarter W., and Forde, M.C., “The Conduction of Electricity through Concrete,” Magazine of Concrete Research, 33, No. 114, 1981, pp. 48-60.

80. Xie, P., and Beaudoin, J. J., "Electrically Conductive Concrete and Its Application in Deicing," Advances in Concrete Technology, Proceedings of the Second CANMET/ACI International Symposium, Las Vegas, Nevada, USA, 1995, pp. 399-417.

81. Xie, P., and Tang, M., "Effect of Portland Cement Paste-Aggregate Interface on Electrical Conductivity and Chemical Corrosion Resistance of Mortar," Il Cemento, 85 [1], 1988, pp. 33-42.

82. Xie, P., Gu, P., and Beaudoin, J. J., "Conductive Concrete Cement-Based Compositions," U.S. Patent 5,447,564, 10 pp., 1995.

83. Xie, P., Gu, P., and Beaudoin, J. J., "Electrical percolation phenomena in cement composites containing conductive fibers," Journal of Materials Science, Vol. 31, Issue No. 15, August 1996, pp. 4093-4097.

84. Yehia, S. A., and Tuan, C.Y., "Conductive Concrete Overlay for Bridge Deck Deicing," ACI Materials Journal, Vol. 96, No. 3, May-June 1999, pp. 382-390.

85. Yehia, S. A., Tuan, C.Y., Ferdon, D., and Chen, B., "Conductive Concrete Overlay for Bridge Deck Deicing: Mix Design, Optimization, and Properties," ACI Materials Journal, Vol.97, No.2, March-April 2000, pp.172-181.

86. Zenewitz, J. A., "Survey of Alternatives to the Use of Chlorides for Highway Deicing," Report No. FHWA-RD-77-52, May 1977.

Page 125: [1] Formatted	**Christopher Tuan**	**2/23/2004 3:46:00 PM**

Font: 12 pt

Page 125: [1] Formatted	**Christopher Tuan**	**2/23/2004 3:45:00 PM**

Font: (Default) Times New Roman, 12 pt

Page 125: [1] Formatted	**Christopher Tuan**	**2/23/2004 3:45:00 PM**

Font: 12 pt

Page 125: [2] Formatted	**Christopher Tuan**	**2/23/2004 3:46:00 PM**

Font: 12 pt

Page 125: [2] Formatted	**Christopher Tuan**	**2/23/2004 3:45:00 PM**

Font: (Default) Times New Roman, 12 pt

Page 125: [2] Formatted	**Christopher Tuan**	**2/23/2004 3:45:00 PM**

Font: 12 pt

Page 125: [3] Formatted	**Christopher Tuan**	**2/23/2004 3:46:00 PM**

Font: 12 pt

Page 125: [3] Formatted	**Christopher Tuan**	**2/23/2004 3:45:00 PM**

Font: (Default) Times New Roman, 12 pt

Page 125: [3] Formatted	**Christopher Tuan**	**2/23/2004 3:45:00 PM**

Font: 12 pt

Page 125: [4] Formatted	**Christopher Tuan**	**2/23/2004 3:46:00 PM**

Font: 12 pt

Page 125: [4] Formatted	**Christopher Tuan**	**2/23/2004 3:45:00 PM**

Font: (Default) Times New Roman, 12 pt

Page 125: [4] Formatted	**Christopher Tuan**	**2/23/2004 3:45:00 PM**

Font: 12 pt

Page 125: [5] Formatted	**Christopher Tuan**	**2/23/2004 3:46:00 PM**

Font: 12 pt

Page 125: [5] Formatted	**Christopher Tuan**	**2/23/2004 3:45:00 PM**

Font: (Default) Times New Roman, 12 pt

Page 125: [5] Formatted	**Christopher Tuan**	**2/23/2004 3:45:00 PM**

Font: 12 pt

Page 125: [6] Formatted	**Christopher Tuan**	**2/23/2004 3:46:00 PM**

Font: 12 pt

Page 125: [6] Formatted	**Christopher Tuan**	**2/23/2004 3:45:00 PM**

Font: (Default) Times New Roman, 12 pt

Page 125: [6] Formatted	**Christopher Tuan**	**2/23/2004 3:45:00 PM**

Font: 12 pt

Page 125: [7] Formatted	**Christopher Tuan**	**2/23/2004 3:46:00 PM**

Font: 12 pt

Page 125: [7] Formatted	**Christopher Tuan**	**2/23/2004 3:45:00 PM**

Font: (Default) Times New Roman, 12 pt

Page 125: [7] Formatted	**Christopher Tuan**	**2/23/2004 3:45:00 PM**

Font: 12 pt

Page 125: [8] Formatted	**Christopher Tuan**	**2/23/2004 3:46:00 PM**

Font: 12 pt

Page 125: [8] Formatted	**Christopher Tuan**	**2/23/2004 3:45:00 PM**

Font: (Default) Times New Roman, 12 pt

Page 125: [8] Formatted	**Christopher Tuan**	**2/23/2004 3:45:00 PM**

Font: 12 pt

Page 125: [9] Formatted	**Christopher Tuan**	**2/23/2004 3:46:00 PM**

Font: 12 pt

Page 125: [9] Formatted	**Christopher Tuan**	**2/23/2004 3:45:00 PM**

Font: (Default) Times New Roman, 12 pt

Page 125: [9] Formatted	**Christopher Tuan**	**2/23/2004 3:45:00 PM**

Font: 12 pt

Page 125: [10] Formatted	**Christopher Tuan**	**2/23/2004 3:46:00 PM**

Font: 12 pt

Page 125: [10] Formatted	**Christopher Tuan**	**2/23/2004 3:45:00 PM**

Font: (Default) Times New Roman, 12 pt

Page 125: [10] Formatted	**Christopher Tuan**	**2/23/2004 3:45:00 PM**

Font: 12 pt

Page 125: [11] Formatted	**Christopher Tuan**	**2/23/2004 3:46:00 PM**

Font: 12 pt

Page 125: [11] Formatted	**Christopher Tuan**	**2/23/2004 3:45:00 PM**

Font: (Default) Times New Roman, 12 pt

Page 125: [11] Formatted	**Christopher Tuan**	**2/23/2004 3:45:00 PM**

Font: 12 pt

Page 125: [12] Formatted	**Christopher Tuan**	**2/23/2004 3:46:00 PM**

Font: 12 pt

Page 125: [12] Formatted	**Christopher Tuan**	**2/23/2004 3:45:00 PM**

Font: (Default) Times New Roman, 12 pt

Page 125: [12] Formatted	**Christopher Tuan**	**2/23/2004 3:45:00 PM**

Font: 12 pt

Page 125: [13] Formatted	**Christopher Tuan**	**2/23/2004 3:46:00 PM**

Font: 12 pt

Page 125: [13] Formatted	**Christopher Tuan**	**2/23/2004 3:45:00 PM**

Font: (Default) Times New Roman, 12 pt

Page 125: [13] Formatted	**Christopher Tuan**	**2/23/2004 3:45:00 PM**

Font: 12 pt

Page 125: [14] Formatted	**Christopher Tuan**	**2/23/2004 3:46:00 PM**

Font: 12 pt

Page 125: [14] Formatted	**Christopher Tuan**	**2/23/2004 3:45:00 PM**

Font: (Default) Times New Roman, 12 pt

Page 125: [14] Formatted	**Christopher Tuan**	**2/23/2004 3:45:00 PM**

Font: 12 pt

Page 125: [15] Formatted	**Christopher Tuan**	**2/23/2004 3:46:00 PM**

Font: 12 pt

Page 125: [15] Formatted	**Christopher Tuan**	**2/23/2004 3:45:00 PM**

Font: (Default) Times New Roman, 12 pt

Page 125: [15] Formatted	**Christopher Tuan**	**2/23/2004 3:45:00 PM**

Font: 12 pt

Page 125: [16] Formatted	**Christopher Tuan**	**2/23/2004 3:46:00 PM**

Font: 12 pt

Page 125: [16] Formatted	**Christopher Tuan**	**2/23/2004 3:45:00 PM**

Font: (Default) Times New Roman, 12 pt

Page 125: [16] Formatted	**Christopher Tuan**	**2/23/2004 3:45:00 PM**

Font: 12 pt

Page 125: [17] Formatted	**Christopher Tuan**	**2/23/2004 3:46:00 PM**

Font: 12 pt

Page 125: [17] Formatted	**Christopher Tuan**	**2/23/2004 3:45:00 PM**

Font: (Default) Times New Roman, 12 pt

Page 125: [17] Formatted	**Christopher Tuan**	**2/23/2004 3:45:00 PM**

Font: 12 pt

Page 125: [18] Formatted	**Christopher Tuan**	**2/23/2004 3:46:00 PM**

Font: 12 pt

Page 125: [18] Formatted	**Christopher Tuan**	**2/23/2004 3:45:00 PM**

Font: (Default) Times New Roman, 12 pt

Page 125: [18] Formatted	**Christopher Tuan**	**2/23/2004 3:45:00 PM**

Font: 12 pt

Page 125: [19] Formatted	**Christopher Tuan**	**2/23/2004 3:46:00 PM**

Font: 12 pt

Page 125: [19] Formatted	**Christopher Tuan**	**2/23/2004 3:45:00 PM**

Font: (Default) Times New Roman, 12 pt

Page 125: [19] Formatted	**Christopher Tuan**	**2/23/2004 3:45:00 PM**

Font: 12 pt

Page 125: [20] Formatted	**Christopher Tuan**	**2/23/2004 3:46:00 PM**

Font: 12 pt

Page 125: [20] Formatted	**Christopher Tuan**	**2/23/2004 3:45:00 PM**

Font: (Default) Times New Roman, 12 pt

Page 125: [20] Formatted	**Christopher Tuan**	**2/23/2004 3:45:00 PM**

Font: 12 pt

Page 128: [21] Formatted	**Christopher Tuan**	**2/23/2004 4:00:00 PM**

Font: 10 pt, Raised by 4 pt

Page 128: [22] Formatted	**Christopher Tuan**	**2/23/2004 4:09:00 PM**

Font: 11 pt

Page 128: [22] Formatted	**Christopher Tuan**	**2/23/2004 4:09:00 PM**

Font: 11 pt, Raised by 4 pt

Table 3. Electrical resistivities of carbon concrete trial mixes

Specimen	Initial Temperature	Temperature Range (^{o}C)	Electrical Resistivity (Ω.cm)
EC-100 (3/8×0)	-4^{o}C	-4° ~ 4.5°	564 -381
EC-100 (3/8×0)	2^{o}C	2° ~ 10°	451 - 323
EC-100 (10×0)	-4^{o}C	-4° ~ 4.5°	721 - 576
EC-100 (10×0)	2^{o}C	2° ~ 15.5°	519 - 392
EC-98C (10×0)	-4^{o}C	-4° ~ -1°	939 - 853
EC-98C (10×0)	2^{o}C	2° ~ 4.5°	733 - 669
EC-97 (3/8×0)	-4^{o}C	-4° ~ 10°	564 - 403
EC-97 (3/8×0)	2^{o}C	2° ~ 15.5°	518 - 357
FP-428 (100×0)	-4^{o}C	-4° ~ 2°	1048 - 958
FP-428 (100×0)	2^{o}C	2° ~ 4.5°	902 - 900
EC-all	**-4^{o}C**	**-4° ~ 38°**	**435 - 108**
EC-all	**2^{o}C**	**2° ~ 49^{o}**	**395 - 101**
41% EL	-4^{o}C	-4° ~ 7°	1006 - 762
41% EL	2^{o}C	2° ~ 13°	846 - 702
BD 20%	-4^{o}C	-4° ~ -3°	8077 -7404
BD 20%	2^{o}C	2° ~ 7°	7500 - 5226
slag + 25% EL	**-4^{o}C**	**-4° ~ 40°**	**808 - 208**
slag + 25% EL	**2^{o}C**	**2° ~ 35°**	**705 - 219**
25% EL	-4^{o}C	-4° ~ 4.5^{o}	1813 - 728
25% EL	2^{o}C	2° ~ 4.5°	830 - 759

Page 137: [24] Deleted **College of Engineering and Technology** **2/24/2004 4:34:00 PM**

T

Page 137: [24] Deleted **College of Engineering and Technology** **2/24/2004 9:42:00 PM**

1.7

Page 137: [24] Deleted **College of Engineering and Technology** **2/24/2004 9:43:00 PM**

7.2

Page 137: [24] Deleted **College of Engineering and Technology** **2/24/2004 9:42:00 PM**

3

Page 137: [24] Deleted **College of Engineering and Technology** **2/24/2004 9:42:00 PM**

45

Page 137: [24] Deleted **College of Engineering and Technology** **2/25/2004 1:13:00 AM**

7

Page 137: [24] Deleted **College of Engineering and Technology** **2/25/2004 1:13:00 AM**

1

Page 137: [24] Deleted **College of Engineering and Technology** **2/25/2004 6:39:00 AM**

Page 137: [25] Formatted **Christopher Tuan** **2/25/2004 11:24:00 AM**

Raised by 3 pt

Page 137: [25] Formatted **Christopher Tuan** **2/25/2004 11:24:00 AM**

Font: 10 pt, Raised by 3 pt

Page 137: [25] Formatted **Christopher Tuan** **2/25/2004 11:23:00 AM**

Font: 10 pt, Raised by 4 pt

Page 137: [26] Deleted **College of Engineering and Technology** **2/25/2004 1:29:00 AM**

a three-day deicing

Page 137: [26] Deleted **College of Engineering and Technology** **2/25/2004 1:29:00 AM**

period

Page 137: [26] Deleted **College of Engineering and Technology** **2/25/2004 1:31:00 AM**

Page 137: [27] Deleted **Christopher Tuan** **2/25/2004 1:24:00 PM**

conductive concrete

Page 137: [27] Deleted	Christopher Tuan	2/25/2004 1:25:00 PM

is demonstration

Page 137: [28] Deleted	College of Engineering and Technology	2/25/2004 6:48:00 AM

e data

Page 137: [28] Deleted	College of Engineering and Technology	2/25/2004 6:31:00 AM

Page 137: [29] Deleted	College of Engineering and Technology	2/24/2004 4:22:00 PM

10

Page 137: [29] Deleted	College of Engineering and Technology	2/25/2004 12:54:00 AM

Temperature Data – February 1-2

Page 138: [30] Deleted	College of Engineering and Technology	2/25/2004 6:31:00 AM

Figure 10 presents the temperature traces of several slabs along with the ambient temperature.

The maximum current recorded varied between 9 and 18 Amps, with an average of 12.5 Amps. The peak power density delivered to the slabs varied between 360-720 W/m^2 (33 to 67 W/ft^2) with an average of 500 W/m^2 (46 W/ft^2). Figure 11 presents the corresponding current traces of the selected slabs. The energy consumed by the conductive slabs during the three-day period varied from 12.6 to 34.6 kW-hr, with an average of 24 kW-hr per slab. The total energy consumption was calculated from

the electric power curves from the slabs to be 1,270 kW-hr, and would cost about $100 based on the rate of $0.08/kW-hr.

TABLE OF CONTENTS

ABSTRACT…… vi

LIST OF FIGURES…… viii

LIST OF TABLES…….. xiii

CHAPTER 1 INTRODUCTION

1.1 Problem Statement…… 1

1.2 Background Information……... 1

1.3 Research Objectives……. 2

1.4 Organization of the Report……... 3

CHAPTER 2 LITERATURE REVIEW

2.1 Protections against Frost Action……... 5

2.1.1 Concrete in Cold Weather……... 5

2.1.2 Deterioration of Concrete…… 6

2.1.2.1 Deterioration line (D-line cracking)…… 6

2.1.2.2 Pattern Cracking……..... 7

2.1.2.3 Spalling…… 7

2.1.2.4 Scaling……. 8

2.1.3 Thawing and Freezing Mechanism…….. 8

2.1.4 Factors Affecting Frost Resistance of Concrete…….. 8

2.1.4.1 Shrinkage and Moisture Movement of Concrete……. 9

2.1.4.2 Alkali-Aggregate Reaction…….. 11

2.2 Using Deicing Chemicals……. 12

2.3 Alternative to the Use of Chloride…… 13

2.4 Insulation against Freezing……... 16

2.5 Heating Systems……... 17

2.5.1 Heating Using Ground Source Heat Pipes…….. 17

2.5.2 Heating Using Infrared Heat Lamps…… 18

2.5.3 Heating Using Electric Heating Cables……... 18

2.5.4 Heating Using Heated Fluids……... 20

2.5.5 Electrically Conductive Concrete……... 22
2.6 Previous Experience with Fiber-Reinforced Concrete……. 24
2.7 Conduction of Electricity through Concrete……. 25
2.7.1 Electrical Conduction Models for Concrete…… 26
2.7.2 Equivalent Circuit Models for Cement Paste Systems…… 28
CHAPTER 3 CONDUCTIVE CONCRETE MIX DESIGN
3.1 Background……... 30
3.2 Conductive Concrete Mix Design…… 30
3.2.1 Mix Design by Xie et al. (1995)…….. 30
3.2.2 Mix Design by Yehia and Tuan (1998)……... 31
3.3 Material Properties……... 31
3.3.1 Steel Shavings…….. 31
3.3.2 Steel Fiber…… 33
3.3.3 Other Materials…… 34
3.4 Mixing Procedure……. 34
3.5 Optimization……. 35
3.5.1 Category 1 and Category 2…….. 35
3.5.2 Category 3…… 36
3.5.2.1 First-Stage Evaluation……. 36
3.5.2.1.1 Mechanical and Physical Properties……. 37
3.5.2.1.2 Small Slab Heating Experiments…….. 38
3.5.2.2 Second-Stage Evaluation……. 44
3.5.2.2.1 Mechanical Properties…….. 45
3.5.2.2.2 Effect of Hydration Time on Electrical Conductivity.. 45
3.5.2.2.3 Slab Heating Tests…… 47
3.5.2.2.4 Conduction of Electricity in Conductive Concrete…... 49
3.5.2.2.5 Slab Heating Rate Comparison – AC vs. DC Power… 50
3.5.2.2.6 Size Effect……. 52
3.5.2.2.7 Evaluation of the Electric Resistivity……... 53

3.5.3 Problems and Solutions……... 53

CHAPTER 4 EVALUATION OF MECHANICAL AND PHYSICAL PROPERTIES OF THE CONDUCTIVE CONCRETE MIX

4.1 Background……... 58

4.2 Specimen Fabrication……... 59

4.3 Mechanical Properties…….. 61

4.3.1 Compressive Strength…….. 61

4.3.2 Stress-Strain Relation and Modulus of Elasticity…… 63

4.3.2.1 Stress-Strain Relation…….. 63

4.3.2.2 Modulus of Elasticity……... 63

4.3.3 Flexural Strength……. 66

4.3.4 Rapid Freeze and Thaw Resistance……. 67

4.3.5 Shrinkage……. 70

4.4 Physical Properties……... 71

4.4.1 Permeability……. 72

4.4.2 Thermal Conductivity…….. 77

4.4.2.1 Theoretical Approach…….. 77

4.4.2.1 Experimental Approach……... 78

4.5 Test Results……... 81

CHAPTER 5 DEICING EXPERIMENTS WITH CONDUCTIVE CONCRETE OVERLAY

5.1 Introduction…….. 82

5.2 Conductive Concrete Overlay Construction……. 82

5.2.1 The Concrete Slabs…….. 82

5.2.2 The Conductive Concrete Mix…… 87

5.2.3 Instrumentation…… 89

5.2.3.1 Thermocouples…… 89

5.2.3.2 Weather Station……... 94

5.2.3.3. AC Power Supply……... 95

5.2.3.4. Data Acquisition System…… 95

5.3 Deicing and Anti-icing Experiments…… 96

5.3.1 Anti-icing Experiments…… 98
5.3.2 Deicing Experiments……... 100
5.3.3 Energy Consumption and Costs…….. 103
5.4. Design Issues……... 106
5.4.1 Electrical Conduction Model Validation…… 106
5.4.2 High Voltage and Safety Concerns…… 107
5.4.3 Thermal Stresses Due to Overlay Heating……. 107
5.4.4 Interface Shear Between Bridge Deck and Overlay……... 108
5.4.5 Minimum Temperature Reinforcement in an Overlay……... 108
5.4.6 Effect of Slab Geometry on Heating Rate……. 109
5.5 Electric Resistance Heating of Conductive Concrete……... 109
5.5.1 Coupled-field Governing Differential Equations…… 110
5.5.2 Transient Thermal Finite Element Analysis…… 111
5.5.3 Comparison of Results……. 115

CHAPTER 6 AN IMPLEMENTATION OF CONDUCTIVE CONCRETE OVERLAY

6.1 Background……... 121
6.2 Conductive Concrete Utilizing Carbon and Graphite Products…… 122
6.3 Test Results……... 123
6.3.1 Workability, Finishability and Compressive Strength…… 123
6.3.2 Heating Rate…… 123
6.3.3 Electric Resistivity……... 126
6.3.4 Long-term Stability of Electric Resistivity…….. 129
6.4 Implementation Project – Roca Spur Bridge…… 130
6.4.1 Construction Sequence…… 131
6.4.2 Integration of Power Supply, Sensors and Control Circuits…… 134
6.4.3 Deicing Operation…… 134
6.4.4 Construction Costs……... 138

CHAPTER 7 CONCLUSIONS AND RECOMMENDATIONS

7.1 Conclusions…….. 140

7.2 Recommendation for Future Research…… 144

REFERENCE……..... 145

ABSTRACT

Traditionally, removing ice from pavement can be accomplished by a combination of several methods, such as plowing, natural melting, traffic movement, and chemical treatment. Because the bond between ice and pavement is strong, removal by plowing alone is not effective. Chemical treatment helps break the bond by melting into the ice and spreading under the ice layer. Most highway winter maintenance depends on using chemicals and fine granular particles as a primary means for deicing. However, using deicing chemicals and salt has caused damage to concrete and corrosion of reinforcing bars in concrete bridge decks which is partially responsible for the rapid deterioration of the transportation infrastructure in the U.S. The search for improved deicing methods has been a research focus for quite some time. The use of electric heating cables and heated fluid in pipes have been attempted, however, those techniques were too expensive to operate and difficult to maintain.

Conductive concrete is produced by adding electrically conductive components to a regular concrete mix to attain stable electrical conductivity. Due to its electrical resistance, a thin layer of conductive concrete can generate enough heat to prevent ice formation on concrete pavement when connected to a power source. A concrete mix containing 1.5 percent of steel fibers and 25 percent of steel shavings by volume was developed specifically for concrete bridge deck deicing. The mix has adequate strength and provides a thermal power density of 600 W/m^2, producing a heating rate of 0.25^oC/min under subfreezing temperature. The average energy cost was about \$0.8/m^2 per snow storm. A comparison of conductive concrete technology against other deicing technologies in the literature has revealed that it has the potential to become the most cost-effective deicing technology in the future.

This research project has national and international implications. Statistics indicate that 10 to 15 percent of all roadway accidents are directly related to weather conditions. This percentage alone represents thousands of human injuries and deaths and millions of dollars in property damage annually. Ice accumulation on paved surfaces is not merely a concern for motorists; ice accumulation on pedestrian walkways accounts for numerous personal injuries, due to slipping and falling. The conductive concrete deicing technology is readily available for implementation at accident-prone areas such as bridge overpasses, exit ramps, airport runways, street intersections, sidewalks, and driveways.

During development of the conductive concrete, several drawbacks about using steel shavings in the mix were noticed. Carbon and graphite products were subsequently used to replace steel shavings in the conductive concrete design. The electrical conductivity and the associated heating rate were improved with the carbon products. A conductive concrete deck has been implemented for deicing on a highway bridge at Roca, located about 24 km (15 miles) south of Lincoln, Nebraska. The Roca Spur Bridge has a 46 m long and 11 m wide conductive concrete deck overlay. The Roca Bridge project was let in December 2001 and construction completed in November 2002. The overlay has been instrumented with temperature and current sensors to provide data for heating performance monitoring during winter storms. Experimental data and operating costs are presented in this report.

LIST OF FIGURES

Figure 2-1 D-line cracking spreading from sidewalk joint 7

Figure 2-2 Spalling of concrete surface, exposing a reinforcing bar 7

Figure 2-3 Scaling of concrete slab surface 8

Figure 2-4 Styrofoam insulating layer used on graded subgrade for flexible pavement in Michigan (1962).....16

Figure 2-5 Electric cables in the bridge approach roadway, New Jersey 1961.....19

Figure 2-6 Deck heating system on approaches of a pedestrian overpass in Lincoln, Nebraska, 1993.....20

Figure 2-7 Deck heating system in the Buffalo River Bridge, Amherst, Virginia, in November 1996 22

Figure 3-1 Steel shavings 32

Figure 3-2 Results from sieve analysis.....33

Figure 3-3 Low carbon steel fibers.....34

Figure 3-4 Typical conductive concrete mix.....38

Figure 3-5 Surface finishability of conductive concrete 38

Figure 3-6 Steel plates are used for electrodes.....40

Figure 3-7 Small conductive concrete slab heating test 40

Figure 3-8 (a) Slab heating test - 20% conductive material 41

Figure 3-8(b) Slab heating test - 15 % conductive material.....42

Figure 3-8(c) Slab heating test - 15 % conductive material 43

Figure 3-9 Conductive concrete test specimens-Category 3 (stage two evaluation).....44

Figure 3-10 Slab under testing using DC-power 47

Figure 3-11 Slab heating tests 48

Figure 3-12 A model for conduction of electricity through conductive concrete ... 50

Figure 3-13 Conduction of electricity through conductive concrete – model parameters 50

Figure 3-14 Power consumption – AC vs. DC 51

Figure 3-15(a) 1 ft x 1ft x 2 in. slabs 52

Figure 3-15(b) 3 ft x 2ft x 3.5 in. slabs 53

Figure 3-16 Smooth surface between the steel plate and concrete surface 54

Figure 3-17(a) Steel plate with opening 55

Figure 3-17(b) 1 in. steel plate welded on WWF with 0.5 in. spacing 55

Figure 3-17(c) 3/4 in. corrugated steel plate welded on steel posts with 1.25 in. spacing 56

Figure 3-18 Sawdust layer was used as insulation layer 56

Figure 4-1 Specimens in curing tank 59

Figure 4-2 400-kip compression testing machine 61

Figure 4-3 Compressive strength with time 62

Figure 4-4 Typical failure mode of concrete in compression 62

Figure 4-5 Test setup for stress-strain relationship 63

Figure 4-6 Stress-strain relations of conductive concrete 65

Figure 4-7 Modulus of elasticity of conductive concrete 65

Figure 4-8 Flexural strength – test setup 66

Figure 4-9 Flexural strength with time [using simple beam with center-point loading]

(ASTM C293-79 – AASHTO T 177-81) 67
Figure 4-10 Freeze and thaw testing equipment 68
Figure 4-11 Freeze and thaw specimens during taking measurements 69
Figure 4-12 Freeze and thaw specimens – before and after 312 cycles 69
Figure 4-13 Specimens for shrinkage test 70
Figure 4-14 Shrinkage strain measurements 71
Figure 4-15 Shrinkage strain vs. ACI 209-97 predicted strain 71
Figure 4-16 1-in. thick specimens for permeability test 72
Figure 4-17 Temperature-controlled box for permeability test 74
Figure 4-18 Permeability test specimen preparation 74
Figure 4-19 Specimens inside moisture-free desiccators 75
Figure 4-20(a) Specimens stored in unsaturated air 76
Figure 4-20(b) Saturated surface dry specimens 76
Figure 4-21(a) Cylinders with sawdust mortar insulation layer 79
Figure 4-21(b) Thermal conductivity test specimen 79
Figure 4-22 Typical temperature distribution during thermal conductivity tests 80
Figure 5-1(a) Slabs ready for casting the conventional concrete layer 83
Figure 5-1(b) 6-in. conventional concrete slab 83
Figure 5-2(a) Slab cross section 84
Figure 5-2(b) Thermocouples and steel plates in the overlay 85
Figure 5-3 Fiber reinforced plastic rebar used as shear studs 86
Figure 5-4 Steel plates with opening were used as electrodes 87
Figure 5-5 Conductive concrete mix showed excellent workability and

surface finishability 88

Figure 5-6 Slabs after finishing 88

Figure 5-7 Thermocouple locations in the insulation layer 90

Figure 5-8(a) Thermocouple locations in the 2m x 2m overlay 91

Figure 5-8(b) Thermocouple locations in the 1.2m x 3.6m overlay 92

Figure 5-9(a) Thermocouples placed at two levels 93

Figure 5-9(b) Thermocouple layout before casting overlay 93

Figure 5-10(a) Temperature, humidity, and wind sensors 94

Figure 5-10(b) An electronic weather station 94

Figure 5-11(a) The VARIAC, transformer and amp-meter for power control 95

Figure 5-11(b) Slabs connected to power source 96

Figure 5-12 Anti-icing experiment – Feb. 11, 1999 99

Figure 5-13(a) Slab before testing (Deicing experiment – Feb. 20, 1999) 100

Figure 5-13(b) Slab during testing (Deicing experiment – Feb. 20, 1999) 101

Figure 5-14 Average anti-icing and deicing temperature data 103

Figure 5-15 Conduction of electricity in the 1.2m x 3.6m x 9cm conductive concrete overlay 106

Figure 5-16 Conductive concrete overlay model 112

Figure 5-17 Electric resistivity of the conductive concrete 114

Figure 5-18 Enthalpy-temperature curve for phase change of snow 115

Figure 5-19 Deicing electric current data (under 420 V AC) 118

Figure 5-20 Electrical resistance heating of conductive concrete overlay 119

Figure 5-21 Temperature time-histories in the snow layer 120

Figure 6-1 Electric resistivity vs. temperature – EC-All mix 128

Figure 6-2 Electric resistivity vs. temperature – Slag + 25% EL mix.....128

Figure 6-3 Comparison of heating rates of trial mixes.....130

Figure 6-4 Time effect on electric resistivity 131

Figure 6-5 Conductive concrete panel layout.....132

Figure 6-6 Power chord and angle iron connection.....133

Figure 6-7 Roca Bridge deck deicing – February 5, 2004 136

Figure 6-8 Ambient vs. average slab temperature.....137

Figure 6-9 Average current-temperature relationship 138

LIST OF TABLES

Table 2.1 Comparison of deicing chemicals 15

Table 2.2 Comparison of different heating systems 23

Table 3.1 Conductive concrete mix design by Xie et al. 31

Table 3.2 Steel fiber characteristics 33

Table 3.3 Materials used in the conductive concrete mixes 34

Table 3.4 Summary for test results – Optimization category 1 and 2 36

Table 3.5 First-stage test results – Category 3 37

Table 3.6 Compressive strength and modulus of rupture – Category 3 45

Table 3.7 Effect of hydration time on electric resistivity 46

Table 3.8 Long-term evaluation of the electric resistivity 47

Table 4.1 Summary of material testing 60

Table 4.2 Modulus of elasticity of conductive concrete 64

Table 4.3 Resistance of concrete to rapid freezing and thawing ASTM C 666-92 -AASHTO (T161-93) 68

Table 4.4 Summary of the permeability tests 73

Table 4.5 Summary of the thermal conductivity tests 80

Table 4.6 Mechanical and physical properties of the conductive concrete 81

Table 5.1 Climatic data in anti-icing and deicing experiments 97

Table 5.2 Temperature range of anti-icing and deicing experiments (Data from 3.6m by 1.2m slab) 102

Table 5.3 Energy consumption and costs (Data from 3.6m by 1.2m slab) 105

Table 5.4 Electrical and thermal properties used in the finite element simulation 114
Table 6.1 Preliminary test results – carbon concrete.....124
Table 6.2 Comparison of heating rate, operating voltage and peak current.....125
Table 6.3 Electrical resistivity of carbon concrete trial mixes ……...127
Table 6.4 Deicing performance of Roca Spur Bridge……. ……...135